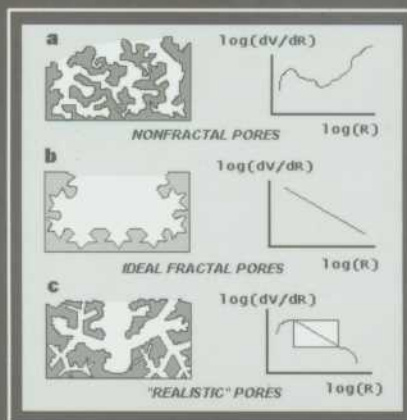
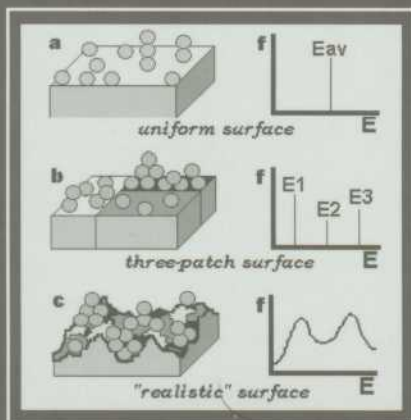


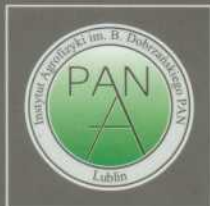
# PHYSICAL CHEMISTRY OF SOIL SURFACE AND PORE PROPERTIES

EDITED BY

GRZEGORZ JÓZEFACIUK, ZOFIA SOKOŁOWSKA, MIECZYŚLAW HAJNOS



Centre of Excellence for  
Applied Physics in Sustainable  
Agriculture AGROPHYSICS



Institute of Agrophysics  
Polish Academy of Sciences



EU 5<sup>th</sup> Framework Program  
QLAM-2001-00428



EU 5<sup>th</sup> Framework Program  
QLAM-2001-00428

**PHYSICAL CHEMISTRY OF SOIL  
SURFACE AND PORE PROPERTIES**

EDITORS:  
Grzegorz Józefaciuk  
Zofia Sokołowska  
Mieczysław Hajnos

Lublin 2004

**Authors:**

Grzegorz Bowanko (Institute of Agrophysics, Lublin)

Mieczysław Hajnos (Institute of Agrophysics, Lublin)

Grzegorz Józefaciuk (Institute of Agrophysics, Lublin)

Dorota Matyka-Sarzyńska (Institute of Agrophysics, Lublin)

Tosho Raychev (N. Poushkarov Institute of Soil Science, Sofia)

Zofia Sokołowska (Institute of Agrophysics, Lublin)

Ryszard Świeboda (Medical Academy, Pharmacy Dept., Lublin)

Opinion for the printing: Professor J. Gliński

ISBN 83-87385-91-3

© Institute of Agrophysics PAS, Lublin 2004

Edition: 180 copies

Project of cover and computer edition: Grzegorz Józefaciuk  
Technical assistance Dorota Matyka-Sarzyńska

---

Print: Drukarnia *ALF-GRAF*, ul. Kościuszki 4, 20-006 Lublin

## INTRODUCTION

Vast number of environmentally important processes occur on surface of soil solid phase and within soil pores. Soil surface and pore build-up is extremely complex due to diversified mineral, organic and ionic composition of soil constituents, and their different degree of dispersion. It constantly changes under various environmental factors.

Soil surface and pore properties become increasingly used for description and modeling of soil physical, chemical and biological processes (e.g. fertility, mass and energy exchange, accumulation of various species, water retention, microbial life, catalysis, pollution, acidification and alkalization, soil organic matter leaching and oxidation) as well as for quantitative analysis of soil typological and genetic properties.

Surface physicochemical models provide a framework within which several multidisciplinary studies of soil and plant can be conducted and complex relation between different soil and plant processes can be understood.

Despite this broad application there has been no book concerning soil surface and pore properties in more details. A need of such book has been frequently expressed by many researchers from agrophysics and related disciplines. Therefore we made a first attempt to fill this gap, providing a broader view on recent theories and experimental approaches to soil surface and pore systems, as well as to present some problems that are enlighten using surface and pore science.

As far as the present issue is a first approach to the subject, we will be glad to all the readers for their comments and criticisms, that will be helpful in eventual preparing of its more reader friendly version in future.

The Editors

## CONTENTS:

<b>INTRODUCTION</b> .....	7
<b>CHAPTER 1.</b>	
<i>T. RAYCHEV, D. MATYKA-SARZYŃSKA</i>	
<b>SOIL SOLID PHASE</b> .....	7
CLAY MINERALS .....	7
SOIL ORGANIC MATTER .....	13
ORGANO-MINERAL ASSOCIATES .....	15
<b>CHAPTER 2.</b>	
<i>G. JÓZEFACIUK</i>	
<b>SOIL pH</b> .....	19
EFFECT OF pH ON SOIL SOLID PHASE .....	23
<b>CHAPTER 3.</b>	
<i>Z. SOKOŁOWSKA, G. JÓZEFACIUK, G. BOWANKO</i>	
<b>ADSORPTION OF GASES OR VAPORS ON SOLIDS</b> .....	30
MEASUREMENT OF ADSORPTION .....	31
ADSORPTION ISOTHERM .....	33
ADSORPTION IN SOILS .....	36
<b>CHAPTER 4.</b>	
<i>Z. SOKOŁOWSKA, G. JÓZEFACIUK</i>	
<b>SURFACE AREA</b> .....	41
SURFACE AREA IN SOILS AND SOIL PROCESSES .....	44
<b>CHAPTER 5.</b>	
<i>Z. SOKOŁOWSKA, G. JÓZEFACIUK</i>	
<b>ADSORPTION ENERGY AND SURFACE HETEROGENEITY</b> ...	54
ADSORPTION ENERGY IN SOILS AND SOIL PROCESSES ....	56
<b>CHAPTER 6.</b>	
<i>M. HAJNOS, R. ŚWIEBODA, G. JÓZEFACIUK</i>	
<b>SOIL POROSITY</b> .....	67
MEASUREMENT OF POROSITY .....	70
POROSITY IN SOILS AND SOIL PROCESSES .....	75
<b>CHAPTER 7.</b>	
<i>Z. SOKOŁOWSKA, G. JÓZEFACIUK</i>	
<b>FRACTAL CHARACTER OF SOIL</b> .....	85
FRACTAL CHARACTER OF SOIL SURFACE .....	87
FRACTAL CHARACTER OF PORE SYSTEM .....	89
FRACTALITY OF GRAIN-SIZE DISTRIBUTION .....	91
FRACTALS IN SOILS AND SOIL PROCESSES .....	93

<b>CHAPTER 8.</b>	
<i>G. JÓZEFACIUK</i>	
<b>SURFACE CHARGE</b> .....	99
MEASURE OF SURFACE CHARGE.....	104
HETEROGENEITY OF SURFACE CHARGE .....	105
SURFACE CHARGE IN SOILS AND SOIL PROCESSES .....	108
<b>CHAPTER 9.</b>	
<i>M. HAJNOS</i>	
<b>SURFACE FREE ENERGY AND WETTABILITY</b> .....	119
WETTABILITY OF SOILS .....	123
<b>LITERATURE</b> .....	129
<b>LIST OF SYMBOLS</b> .....	147

## CHAPTER 1.

### SOIL SOLID PHASE

*T.RAYCHEV, D. MATYKA-SARZYŃSKA*

Solid phase of a soil is a mixture of different inorganic constituents as non-porous materials of different size and shape, porous materials with microcapillaries or pores and phyllosilicates with the interlayer structure, as well as organic species, mainly plant residues and specific humus substances (Fig.1.).

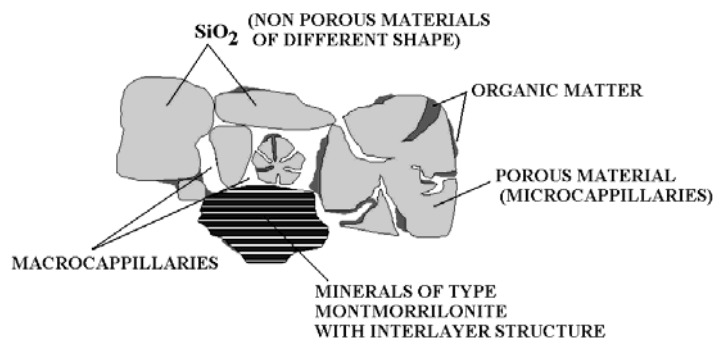


*Fig. 1. Scheme of solid phase of the soil*

The most important for development of specific surface and fine porosity is soil clay fraction, containing soil material of finest sizes (<2 $\mu$ m particles, Elonen 1971), wherein clay minerals, humus and organo-mineral components dominate.

#### CLAY MINERALS

Clay minerals, formed as secondary weathering minerals, are hydrated aluminum (or rarely magnesium) silicates of layer structure (Grim 1959). They are built from couple of subsequent flat layers of silicon oxide and aluminum oxide. The general formula of aluminosilicates  $n\text{SiO}_2\text{Al}_2\text{O}_3 \cdot m\text{H}_2\text{O}$  and a mole ratio  $\text{SiO}_2:\text{Al}_2\text{O}_3$  varies between 2 to 5 depending on impurities and type and extent of isomorphism. Although some of the clay minerals are stable at very high temperatures, they can be also synthesized at ambient temperature, during various sedi-

mentation processes, diagenesis and weathering, as well as could be of biogenic origin, i.e. from mineralization products of plant residues.

Their common properties are the crystal layer structure, the colloid dispersion, the sorption characteristics and the presence of the constitutional water. Each group, however has specific behavior and importance in the formation and properties of the different soil types. On the basis of the structure of the crystal lattice of the majority of the clay minerals, two structural patterns can be distinguished: Si-O-Si tetrahedral ( $T_d$ ) and O-Al-OH octahedral ( $O_h$ ).

### ***Tetrahedral layer ( $T_d$ )***

In the tetrahedral structure Si atoms are surrounded by 4 O atoms. The binding between them takes place through overlapping of the innate  $sp^3$ -hybrid orbitals, resulting in the formation of  $4\sigma$ -bonds (Fig. 2) (Lazarov 2001).

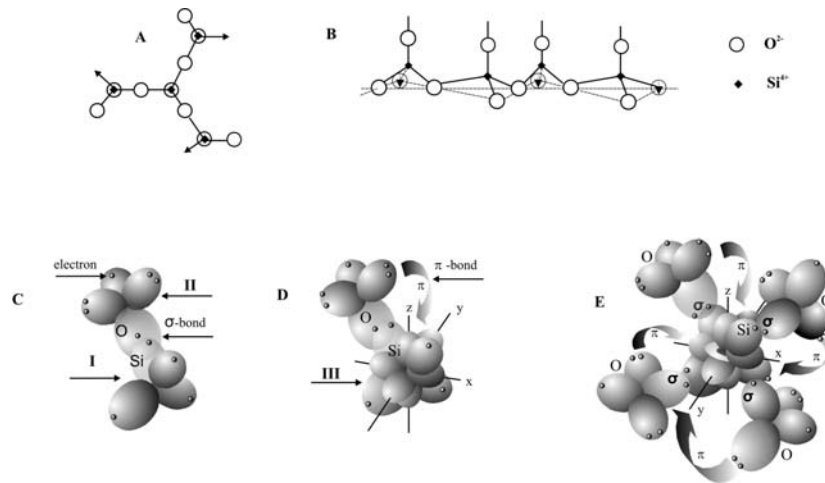


**Fig. 2.** Formation of tetrahedral layer of clay minerals:

**A** – fragment of the hexagonal network of the repeating fragment with composition  $(Si_4O_{10})^{4-}$ ; **B** – schematic representation of the basal surface, formed by the fragment  $(Si_4O_{10})^{4-}$ . With flashes are marked the ions of the oxygen, which belong to other structural fragment; **C** – formation of  $\sigma$ -bond between silicon and oxygen: **I** –  $sp^3$  hybridisation of the silicon atom; **II** –  $sp^3$  hybridisation of the oxygen atom; **D** – formation of the  $\pi$ -bond between silicon and oxygen: **III** – steric configuration of the four  $sp^3$ -hybrid orbitals and two free  $d$ -orbitals ( $d_{z^2}$ ;  $d_{x^2-y^2}$ ) of the silicon; **E** – chemical bonds in a fragment of the tetrahedral layer.

Since every O atom is bound to two Si atoms, its second  $sp^3$ -hybrid orbital is overlapped with the respective orbital of the neighboring Si atom. The other ready electron pairs on the remaining two hybrid orbitals additionally strengthen the  $\sigma$ -bonds through overlapping with free d-orbitals of the outer electron layer of Si.

This is the way of formation of donor-acceptor interaction and respectively  $\pi$ -bonding with the participation of the ready electron pair of the atom bonded to Si and Si free d-orbital. The formation of a  $\pi$ -bond strengthens the  $\sigma$ -bonds between Si and O and predetermines the stability of the tetrahedral structure of layer silicates (Cotton and Wilkinson 1997a,b).

### **Octahedral layer ( $O_h$ )**

The other major construction element of layer silicates is composed of two layers tightly packed O atoms and OH groups and Al, Fe or Mg atoms situated between them (Fig. 3). The central cation is surrounded by 6 anions each situated on the top of  $O_h$  e.g. for the Al atom the formula is  $[Al(OH)_6]^{3-}$ . Since the anions belong to adjacent  $O_h$  the resulting net formed is called the “ $O_h$  layer”. This type of structure is characteristic for gibbsite  $[Al(OH)_3]$  and brucite  $[Mg(OH)_2]$ .

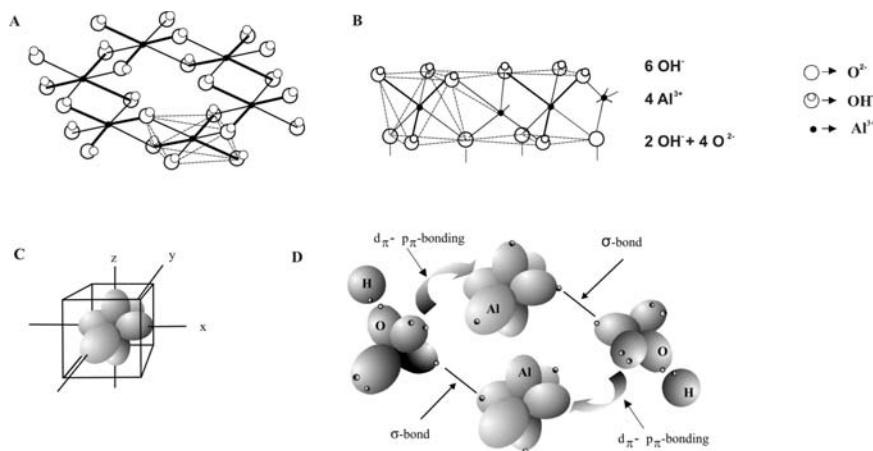


**Fig. 3.** Formation of octahedral layer of clay minerals:

**A** – single layer from the structure of the gibbsite where Al occupied 2/3 of the octahedral positions; **B** – schematic representation of the basal surface, formed by the fragment  $Al_4O^4(OH)_8$ ; **C** –  $sp^3d^2$ -hybridisation between one  $s$ -, three  $p$ - and two  $d$ -orbitals; **D** – formation of  $\sigma$ - and  $\pi$ -bond ( $d_{\pi}-p_{\pi}$  - bonding) between aluminium and oxygen in a fragment of the octahedral layer.

In the structure of gibbsite the atoms of Al in the octahedral coordination leave six  $sp^3d^2$ -hybrid orbitals, three of which possess one electron. The binding between the Al atoms and the OH-groups through  $\sigma$ -bonds is carried out through overlapping of the hybrid orbitals. There is also a possibility of leaving ready electron pairs of the O-atoms for a formation of a  $d_\pi$ - $p_\pi$ -bonding and a realization of a  $\pi$ -bond (Fripiat et al. 1971).

With two orbitals of one O atom two valent bonds are formed: one with the H atom and another “resonance” bond with two atoms of Al. The rest two hybrid orbitals with ready electron pairs, and at suitable geometry could overlap with free  $sp^3d^2$ -hybrid orbitals of Al.

The mobility of the donor electrons and  $\pi$ -electrons allows their transition from one atom to another. This results in delocalization of the orbitals, enveloping several atomic nuclei. Each of the O-Al- bonds might be presented as  $1/2\sigma$ - and  $1/2d_\pi$ - $p_\pi$ -bond. The lack of symmetry of the charge centers predetermines also the realization of H-bonds between adjacent OH groups. Because of the accumulation of the above-mentioned phenomena, around the Al-OH a dipole field is formed whose influence is induced over the molecular field of the entire crystal lattice.

### ***Electric neutrality of the package***

The electric neutrality requires the compaction of one  $O_h$  layer and one  $T_d$  layer in an electroneutral package. The neutralization between the positive and the negative ion charges takes place through the adjacent intermediate layer of O and OH anions of the neighboring layers. Generally judged their condensation leads to the formation of mixed  $T_d$ - $O_h$  packages and actually to formation of specific clay mineral structures. They can consist of two separate layers (two-layer structure or 1:1 type of minerals: kaolinite, dickite, halloisite), but also the  $O_h$  layer may be inserted between two  $T_d$  layers (three-layer structure 2:1 type of minerals: smectite, beidellite, muscovite, vermiculite, hectorite, etc.), that is shown in Fig. 4.

The electronic configuration of the unified layers in the two-layer package (e.g. in 1:1 minerals such as kaolinite) and the bonds distribution in the  $T_d$ -coordination of Si and the  $O_h$  coordination of Al with the strongly electronegative ligands of O (respectively OH-groups) has the following peculiarities:

- Increased electronic density in the outer surface planes relative to the inside of the package;
- Appearance of  $H^+$ -cations on the basal plane of the  $T_d$  layer in acid medium provokes the formation of H-O bonds;
- Formation of hydrogen bonds takes place also between adjacent OH groups on the basal plane of the Al-OH motif;

- Formation of inner structure bonding between the  $O_h$ -OH groups and the common to Si and Al oxygens;
- The  $\sigma$ -bond between the atomic orbitals of Al and O ( $sp^3d^2$ - $sp^3$ ) is weaker than the  $\sigma$ -bond Si - O ( $sp^3$ - $sp^3$ );
- Formation of  $\pi$ -bonds strengthens the  $\sigma$ -bonds.

*Fig. 4. Formation of the combined package of kaolinite (A) and montmorillonite (B) and chemical bonds between silicon-oxygen and alumo-hydroxylic layers (C).*

#### ***Consequences for soil properties***

To understand the participation of the clay minerals in the formation of the soil adsorbent and its colloidal and chemical behavior, some major consequences resulting from the character of the electronic configuration and the types of bonding on the crystal surfaces are important, i.e.:

- The decreased electronic density in the oxygen area on the basal plane of the  $T_d$  layer because of appearance of exchangeable  $H^+$ -cations increases the polarity of H-O bonds and respectively the acidic character on the surface of the hexagonal rings.
- Delocalized multi-centre electronic configuration in the area of the hexagonal gibbsite layer on the  $O_h$ -plane creates non-symmetrical dipole field. Its characteristics are determined by increased electron density around OH-groups and the appearance of partial positive charge in the vicinity of Al atoms.
- The different length of Si-O-Al bonds may cause a change of the  $T_d$  coordination and the presupposed allowed angle of Si-O bond orientation, and may lead to geometry deformations in the crystal structure. A possible consequence is a shift of the ideal hexagonal symmetry formed by inclination of the oxygens towards the gibbsite layer with following deformation of the  $T_d$  layer. This is a reflection of the appearance of the partial charges both in the area of  $T_d$  bonded with Si oxygens and in the vicinity of the octahedral Al.

Some peculiarities in the behavior of soil clays in real conditions are probably consequences of the influence of such deformation effects. Aluminum, for instance initially plays the role of a central atom in the  $O_h$  layer of the package. In the gibbsite structure, each hydroxide ion is situated above the two cations and above the respective cavity. Its oxygen is oriented towards aluminum, and hydrogen towards the outermost coordination relative to Al. All of these results in the change of the angle of hydroxyl ions position against gibbsite surface. Such geometry pulls up the proton to the bridge oxygen (Si-O-Al) between the two layers of the package. Because of the orientation effect and the induced interactions, a hydrogen bond is formed. That's why prerequisites occur for local shrinking of the  $O_h$  layer, followed by the reciprocal reaction also in the  $T_d$  layer. In strongly acidic medium the  $H^+$  ions can easily migrate inside the crystal lattice. Their hydrolytic attack may be directed both to surface OH-groups, and towards oxygen bridges between atoms of Al and Si. The hydrolysis process of Al (having central place in the octahedral) leads to accordingly hydroxyl- and aqua- complexes of Al. Its coordination in the lattice structure is disturbed and allows movement of the complexed forms towards negatively charged centers of basal planes.

The actual presence of these colloid forms of Al in the cavities of the crystal structure and in the vicinity of its initial coordination center maintains the level of its partial positive charge. This charge is transmitted (induced) on the outer crystal surfaces. The comparatively higher dimensions of this colloid may cause inner tension in the structure and appearance of secondary deformations in its geometry. Its "emerging" on the basal plane will neutralize part of the negative charges and decrease the cation sorption capacity and facilitate the package interaction.

Consequently positively charged zones may appear also on the basal plane of the  $T_d$  layers, as a result of the destructive role of acidification and the following “emerging” of colloid forms of Al for neutralization of part of the negatively charged geometric centers. The behavior of the hydrolyzed forms of the transition elements on the surface of allumino-silicates probably also depends on similar geometric deformations. It was shown (Atanassova and Ilieva, 2003) that the pH-dependent specific sorption (based on the discrepancy between  $Cu^{2+}$  adsorbed/ $Ca^{2+}$  desorbed shifted to the lower pH ( $< 4$ ) with increasing Cu concentrations and specific sorption with kaolinite was recorded even at pH 3.6. The surface of kaolinite exhibited a higher affinity for Cu ( $\log K_d$  values of the distribution coefficient) with increasing pH than the smectite and vermiculite surfaces (Atanassova, 1995).

In some cases the geometric position of the OH groups should open the space above the Al atoms in their  $O_h$  coordination, thus increasing their susceptibility to cationic attack and facilitating the isomorphic substitution. Such interactions induce considerable changes in the ion-exchange properties of clay minerals. The lower sorption capacity of the  $O_h$  surfaces relative to the  $T_d$  ones and the smaller distance between the packages of clay minerals such as kaolinite can be explained with the above mentioned arguments.

## **SOIL ORGANIC MATTER**

Soils contain large variety of organic materials that can be grouped into humic and non-humic substances (Schnitzer 1991). The process of humus formation is called humification. Until now the humification process has been a subject of much speculations and studies. In natural systems, biomass consisting of dead plant and animal residues is converted into soil organic matter (humus) by degradation reactions catalyzed by enzymes. A part of organic compounds is partially oxidized. So, humification can be defined as a conversion of degradation products by series of polymerization reactions into new types of polymeric species that are different from the precursor molecular species in the original biomass (Schnitzer and Khan, 1978; Wershaw, 1994).

### ***Structure of humic substances***

Humus is probably the most chemically and physically active component of soils but it is still the least understood. Nevertheless its several general common features can be distinguished: the presence of an aromatic ring, nitrogen as an obligatory component and functional groups. A schematic view of the structure of humic acid is shown in Fig. 5.

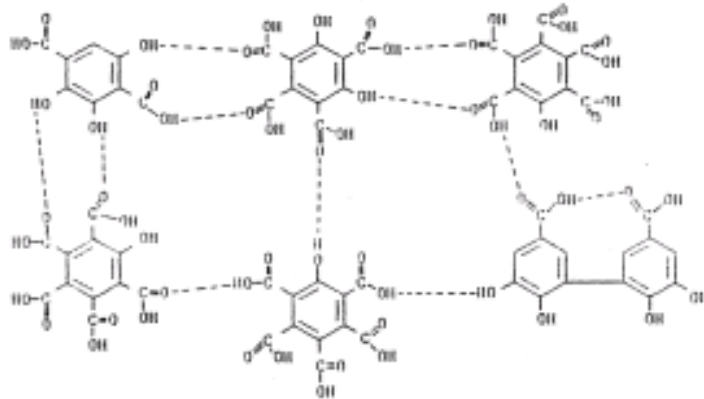


**Fig. 5.** Hypothetical structure of humic acids after Stevenson (1982).

Historically humus (humic substances) can be divided into the following three main fractions: humic acids (HA), fulvic acids (FA) (Fig. 6.) and humines. In this classification (Kononova, 1966), humic acid is soluble in strong base but precipitates at pH values less than 2; fulvic acid is soluble in both basic and acidic solution; humin is insoluble in both basic and acidic solutions. These three fractions differ mainly in molecular weight and functional groups content with FA having a lowest molecular weight, containing more oxygen but less carbon and nitrogen, and having a higher content of oxygen-containing functional groups per unit weight than the other two humic fractions.

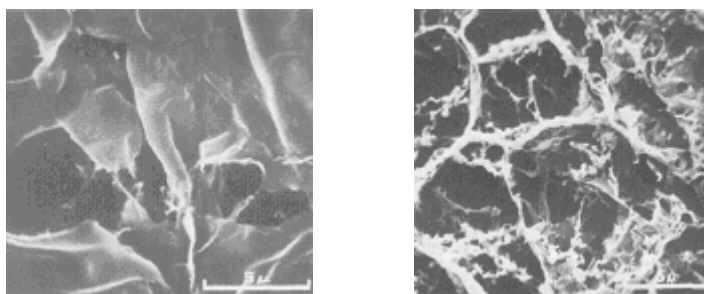


**Fig. 6.** Scanning electron micrographs of FA (left) and HA (right) at pH 8 (after Schnitzer and Khan, 1978).

### ***Function of organic matter in soil***

The importance of humus as a major factor in controlling the physical and chemical properties of soils has long been recognized. The organic matter plays a significant role in cations exchange and can interact with inorganic anions (phosphorus) via polyvalent cations. So, humus has physical and physico-chemical function in that it promotes good soil structure (stability of aggregates of soil particles), thereby improving soil fertility, aeration, retention of moisture, buffering and exchange capacity of soils (Gawlik 1992, Gawlik and Harkot 2000). Organic matter contributes to plant growth through not only its effect on the physical, chemical but also biological properties of the soil. It has: nutritional function in that it serves as a source of N, P for plant growth. Humus content is also important in maintaining biological function in soils. It affects the activities of microflora and microfauna organisms (Schnitzer and Khan, 1978).

### ***Dissolved organic matter (DOM)***

In nature some of organic matter substances (humus) are sorbed by soil solid particles and some are transported through unsaturated zone into the saturated zone, where they can remain dissolved in, and move with the groundwater. So, DOM is an important component of not only soil but also aquatic environments. The nature and the amount of DOM in soil solution can influence the quality of groundwater and surface waters. Furthermore, DOM is involved in a number of biogeochemical processes, including pH buffering, nutrient cycling, ionic balance, mineral weathering, metal leaching, pollutant toxicity, mobility and bioavailability.

### **ORGANO-MINERAL ASSOCIATES**

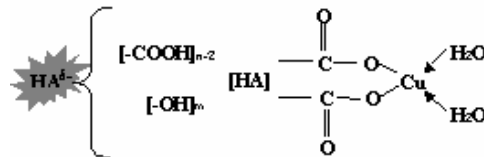
Organo-mineral compounds may be formed from negatively charged clay minerals, humus and positively charged ions or hydroxycomplexes of amphoteric elements into forms of “sandwich” colloidal structures. Such “mosaic” materials of various local structures determine ionic equilibria between the root system and soil sorption complex (Chassin et al. 1977; Ganey, 1990; Orlov, 1985).

The specific role of organo-mineral compounds in soil adsorption complex depends on their genesis and evolution (Duchaufour, 1968, 1972). Their peculiar character is determined just from the beginning of a decay of plant or animal residues.

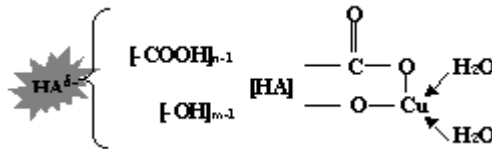
Formation of organo-mineral compounds is governed by activity of soil biochemical and enzymatic processes that produce a range of forms of decomposed

organic material of various stereochemical character, elasticity and dimensions, finally interacting with mineral phases (Raychev 1996, Raychev et al. 2001).

High concentration of acidic groups on organic macromolecules promotes binding of polyvalent ions into chelate complexes:



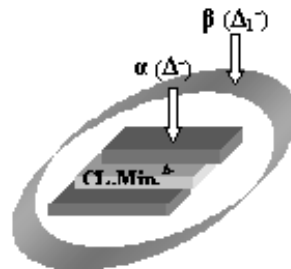
At high pH values, dissociated phenolic hydroxyls may participate in the above reactions (Orlov, 1985):



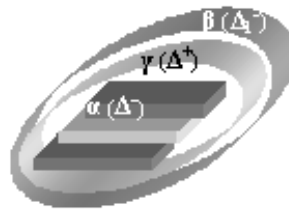
Polyvalent cations adsorbed on surfaces of stable organo-mineral complexes promote subsequent adsorption of next organic layers, and so on, and in time these formations reorganize and polymerize reaching more aromatic character.

Colloid micelles can arise around polymeric hydroxyions having pH dependent surface charge. These hydroxyions have extremely high sorption ability due to high charge and mass of the micelles (Boldyrev, 1983; Ganev, 1990; Orlov, 1985; Charlot, 1969). Interactions of individual atoms or their groups leading to new structures formation may occur via atomic or ionic bonds (Raychev et al. 2001).

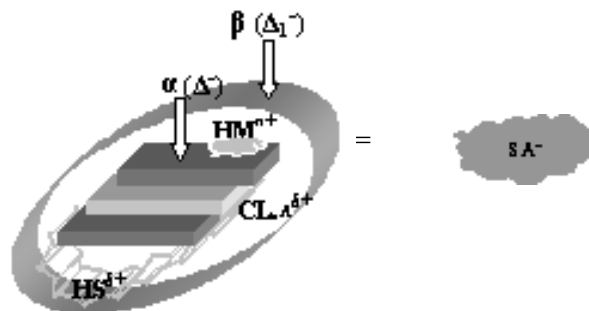
The basic source and carrier of the negatively charged centers in soils are basal planes ( $CL_{sA}^{\delta-}$ ) of clay minerals ( $CL_{Min}^{\Delta-}$ ), that form an internal zone ( $\alpha$ ) with partial negative charge ( $\Delta^- = \Sigma(\delta^- + \delta^+)$ , where  $\delta^- \gg \delta^+$ ) and the acidic groups ( $HA^{\delta-}$ ) of soil humus substances that belong to the external zone ( $\beta$ ) of the negative charge ( $\Delta_1^-$ ):



Except of hydrophobic and Van der Waals interactions, a partial positive charge on soil components may be involved in formation of the above structures. The source and carrier of the positive charge ( $\Delta_1^+$ ) are colloidal forms of polyvalent heavy metals ( $\text{HM}^{n+}$ ), edge surfaces of clay minerals ( $\text{CL}_A^{\delta+}$ ) and some fragments of humic substances ( $\text{HS}^{\delta+}$ ):



The compensation of the negative surface charge goes mainly by cation ( $\text{M}^{n+}$ ) adsorption, positively charged mineral colloids ( $\text{HM}^{n+}$ ) and fragments of humic substances ( $\text{HS}^{\delta+}$ ). Due to this, near the surface of the mineral center of the soil adsorbent a transition („bridge”) zone ( $\gamma$ ) is formed that strengthen the overall interactions between humus and clay minerals:

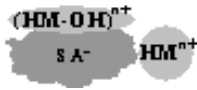


Such structure of the organo-mineral center (abbreviated further as  $\text{SA}^-$ ), has its own external adsorption centers that may bind additional amounts of heavy metal micelles and next organic substances, and so on, and the system is stabilized in time in such way that polar (charged surfaces) remain inside and nonpolar (aromatic or aliphatic) groups are exposed. Most of heavy metals in acidic soils are in forms of hydroxyions ( $\text{HM-OH}^{n+}$ ), and a smaller part of free cations ( $\text{HM}^{n+}$ ) is mainly bound to soil exchange positions. This is accepted that positively charged hydrosols form coagulation zones for particles of opposite sign of charge i.e. negative parts of clays and humus. The above reactions may be illustrated as following:

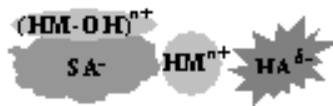
At a presence of colloidal forms of heavy metal hydroxides  $(HM-OH)^{n+}$ , in acidic environments the following formation will dominate:



On negatively charged basal planes of clays ( $CL.SA^{\delta-}$ ) occurs adsorption of free metal cations ( $HM^{n+}$ ):



This allows for an excess sorption of humic acids ( $HA^{\delta-}$ ):



The diffuse double layer in such systems has now “triple zone“ configuration remaining this illustrated above, where the surface potential may change not only in the amount, but in sign, as well (Friedrichsberg, 1984; Kokotov et al., 1986).

Distribution of negatively and positively charged specific adsorption centers in the colloidal soil components allows for structure formation and stabilization. The soil structure may be further stabilized by different forms of polyvalent heavy metals via a range of adsorption, colloidal and ionic interactions.

The structure may have zonal character wherein the mineral center is surrounded by subsequent layers of organic substances bind together by various polyvalent cations forms.

## CHAPTER 2.

### SOIL pH

*G. JÓZEFACIUK*

The pH is probably the most important soil parameter (Davis 1943; Ganey 1987). The actual soil pH governs most of soil physicochemical properties as nutrient availability and uptake by plants, aluminum and heavy metals equilibria and toxicity, microbial activity, organic matter transformations, soil microstructural properties, the amount and sign of soil charge and many others. Thus it is not surprising that the determination of pH is the most commonly performed soil test. However, there still exist different definitions and standards for pH measurement as well as for interpretation (Sumner, 1994).

The pH is defined as the negative logarithm of hydrogen ion activity:

$$\text{pH} = -\log(a_{\text{H}^+}). \quad (1)$$

The above definition implicates that the determination of pH is equivalent to the knowledge on the individual ion activity, what is thermodynamically restricted (Bache, 1979). However, for many practical purposes the single ion activity,  $a_i$ , can be formally defined as (Kortum, 1966):

$$a_i = c_i f_i, \quad (2)$$

where  $c_i$  denotes ion concentration and the individual ion activity coefficient,  $f_i$ , is given by:

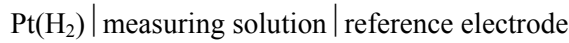
$$\ln f_i = \ln f_{\pm} (v_i z_i^2) / (v_+ z_+^2 + v_- z_-^2), \quad (3)$$

where  $v$  and  $z$  are the number and the valence of ions coming from a salt dissociation, respectively. According to the corrected Debye-Huckel theory, the average ionic activity coefficient,  $f_{\pm}$ , is given by:

$$\log f_{\pm} = -[A |z_+ z_-| \sqrt{J}] / [1 + Ba \sqrt{J}] + CJ, \quad (4)$$

where  $A$  and  $B$  are constants related to the temperature and the dielectric constant of the medium,  $a$  (``an effective ionic diameter``) and  $C$  are empirical parameters and  $J$  is the ionic strength of the solution. Due to the complicated and a semi-empirical character of the dependencies between the concentration and activity, the translation of pH onto concentration should be avoided.

The potentiometric methods of pH measurement do not, however, give the values defined by Eq. (1) but the values corresponding to some conventional pH scale, obtained in arbitrary (and carefully) selected systems. The most common conventional pH scale is based on the measurement of the electromotive force between a reference (constant potential) electrode and the normal hydrogen electrode:



where  $\mid$  denotes the interphase. The electromotive force of the above system,  $\Delta E$ , can be expressed as:

$$\Delta E = E_0' - RT/F \ln a_{\text{H}^+} + \Sigma E_d, \quad (5)$$

where  $E_0'$  is the potential of the reference electrode and  $\Sigma E_d$  is the sum of the diffusion potentials across all interfaces. In the most general case, the diffusion potential is:

$$E_d = -RT/F \int_{a_2}^{a_1} \sum_i \frac{t_i}{z_i} d \ln a_i, \quad (6)$$

where  $t_i$  is the transference number of the ion kind  $i$  and the integration is performed across the interface of the ionic activities  $a_1$  and  $a_2$ .

The solution of Eq. (6) is possible only for some simple systems, for which usually the transference number of a given ion is assumed to be constant across the interface. Despite the difficulties in calculating the diffusion potential, this can be minimized in practice e.g. by making the junction between the measuring solution and the reference electrode with a saturated KCl solution (salt bridge). The mobilities of K and Cl ions are nearly that same and high salt concentration provides the current is transported practically by K and Cl ions only. To be sure that this diffusion potential is reproducible, the KCl bridge  $\mid$  measuring solution interface should not change during the measurement. This is provided by the KCl leakage from the salt bridge. In modern electrodes the leakage can be as small as less than  $1\text{mm}^3$  per hour.

This is important to note on particular problem arising when the measuring system involves charged colloidal particles. In this case the transference number of the ions of the opposite sign than the charge of the particles decrease due to the retardation of their mobility in the electric field. Thus the transference numbers of the ions from the salt bridge can markedly differ and high diffusion potentials can occur. This is called the suspension effect. The suspension effect is favored by high particle concentration, low counterion valence and high difference between the suspension and the salt bridge ionic strengths. It was recommended by Peech et al. (1953) to place the salt bridge in the clear supernatant liquid after the soil

particles have settled out from the suspension. As resulting from the above, also stirring of the suspension during pH measurements should be avoided. The suspension effect can be eliminated when the salt bridge has that same composition as the suspension equilibrium solution (Chernoberezskij, 1980).

Let us now return to Eq. (5). As this was mentioned earlier, even for pure solutions the calculation of the value of the diffusion potential as depending on the geometry and composition of the interface is not possible in general. However, for a given electrode the  $E_0' + \Sigma E_d$  can be measured experimentally with a good precision. For saturated calomel electrode (SCE), this quantity can be quite well approximated by the empirical formula:

$$E_0'_{SCE} + \Sigma E_d = 0.2490 - 6.5 \cdot 10^{-4}(t - 20), \text{ Volts,} \quad (7)$$

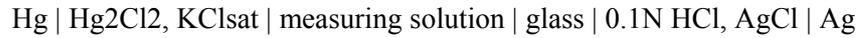
where t is the temperature (Celsius).

Thus from Eqns (1), (5) and (7) the pH value is:

$$\text{pH} = [\Delta E - 0.2490 - 6.5 \cdot 10^{-4}(t - 20)]/[0.0001983(t + 273)]. \quad (8)$$

This equation is a base for establishing pH's of standard buffer solutions.

Because of the practical complications of the use of hydrogen this has been commonly replaced with a glass electrode. The pH is measured in the system:



Due to the dependence of the glass electrode potential on the type of the internal reference electrode, kind of glass used as well as on time (ageing) the pH measurements are made by comparison with standard buffer solutions. Usually two buffer solutions  $S_1$  and  $S_2$  are taken and the linearity between pH and  $\Delta E$  is assumed. When the diffusion potentials in all the solutions can be assumed to be that same, the pH of the unknown solution X is given by:

$$[\text{pH}(X) - \text{pH}(S_1)]/[\text{pH}(S_2) - \text{pH}(S_1)] = (\Delta E_X - \Delta E_{S_1})/(\Delta E_{S_2} - \Delta E_{S_1}) \quad (9)$$

In contrary to most other ions, the determination of proton activity in solutions extracted from soils leads to unrealistic values, most probably due to the disturbance of the total three-phase equilibrium during extraction and a usually low buffer capacity of the soil solution (Csillag, 1987). Thus the soil pH is commonly measured in the supernatants over the sedimented soil solid phase.

The soil pH depends not only on soil composition but also on external conditions such as solid to liquid ratio, concentration and ionic composition of equilibrium solution, carbon dioxide partial pressure. While the effect of carbon dioxide is negligible in soils of pH values below 7 and the measured samples can be assumed to be in equilibrium with the atmosphere, the most important influence on the measured pH have soil solution composition and its ratio to the soil.

Within the entire range of soil to solution ratio for acidic soils the effect of dilution is to increase the pH of soil suspension. That same holds for alkaline soils providing the dilution is not extremely high. To make soil pH values comparable, the soil to solution ratio of 2.5 was adopted in 1930 by International Society of Soil Science (Peech, 1965).

The pH of the soil measured in water suspensions is very sensitive to biological and meteorological conditions. To obtain stable readings, reflecting the more intrinsic characteristic of the soil, the researchers early started to measure pH in neutral salt solutions.

The most important mechanisms occurring when increasing of salt concentration are:

- replacement (exchange) of electrostatically adsorbed protons from negatively charged surfaces. As this was proven (Gilbert and Laudelout, 1965) the hydrogen ions behave like any other exchangeable monovalent cations. Approximate calculations assuming average soil properties (total concentration of the soil solution around 0.01N, surface coverage by polyvalent cations around 80% of the CEC and exchange capacity about  $50\text{cmol kg}^{-1}$ ) and no buffer capacity of the soil solution, show that the drop in pH caused by the release of all adsorbed protons to i.e. N KCl solution can be up to 1 pH unit at 1:2.5 soil:water ratio regardless the initial pH. The input of adsorbed protons can thus be significant providing the buffer capacity of the soil solution is low;

- release of surface protons from organic matter functional groups of acidic character in entire range of pH values due to increase degree of dissociation;

- release of adsorbed Al ions (for acidic soils) which may hydrolyze in the solution producing protons (Thomas and Hargrove, 1984);

- dissociation-association reactions of surface protons (potential determining ions) of variable charge / constant potential surfaces. In acidic soils some of variable charge surfaces may consume protons if actual soil pH is lower than PZC thus reducing the decrease of pH after increasing salt concentration. At neutral and alkaline soil reactions the protons release prevails. To quantify these effects on the pH after addition of salt, still much attention should be given to the buffer capacity of the soil solution;

- increase of the coagulation of soil colloidal particles (DLVO theory, (Bolt, 1982)), what is important to minimize the suspension effect.

In carbonate soils, the pH is governed mainly by calcium ion activity and the partial pressure of carbon dioxide (Turner, 1958). Since the solubility of  $\text{CO}_2$  strongly decreases with the increase of salt concentration, the increase of pH after the salt addition might possibly be expected if other effects are not involved. At least, in calcareous soils the decrease of pH with salt level increase can be markedly lower than in other, non carbonate soils.

To measure soil pH, early in Europe the use of N KCl solution was the most common. However, the  $\text{pH}_{\text{KCl}}$  values of many soils may be as much as 2 units lower than measured in aqueous suspensions. More recently Schofield and Taylor (1955b) have proposed to use 0.01M calcium chloride as measuring medium. The use of this solution to measure the soil pH has some important advantages:

-0.01M  $\text{CaCl}_2$  is approximately equivalent to the total electrolyte concentration of most fertile soils at optimum water content. Thus the pH in  $\text{CaCl}_2$  reflects more closely the natural soil conditions;

-0.01M  $\text{CaCl}_2$  is a very good coagulation medium. This is important to minimize the suspension effect. According to Schulze-Hardy rule, coagulation ability depends on the sixth power of the counterion valence. Thus 0.01M  $\text{CaCl}_2$  is that same effective as more than 0.5M KCl. Moreover, Ca ions can form bridges between organic matter macro-molecules thus preventing their peptization.

-pH measured in  $\text{CaCl}_2$  corresponds closely to the value of lime potential which is remarkably constant over a wide range soil to solution ratio and  $\text{CaCl}_2$  concentration in the soil suspension (Aslyng, 1954; Schofield and Taylor, 1955a). The lime potential is considered to be the more correct soil characteristic than the pH as the reduced activity ratio i.e.  $a_{\text{H}}/(a_{\text{Ca}})^{1/2}$  has more thermodynamic meaning than the activity of a single ion (Bache, 1979).

### **EFFECT OF pH ON SOIL SOLID PHASE**

Recent increase in soil acidification caused by atmospheric deposition (Cresser et al. 1989, Debicki et al., 1994; Dechnik et al. 1990; Ulrich, 1990) and improper soil nutrition (Wallace, 1994) as well as a consecutive rise of alkali- and salt-affected soils (Tanji, 1995) induce marked changes in soil pH. Soil reaction can alter soil structure, water and ion adsorption, acid-base equilibria, transport phenomena (Jozefaciuk et al., 1993; Thomas and Hargrove, 1984). Acid and alkali effects are important controls over mineral weathering (Bogda and Chodak 1991; Frank and Gebhardt, 1991; Jackson and Sherman, 1952; 1989; Yatsu, 1998) and genesis (Chermak and Rimstidt, 1987; Drief et al., 2001; Eberl et al., 1993; Huang, 1993). The effect of pH on clay minerals is also important from industrial point of view: treatment of minerals with inorganic acids of rather high concentrations and usually at elevated temperatures, referred to as 'acid activation', is commonly used for production of sorbents or catalysts (white carbon blacks) used in industry or environmental protection measures (Bandosz et al., 1992; Breen et al., 1995; Brown and Rhodes, 1995; Ravichandran and Sivasankar, 1997; Rupert et al., 1987; Schall and Simmler-Hubenthal, 1995).

Acid or alkali attack induces marked changes in crystal lattice of aluminosilicate minerals due to dissolution of lattice ions and/or rearrangement of the struc-

ture (Lal et al. 1989). Generally similar dissolution pathways are observed for various minerals under acid treatment involving structure destruction and formation of silicon oxides. Below pH 3 and depending on contact time smectites delaminate and partially dissolve. Destruction of the smectite structure is connected with the removal of octahedral cations, among which Mg is most readily removed (Christidis *et al.*, 1997). The rate of acidic dissolution of smectites increases with increasing octahedral Mg or Fe content, however the mechanism of the dissolution is independent of layer composition (Madejova *et al.*, 1988). The depopulation of the octahedral sheet of the montmorillonites may lead to different levels of structural decomposition depending on individual resistance to acid attack of the initial minerals (Breen *et al.*, 1995). The final product of acid leaching of smectites is a hydrous amorphous silica phase (Komadel *et al.*, 1990). Sucha *et al.* (2001) found that the weathering of a montmorillonite under natural conditions results in the mineral dissolution and precipitation of amorphous SiO<sub>2</sub>, however, during the weathering of illite-smectite the dissolution was accompanied by appearance of smectite as a separate phase. The kaolinite on acid treatment releases preferentially the octahedral aluminium ions from the clay lattice and forms additional Al-OH and Si-OH bonds, without disturbing the mineral structure (Suraj *et al.*, 1998). During acid treatment of sepiolites the rearrangement of Si and Al atoms in the lattice occurs and the clay structure is progressively transformed into amorphous silica-alumina (Dekany *et al.*, 1999). Acid treatment of a palygorskite leads to the removal of the octahedral Mg and Al, and the formation of amorphous silica from the tetrahedral sheet. The silica obtained after the treatments maintains the fibrous morphology of the natural mineral (Suarez Barrios *et al.*, 1995). Myriam (1998) found that under acid treatment sepiolite is destroyed more rapidly than palygorskite because of its magnesian composition and larger size of structural microchannels. The acid attack progressively destructs the structure of a saponite by partial dissolution of the octahedral Mg cations, generating amorphous silica coming from the tetrahedral sheet (Suárez Barrios *et al.*, 2001). Kooyman *et al.* (1997) observed a progressive dealumination of various samples of synthetic ZSM-5 zeolites in mineral acids with increase in concentration, temperature, and duration of the treatment. However, at high Al content in solution the realumination of dealuminated zeolites was observed by Sano *et al.* (1999). Among various mineral acids employed, HCl solution was the most effective for the realumination. They observed no structural degradation of HZSM-5 zeolite crystals during the acid treatment and reinsertion of some non-framework aluminum in dealuminated HZSM-5 zeolites is into the framework. Natural low-silica zeolites (natrolite and thomsonite) were more reactive against acid than high-silica zeolites heulandite and stilbite. Surface-erosion of zeolite crystals was observed at low degree of acid degradation-dissolution by (Filippidis *et al.*, 1996).

Usually under alkali treatment the dissolution processes affect mineral lattices to the less extent, however formation of new mineral phases is a frequent phenomenon. Taubald *et al.* 2000 observed that X-ray diffraction of a smectite revealed no significant appearance or disappearance of diffraction peaks in an alkaline solution in column experiments. Higher salt concentration in the percolating fluid minored the evolution of pH. Rassineux *et al.* (2001) found that the reaction of a Wyoming-type bentonite with pH 13.5 solutions at 35 and 60°C for periods of 1 to 730 days did not alter stability of the octahedral sheet as well as the composition and the structure of the smectite layers. However the number of expandable layers increased after octahedral charge neutralization and the number of interlayers surrounded by two charged tetrahedral sheets increased with reaction time. The particle morphology changed from flakes to hexagonal shape. More pronounced structural changes of a bentonite were observed by Ruiz *et al.* (1997) who found that the laminar structure of the starting material was converted into spherical units of the zeolitic nature by alkaline treatment in distilled and seawater media. Bauer and Velde (1999) observed that high molar KOH solutions changed the diffracting domain size of a smectite, which decreased in time, reflecting a change in crystal shape. The structure became more illite rich and the diffracting domain continued to decrease. Formation of a phillipsite from a bentonite at pH 11.7-12.6 was observed by de la Villa *et al.* (2001) in a series of closed-system hydrothermal tests at 35-90 degrees C. The chemistry of the equilibrium solutions, rather than the crystallization substrata, controlled the Si/Al atomic ratio and the type of zeolite formed. The decrease of Si/Al was noted at higher pH's. Illitization of a smectite in high pH hydrothermal environment was observed by Ylagan *et al.* (2000) and of a kaolin by Chermak and Rimstidt (1987). Baccouche *et al.* (1998) found that an interstratified illite-smectite treated with 1 to 5 mole dm<sup>-3</sup> NaOH solutions on reflux during 2 to 24 h formed zeolitic products. For 1 and 1.5 mole dm<sup>-3</sup> NaOH solutions zeolite Na-P1 was formed whereas for 2 to 5 mole dm<sup>-3</sup> alkaline solutions sodalite octahydrate zeolite was obtained. As a product of natural zeolites (clinoptilolite and mordenite) reaction with 2 mole dm<sup>-3</sup> NaOH solution at 103°C, zeolite Na-P was identified (Shin-Jyung Kang and Kazuhiko Egashira, 1997). During the reaction, a large amount of Si was dissolved into solution. Natural low-silica zeolites (natrolite and thomsonite) were more reactive against alkali as compared to the high-silica zeolites (heulandite and stilbite). Phase transformations in the base-treated low-silica zeolites to analcime were noted (Sano *et al.*, 1999).

Alterations of soil minerals with changes in pH are well seen from the XRD spectra that are presented in Fig. 7 (Jozefaciuk and Bowanko 2002). for selected minerals. Frequently the alkaline treatment leads to sharpening of the basal reflexes, which may be due to the dissolution of most irregular (amorphous) parts of

the crystal lattice (cleaning of the minerals). Taking into account high amount of silicon dissolved in alkaline media, a removal of outer silica sheets of the minerals can occur, as well. As a rule the acid treatment leads to much severe alteration of the crystal lattice of the minerals which is seen from lowering and broadening of the characteristic peaks on the spectra, indicating a decrease in the mineral lattice regularity. An increase in the diffraction intensity at very low angles can be due to the dispersion and amorphisation of the minerals.

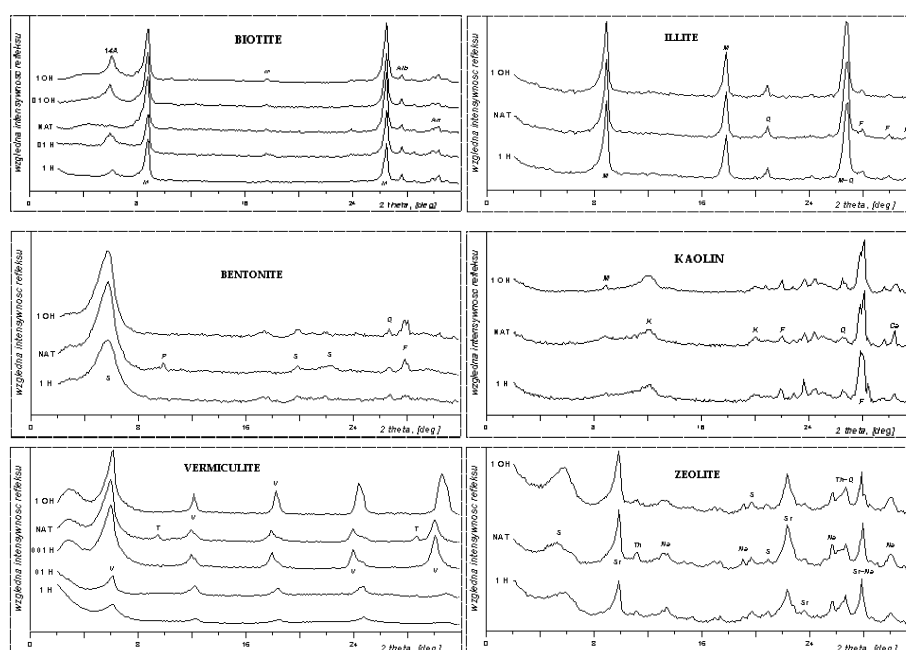


**Fig. 7.** XRD spectra of selected minerals before and after acid and alkaline treatment. Abbreviations: Ab-albite, An-anorthite, Ca-carbonates, F-feldspars, K-kaolinite, M-mica, 14A- 14 Angstroms peak, P-paragonite, Q-quartz, S-smectite, T-talc, Th-thomsonite, V-vermiculite, Na-natrolite i St-stilbite (zeolites). 0- natural mineral; 01H, 1H i 5H: 0.1, 1 i 5 mol dm<sup>-3</sup> HCl treatments.

The XRD spectra for the bentonite can indicate that the destruction of the smectite crystallites during acid attack goes through interlamellar cations depletion and dissolution of the crystal lattice which leads to dispersion and amorphisation of the mineral. In the biotite after both treatments a new, 14 Å peak (2 theta ≈ 7 deg) arises, which is practically absent in the nontreated mineral, indicating a formation expanded lattice structures. Such structures formed in biotites

via nonexchangeable potassium depletion are accompanied by interlamellar expansion (Fanning *et al.*, 1989). Formation of similar structures in weathered biotite flakes was found also by electron-microscopic observations (Boyle *et al.*, 1967). Kaolin and illite seem to be most resistant on acid and alkali attack. The intensity of all basal XRD reflexes of the vermiculite decreased sharply under acid attack and the position of the peaks shifts, which can indicate that not only the octahedral but also the tetrahedral sheet undergoes severe alteration. The latter phenomenon can be also connected with high silicon dissolution. The presence of mobile octahedral Mg and FeII ions in vermiculite lattice is a reason of its easy destruction on oxides. The zeolite showed is not a pure mineral, however high amorphisation of its components is seen from the XRD spectra.

The effect of soil reaction on the composition of soil solid phase is a result of its complex influence on clay minerals, organic matter and amorphous compounds. Exemplary changes of the content of the amount of soil clay fraction and the amount of soil organic matter are shown in Fig. 8. This figure concerns upper 0-20 cm layers material of six Polish and three Korean soils of various of composition and typology. The soils were treated during six weeks with hydrochloric acid and/or sodium hydroxide at various pH values. In this figure, on the y-axis the ratio of the clay content in the treated sample to its content in the control sample is given. Similarly the forthcoming spider-like graphs were constructed.

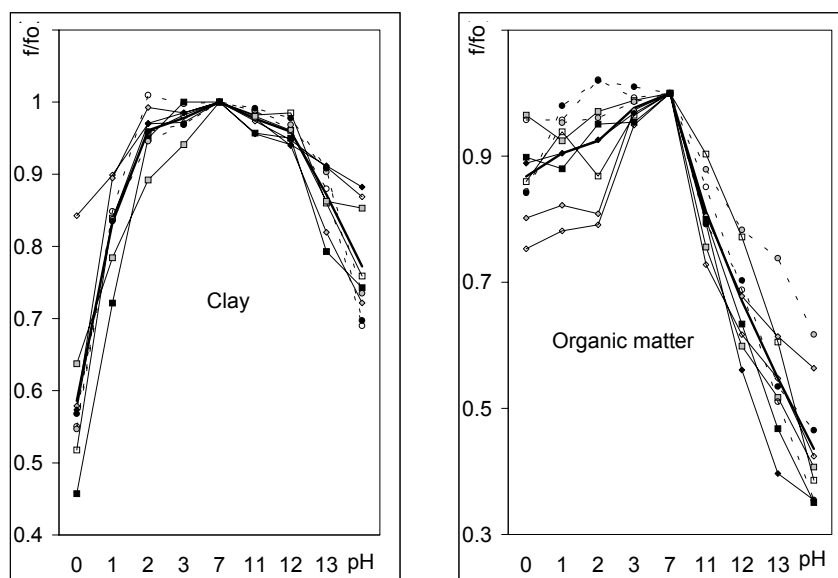


**Fig. 8.** Effect of pH on the relative content of clay fraction (left) and of organic matter (right) in selected soils.

During acid and alkaline treatments the content of clay fraction decreases for all soils. The amount of the clay decreases more under acidic than under alkaline conditions indicating more aggressive influence of protons on soil mineral components dissolution. The organic soil material is much easier removed from the soil under alkaline conditions. This is due to an increase of a negative charge of organic material with the rise of pH, accompanied by an increase of the electrostatic repulsion forces and so the peptization ability with the rise of pH.

The XRD spectra of the clay fraction separated from exemplary natural and at acid and alkali treated soils are shown in Fig. 9. As a rule the acid treatment leads to much severe alteration of the crystal lattice which is seen from lowering and broadening of the characteristic peaks on the spectra, indicating a decrease in the mineral lattice regularity.

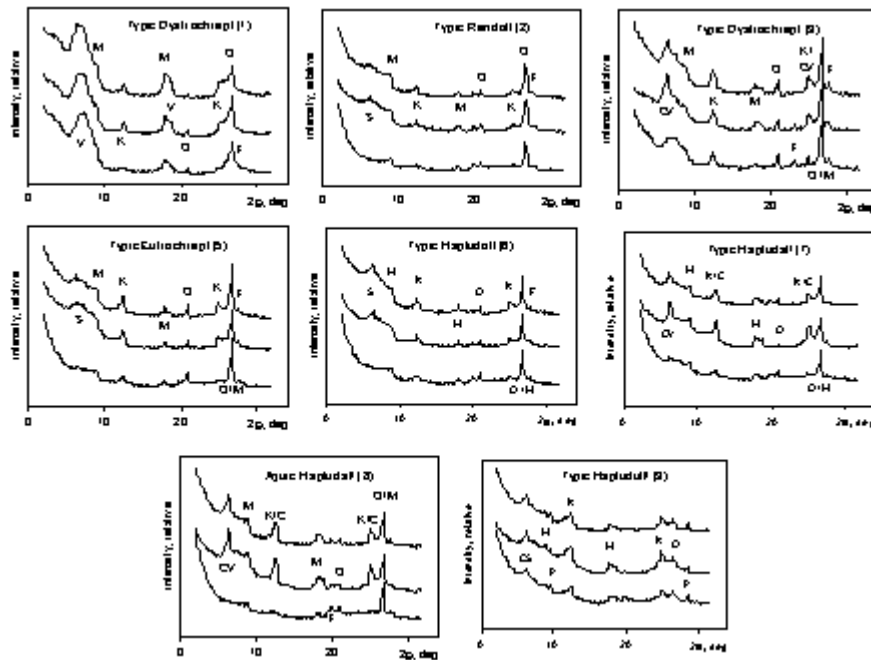


**Fig. 9.** X-ray diffraction patterns for clay fraction separated from natural soils (curves in the middle) and soils treated at maximum acid (lower curves) or base (upper curves) concentrations. Abbreviations within the figure denote: CS-chloritized smectite, CV-chloritized vermiculite, F-feldspars, K-kaolinite, M-mica(illite), P-paragonite, Q-quartz, S-smectite, V-vermiculite.

Soil smectites are most sensitive on acid attack. In all illustrated soils the XRD peaks of smectite disappears. However, the chloritized smectite present in the Typic Hapludult soil persisted the 1N HCl treatment. A vermiculite in the Typic Dystrochrept soil seems to be extremely resistant on acid attack, which can be due to long time influence of low pH on this soil under natural conditions. The chloritized vermiculite in soils is very sensitive on acid attack and slightly on the alkali one. Kaolin and illite (mica) seem to be most resistant on acid and alkali attack. No disturbance of the kaolin structure is observed frequently under acid activation (Suraj *et al.* 1998), as well. However the kaolinite-chlorite XRD peak in the Aquic Hapludalf soil disappears after acid treatment. Individual and different levels of structural decomposition observed for the studied soil minerals may depend on the degree of their crystallinity, particle size, size of structural micro-channels as well as on the content of the lattice substitution ions. In all acidified soils high dispersion and amorphisation of the mineral phases occurs as this is seen from an increase in the diffraction intensity at the lowest angles. This may be due also to the occurrence of a hydrous amorphous silica phase, as far as this is the final product of acid leaching of aluminosilicate minerals (Dekany *et al.* 1999, Komadel *et al.* 1990, Madejova *et al.* 1988, Suarez Barrios *et al.* 1995, 2001, Sucha *et al.* 2001).

Average amounts of selected elements dissolved during acid and alkali treatments of selected soils are shown in Fig. 10. Acid treatment is more aggressive than alkaline one. Twice as much aluminum dissolves under maximum acidic than under maximum alkaline treatment, whereas few times more silica dissolves under alkaline conditions. Iron dissolves practically only in acidic media. Much more Ca, Mg and K are present in acid than in alkaline treatment solutions. These elements may, at least partially, come from the acidic destruction of the octahedral sheets of the permanent charge clay minerals. Rather high amount of potassium was dissolved at maximum NaOH treatment, which may come from nonexchangeable potassium depletion from micaeous soil minerals.

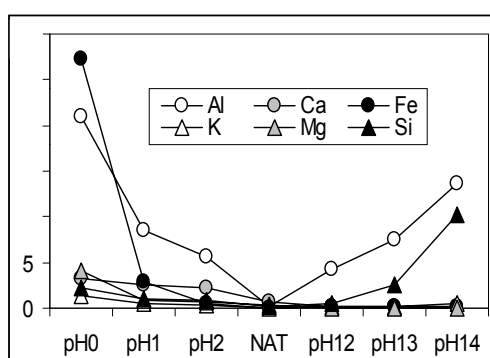


**Fig.10.** Dissolution of selected elements from acidified and alkalized soils (average values for 9 soils)

## CHAPTER 8.

### SURFACE CHARGE

G. JÓZEFACIUK

Except of organogenic elements (carbon, hydrogen and oxygen), being the basic tissue material, the plants need also mineral elements taken from soils via their root system. Mineral elements may occur in soils as soluble salts in the soil solution, as hardly soluble precipitates, and as ions electrostatically bound to charged soil components.

Electric charge of soil components may be divided onto two general types: permanent charge and variable charge (Mc Bride 1989).

The permanent charge occurs mainly in clay minerals. It originates from imperfections of the crystal structure of the minerals (Mc Bride 1976). The most frequent phenomenon responsible for these imperfections is that higher valence cations in the crystal lattice (for example silicon in the silica layers) are substituted by lower valence cations (for example by aluminum) during the genetic processes. This results in the “unsaturation” of oxygen bonds and excess of the negative charge. The substituting cation should be of similar size to this being replaced, therefore this process is called isomorphous substitution, which is schematically presented in Fig. 74.

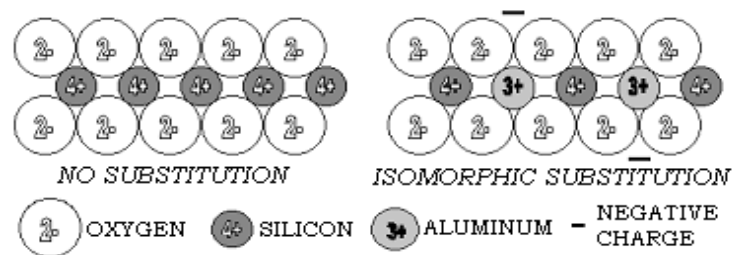
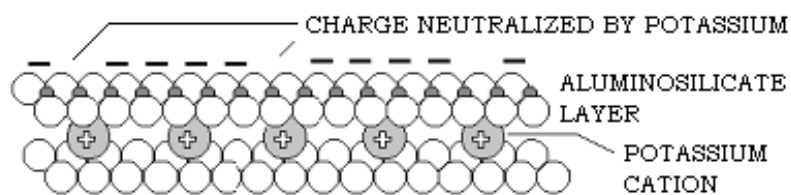


Fig. 74. Isomorphous substitution of silicon by aluminum in the clay lattice.

Frequently the summarical amount of the charge resulting from the isomorphous substitution is not equal to the permanent charge of the mineral. For example a part of the lattice charge may be neutralized by specifically bound cations inside the mineral particle structure (i.e. in the spaces between several subsequent struc-

tural layers – interlayers), as this frequently occurs in illites (binding of potassium cations) and is schematically presented in Fig. 75.



*Fig. 75. Blocking of permanent charge by interlayer cations.*

The amount of permanent charge is characteristic for the mineral and conditions of its genesis. For most frequently occurring clay minerals this charge amounts from a few (kaolin group) by few tens (mica group – illites) to hundreds (smectites, zeolites) of centimoles per kilogram of the mineral (1 centimole = 965 Coulombs =  $6,023 \times 10^{21}$  elementary charges).

Permanent charge minerals dominate in mineral soils of the temperate climatic zone, therefore soils of these regions are called permanent charge soils.

Variable charge occurs on surfaces of most soil solid phase constituents: organic matter, aluminum, iron and silicon oxides, edges of clay minerals (on their basal surfaces the permanent charge is exposed) and many more. Contrary to the permanent charge, the magnitude of the variable charge depends on the composition of the soil solution (pH, concentration, ionic composition). The variable charge originates from dissociation and association of hydrogen ions (protons) from/to surface functional groups.

On surfaces of soil organic matter functional groups of acidic character dominate. An increase of the pH of the soil solution leads to the neutralization of the active protons of these groups thus they become negatively charged, forming negative surface charge (Bloom 1979).

Acidic functional groups of soil organic matter have very different acidic strength, depending not only on the kind of the group, but also on its locality. Surface groups of stronger acidic character (similarly as stronger acids) are neutralized at lower pH values. The weaker acidic is the group, its neutralization requires higher pH value. Therefore the higher is the soil pH, the larger surface charge occurs on organic matter surfaces.

These acidic surface groups, which are located closely to each other, create common electric field surrounding these groups and within this field their protons become delocalized (proximity effect). The delocalized protons behave as strong

acids and so the neighboring groups are strongly acidic and the soil organic matter has some negative charge even at very low pH values. So, the number and acidic strength (dissociation constants) of functional groups constitute a primary characteristics of soil organic matter (Stevenson, 1982; Sposito, 1989). Above processes are illustrated in Fig. 76.

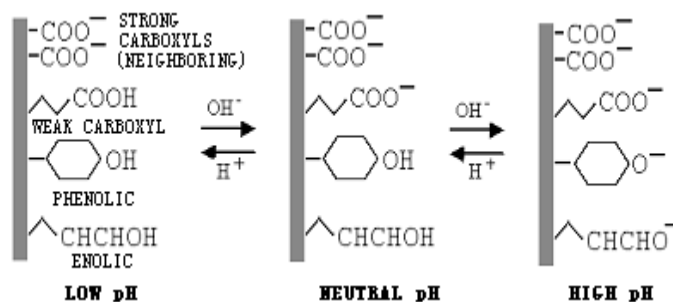


*Fig. 76. Formation of negative variable charge on soil organic matter.*

Depending on soil pH value, surfaces of some mineral soil constituents can have either positive, zero or negative charge. In relatively low pH range, surface hydroxylic groups (SURFACE-OH) of these constituents may associate protons from soil solution via hydrogen bonds thus the surface becomes positively charged. In relatively high pH range, these surface hydroxyls may also undergo acidic dissociation, resulting in formation of negative charge. At a defined pH value the surface hydroxyls neither associate the protons from the solution nor dissociate their own ones and the surface has no charge. The latter value of pH is called point of zero charge (PZC). One can imagine the above reactions are similar to these illustrated in Fig. 77 for aluminum (or iron) oxide.



*Fig. 77. Formation of variable charge on surface of aluminum and iron oxides.*

The point of zero charge for some most frequently occurring soil constituents is: 3-4 for silicon oxides, 5-8 for iron oxides, 6-10 for aluminum oxides. The PZC of edge surfaces of clay minerals is most frequently around 8.2.

Variable charged mineral constituents, mainly oxides and hydroxides of iron, aluminum and silicon and mixed aluminum-silicon oxides – allophanes and imogolites occur in large amounts in highly weathered soils of humid tropics and subtropics, therefore soils of these climatic zones are called variable charge soils. The charged surface attracts ions of opposite sign of charge (counterions) from soil solution and repels ions of the same sign (coions). The tendency of the whole system to reach minimum potential energy would request the counterions to locate just near the surface and the coions to be repelled far away. The simultaneous tendency to reach maximum dissipation (entropy) would request a uniform distribution of both counter and coions in the solution. Thus, in the system, the potential energy factor is responsible for accumulation of most counterions close to the surface and repulsion of the coions while the entropy factor causes diffusion of some counterions out from the surface and of coions to the surface. As a result of these two opposite tendencies, the specific distribution of the ions near the surface occurs which meets the conditions of minimum free enthalpy. The ions balancing surface charge together with the charged surface are called diffuse double layer (DDL). The schematic build-up of this layer is shown in Fig. 78., wherein only counterions distribution is depicted.

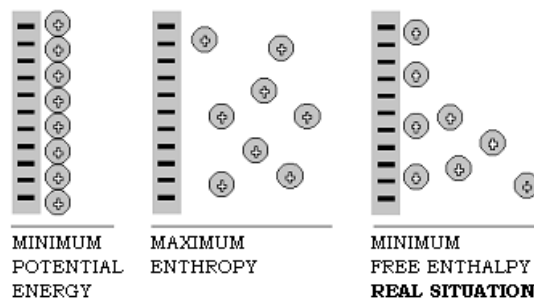


*Fig. 78. Distribution of counterions near negatively charged surface.*

Prevalence of negatively charged surfaces in temperate climatic zone soils causes that they bound mainly cations. And so the troubles with anionic fertilization may arise. For example the negatively charged nitrate anions are repelled to the solution and they are easily washed out from the soil with the rainwater. Therefore this is better to apply the nitrate fertilizers in a few doses rather than in

a single one, or to use foliar application. In mineral soils of humid tropics, having usually lower pH than the PZC, the deficit of cationic nutrients is a frequent phenomenon.

The counterions present in the DDL, as bound to the surface with rather low energies via electrostatic forces, may be easily exchanged with other ions being actually in an excess in soil solution as soluble salts. This process is called ion exchange and is schematically presented in Fig. 79. The formal boundary between the DDL and the bulk solution is drawn as a dashed vertical line.

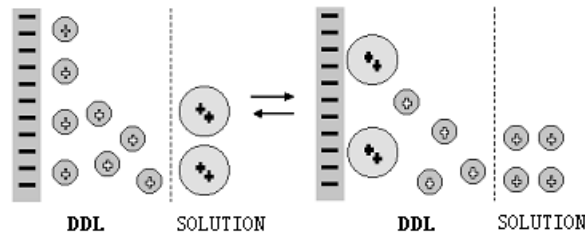


*Fig. 79. Schematic view on cation exchange.*

The fundamental Guy-Chapmann formula for surface charge- electrolyte concentration- electrical potential relationship is (Singh and Uehara, 1986):

$$\sigma = (2c\varepsilon RT/\pi)^{1/2} \sinh[zF\Psi_0/(2RT)], \quad (39)$$

where  $\sigma$  is the diffuse layer charge,  $\varepsilon$  is the dielectric constant of the medium and  $\Psi_0$  is the surface potential. For constant charge soil components ( $\sigma =$  lattice charge), the rise in concentration and/or in counterion valence leads to the drop of surface potential. For variable charge- constant potential components, the surface potential is constant at a given pH:

$$\Psi_0 = 2.303RT/F (\text{pH}_0 - \text{pH}), \quad (40)$$

where  $\text{pH}_0$  is the point of zero charge (PZC). Thus, for such components, the increase of salt concentration and/or counterion valence leads to the increase of surface charge by the dissociation (above PZC) and/or association (below PZC) of the potential determining ions.

The Guy-Chapman theory predicts also that the ratio of ions of the higher valence to these of the lower valence is higher near the surface than in the bulk solution. When the surface potential drops to zero, this ratio approaches this in the bulk solution (Bolt, 1982).

The higher is the charge of the counterion and the higher is its mass, the higher is the force of its binding in the DDL and so this ion is more difficult to be

exchanged by other ions. Therefore acidic soils may lose their ability to bind nutrient cations: trivalent aluminum cations or polymeric aluminum cations of large charge and mass may be so strongly bound that the soil charge becomes almost totally blocked. Deblocking of soil surface charge and renovation of exchange properties of the soil requires neutralization of aluminum and its precipitation as oxides, which can be performed by liming.

Cations adsorbed in the DDL (cations of soil exchange complex) are easily taken by plants. To fulfill the condition of an electric neutrality of the system, the plant should release the equivalent amount of cations to the soil. These ions are hydrogen ions, because the plant can not produce the other ones. This is one of the important mechanisms of soil acidification, and is more pronounced in agricultural areas from which the soil nutrients are removed from soils together with the taken biomass. Therefore the crops need the mineral nutrients supply. In natural environments the cations taken from soils, or at least their large part, may return to the soil after decomposition of the died plants. From this reason this is advantageous to leave the crop residues in the field after harvesting.

## **MEASURE OF SURFACE CHARGE**

Any method of soil exchange capacity estimates soil surface charge at the conditions of the experimental procedure. Anion exchange capacity (AEC) is thus equivalent to the amount of soil positive charge whereas the cation exchange capacity (CEC) to the amount of the negative charge. A number of methods have been introduced to estimate the CEC of soils. The most popular are measurements of ion exchange in salt and buffer solutions, exchange acidity of soil homoionic hydrogen forms, cation activities with ion-selective electrodes, isotopic exchange, or potentiometric titration (van Reeuwijk, 1993). In general the CEC value depends on the measuring conditions e.g. the kind and concentration of exchange cation, pH, equilibration time etc.

Since the above methods are well known, we mention here a relatively new and simple electrokinetic technique called particle-charge detection (PCD) (Gerdes, 1966). The principle of the experiment is based on the sample titration with a charge-compensating polyelectrolyte (of the opposite charge sign than this of the surface) and a simultaneous observation of a streaming current (electric current caused by a movement of charged particle in the liquid medium). During addition of increasing amounts of the polyelectrolyte the titration curves form a quasi plateau followed by a steep decrease of the signal across the isoelectric point (IEP), which marks the end of the titration. The PCD signal can only be used in combination with polyelectrolyte titration to detect the sign of particle charge and to indicate the point of zero charge. Polyelectrolytes used for charge

titration should have functional groups with strong acid or strong base character, to provide nearly completely dissociated counterions. Whereas surface charge determined by acid-base titration or exchange techniques measures the amount of total charge, electrokinetic techniques furnish information about the mobile and weakly bound fraction of the counterions Hunter (1993). This fraction, which is also called the electrokinetic charge or the effective particle charge, plays an important role in electrostatic interaction among charged particles and hence affects the stability of colloidal suspensions (James and Parks, 1982).

For negatively charged samples with exclusively strong acid functional groups, an excellent agreement was obtained between cation-exchange capacity and the charge measured by PCD over a wide pH range. For samples with additional carboxyl groups, the PCD charge was significantly lower than the total charge calculated from cation-exchange results. The good agreement between the titrated PCD charge of negatively charged colloids and the cation exchange capacity, for systems with strong acid functional groups, demonstrates that the PCD technique is capable of accurately detecting the dissociated charge. Differences between total charge and PCD charge are indicative of the presence of an immobile counterion layer, such as a Stern layer. PCD charge measurements are, therefore, an excellent tool for investigating interactions of ions with charged surfaces and the structure of electrolyte interfacial regions.

The upper limit of the particle size for which the charge can be measured in the PCD is around 20 (particle sedimentation during the titration can affect the reproducibility of the results. Assuming that electrokinetic effects result from the replacement of dissociated counterions, the relationship between total charge and PCD charge represents the extent of dissociation.

## **HETEROGENEITY OF SURFACE CHARGE**

Both permanent and variable charge sites on mineral surfaces are heterogeneous. Petit *et al.* (1999) basing on the IR spectra of  $\text{NH}_4^+$ -saturated and KBr-exchanged smectites found that the layer charge have permanent low charge density and/or variable charge sites whereas the interlayers were characterized by high permanent charge density. Different proton interacting sites were found by Janek and Lagaly (2001) on freshly H-saturated and autotransformed smectites using potentiometric titration data. Sites with  $pK$  values of  $\sim 2.8$  were assigned to protons exchanged for sodium ions and of  $\sim 11.3$  to deprotonisation of silanol groups. Hydrated aluminum ions in freshly proton-saturated dispersions were characterized by  $pK \sim 6$ . This group of weakly acidic centers also included oligomeric hydroxoaluminum cations because the amount of these sites increased during autotransformation and was accompanied by a shift in  $pK$  to  $\sim 5.5$ . Autotransformation removed all strongly acidic sites with  $pK \sim 2.8$ . A specific form of

Al oxyhydroxide with amphoteric properties, having two constants of deprotonation  $K_1=10^{-5}$  and  $K_2=0.32 \cdot 10^{-6}$  were found by Mrad *et al.* (1997) as the product of  $Al_{13}$  polycation transformation in aluminium intercalated montmorillonite. Inhomogeneity of an illite charge indicating the existence of a multiplicity of energetically distinct surface types was found by Sinitsyn *et al.* (2000) basing on potentiometric titration. These surface sites included amphoteric silanol and aluminol groups, basal planar surfaces, and "frayed edges". The frayed edges are observed only in low ionic strength solutions.

Back titration procedure (Duquette and Hendershot 1993, Józefaciuk and Shin 1996a, Nederlof *et al.*, 1991, 1993) has been widely used for characterizing surface charge heterogeneity of soils and its constituents. The titration is performed separately for the suspension and for its equilibrium solution (supernatant), starting from low pH upwards. The idea of this method is based on the assumption that the hydroxylic ions of the base added to the suspension are consumed by acids present in the equilibrium solution and by acidic functional groups present on the surface of the suspended solid. Therefore after subtraction of the titration curve of the equilibrium solution from this of the whole suspension, one obtains the titration curve of the solid.

The solid phase titration curve i.e. an amount (mole) of base consumed by the suspension,  $N_{susp}$ , minus the amount consumed by the supernatant,  $N_{sol}$ , is treated as an increase of the variable surface charge of the solid phase,  $\Delta Q_V(\text{pH})$ , during the titration:

$$\Delta Q_V(\text{pH}) = N_{susp} - N_{sol}. \quad (41)$$

The  $\Delta Q_V(\text{pH})$  accounts for an increase of negative charge and a decrease of positive charge.

The variable charge vs. pH dependence can be interpreted in terms of proton dissociation/association of surface functional groups using site-heterogeneity theory (De Wit *et al.*, 1990; Jozefaciuk and Shin, 1996b; Koopal *et al.*, 1987, Van Riemsdijk *et al.* 1987), that is briefly outlined below.

Assuming that the variable charge origins from dissociation of surface acidic groups of kind  $i$ :  $SOH_i = SO^-_i + H_s^+$ , ( $H_s$  denotes a proton in a plane of dissociation) and the (intrinsic) dissociation constants  $K_i$ :

$$K_i = [SO^-_i][H_s^+]/[SOH_i], \quad (42)$$

where the brackets denote surface activities, the variable charge at a given pH is:

$$Q_V(\text{pH}) = \sum_{i=1}^n [SO^-_i](\text{pH}) = \sum_{i=1}^n N_i \alpha_i(K_i, \text{pH}_s), \quad (43)$$

where  $\alpha_i(K_i, \text{pH}_s) = [SO^-_i]/[SOH_i]$  is the degree of ionization of groups kind  $i$  and  $N_i = [SOH_i]$  is their amount. For any pH during the titration:

$$Q_V(\text{pH})/N_t = \alpha(\text{pH}) = \sum_{i=1}^n \alpha_i(K_i, \text{pH}_s) N_i/N_t = \sum_{i=1}^n \alpha_i(K_i, \text{pH}_s) f(K_i), \quad (44)$$

where  $N_t$  is the total amount of surface groups and  $f(K_i) = N_i/N_t$  is a fraction of  $i$ -th groups. Using condensation approximation (Nederlof *et al.* 1993) the  $f(K_i)$  values are:

$$f(K_i) = 1/N_t \Delta Q_V(\text{pH})/\Delta K_i; \quad K_i = [\text{H}_s^+], \quad (45)$$

and in logarithmic scale:

$$f(\text{p}K_i) = 1/N_t \Delta Q_V(\text{pH})/\Delta \text{p}K_i; \quad \text{p}K_i = \text{pH}_s. \quad (46)$$

The distribution function of surface dissociation constants, i.e.  $f(K_i)$  vs.  $K_i$  dependence, can be calculated knowing both surface protons activity ( $\text{pH}_s$ ) and  $N_t$  values. Soil components, as well as plant root surfaces may have different shapes and different charges thus may vary in surface potential values. For  $\text{pH}_s$  (and  $K_i$ ) calculations, basing on the diffuse double layer theory, a single potential value spread uniformly over all surfaces of the same shape is a common assumption, which seems not to be valid in the case of soils and plants. Also, there still exist much controversies on the application of the DDL theory to surface chemistry (Mc Bride, 1997). Therefore, the surface proton activity is replaced by the solution activity and  $N_t$  is taken as  $N_{max}$  = maximal value of  $(N_{susp} - N_{sol})$  measured within the experimental window and, instead of the intrinsic, the distribution functions of apparent surface dissociation constants,  $K_{app}$ , are determined:

$$f(\text{p}K_{app,i}) = 1/N_{max} \Delta Q_V(\text{pH})/\Delta \text{p}K_{app}; \quad \text{p}K_{app} = \text{pH}. \quad (47)$$

The average value of  $\text{p}K_{app}$ ,  $\text{p}K_{app,av}$ , is calculated as:

$$\text{p}K_{app,av} = \sum_{i=1}^n \text{p}K_{i,app} f_i(\text{p}K_{app}), \quad (48)$$

which is direct measure of the average energy of the proton binding.

Having the variable charge vs. pH dependence one can find the relation of actual surface charge,  $Q_A$ , vs. pH. To do this the  $Q_V(\text{pH})$  curves are shifted against y-axis to meet the actual charge value at any pH e.g. a cation exchange capacity of the studied solid, estimated at the same ionic strength, at which the titration is performed. One should select a higher pH value to diminish eventual occurrence of positive surface charge that is not determined during the CEC measurements.

The titration curve of the soil, may include free acidic ions adsorbed on the surface (exchange acidity), which are not surface acidic groups. Therefore there exist a danger of interpretation of exchange acidity in terms of variable charge. To avoid the latter prior to the titration, the soil suspensions should be exchange acidity depleted. This can be done by standard neutral salt washing.

Usually the deviation of the titration curves is lower for the suspensions (around 5%) and higher for the supernatants (around 15%). If washing of the solid and the pretreatment for the titration are properly performed, the titration curves of the supernatants are similar to a titration curve of 1 mole dm<sup>-3</sup> NaCl pH=3 solution, which indicates also that the dissolution of the solid phase under experimental conditions is negligible. This is important to note that in the above procedure the equilibrium conditions are not reached, so the titration curves can be used rather for comparative purposes. 24 hours equilibrium titration of a soil consumes up to twice as much titer as the continuous titration described here and a high dissolution of the solid phase occurs as is indicated by high deviation of the titration curves of the supernatants from the titration curve of NaCl solution (Jozefaciuk and Shin, 1996a).

Applying constant and high concentration of neutral salt during titration has a few advantages. It minimizes adsorption of exchange protons at low initial pH value and their further titration (replacing exchange protons by neutral salt cations), dilution effects (changes of variable charge with salt concentration), dissolution of solid phase, and allows for a better development of variable surface charge (surface groups dissociation is less hindered by electrostatic effects at high ionic strengths).

## SURFACE CHARGE IN SOILS AND SOIL PROCESSES

The total (actual) charge vs. pH dependence for some exemplary soil minerals is illustrated in Fig. 80.

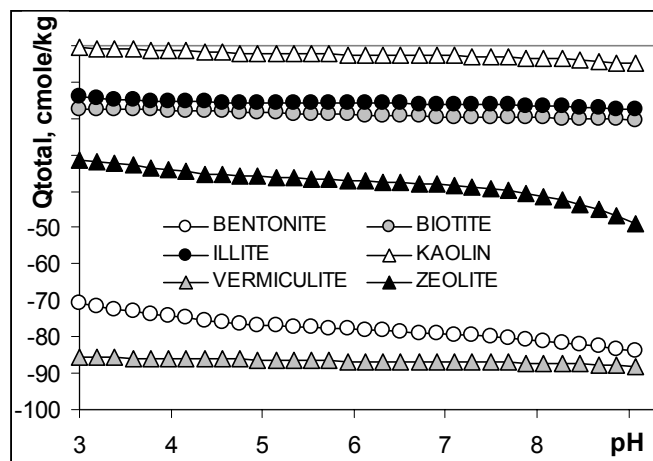
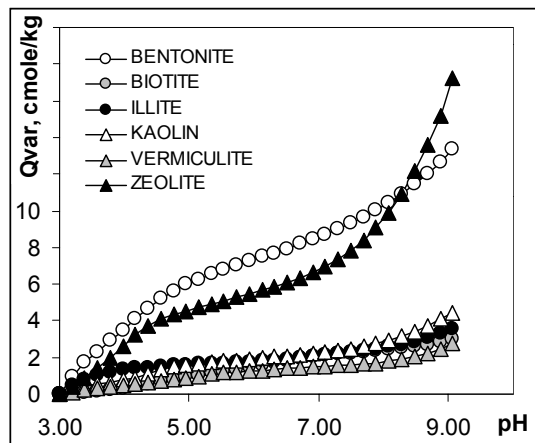


Fig. 80. Total charge vs. pH dependence for exemplary soil minerals.

The amount of total surface charge for the minerals seems to be more or less constant regardless the pH of the environment. As far as the permanent lattice charge does not depend on pH, the deviations of the above curves from parallel straight lines is caused by variations of the variable charge with pH. Figure 81 illustrates the latter dependence (in some magnification, because the amount of variable charge on minerals is usually much smaller than the permanent one).



**Fig. 81.** Variable charge vs. pH dependence for exemplary soil minerals.

The distribution functions of dissociation constants of surface functional groups of various acidic character, dissociation of which is responsible for variable charge of minerals is shown in Fig. 82.

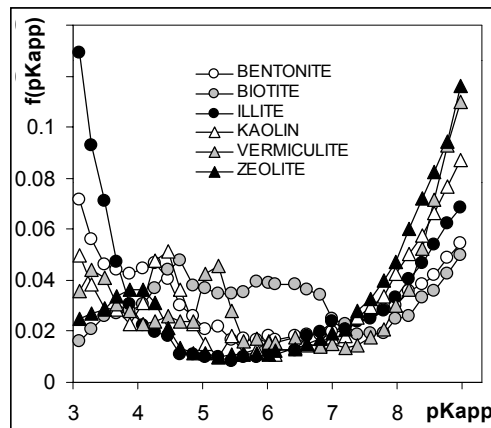


**Fig. 82.** Surface dissociation constant distributions for exemplary soil minerals.

This function for bentonite is u-shaped and contains a peak developed around pH 4.3. Similar shape is observed for kaolin, however the relative amounts of weakly acidic sites (high  $pK_{app}$  values) is higher than of strongly acidic sites (low  $pK_{app}$  values). The u-shaped function with higher amount of strongly acidic sites is observed also for illite, however the peak at  $pK_{app} \approx 4$  is lacking. Vermiculite and zeolite appear to have low amount of strongly acidic surface sites. The  $pK_{app} \approx 4$  peak occurs for the zeolite. Biotite seems to have most heterogeneous surface, however for this mineral, and also for the vermiculite. The peaks observed at  $pK_{app} \approx 4$  may come from positively charged aluminum hydroxyls of mineral edges having the PZC of around 7.5 (Parks, 1965) as well as from metal oxide impurities. The aluminum and iron oxides (especially hydrated ones) have high isoelectric points, up to 10 for Al and 9 for Fe species (Parks 1965). A few pH units below the isoelectric point such surfaces can be almost totally charged thus developing most of the charge in rather narrow pH range, which leads to the occurrence of the peak on the distribution function. A peak coming from the negative surface charging should occur symmetrically above PZC, however this range is outside the experimental window applied.

While the general dependencies of the variable charge on pH for soils are similar to these for the minerals, the amount of variable charge is usually larger that is presented in the left panel in Fig. 83. This is due to high amount of variable charge amorphous components and organic matter present in soils. Typical distribution functions of surface dissociation constants for soils are presented in the right panel of Fig. 83. In most cases the distribution functions are u-shaped (gray points), however for soils rich in iron or aluminum oxides, a peak in the above functions can occur (white points) between  $pK_{app}$  4-5 values.

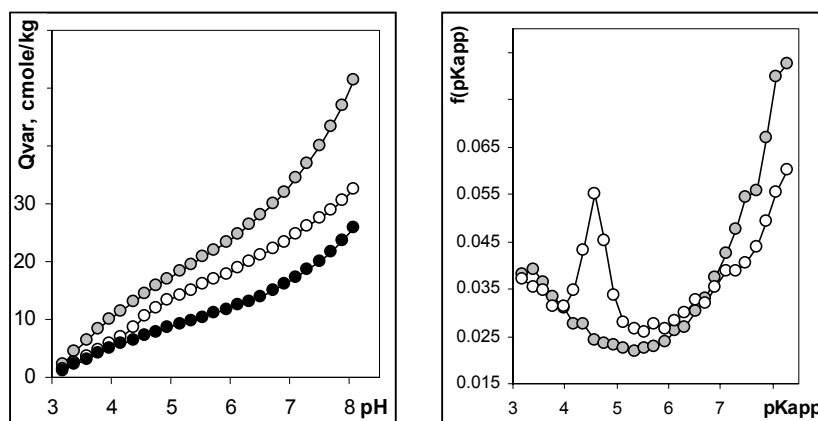


**Fig. 83.** Typical variable charge vs. pH dependence (left) and apparent surface dissociation constant distributions(right) for soils.

Surface charge, and particularly its variable part, is very sensitive in changes in soil reaction. Acid and alkali treatments lead to the decrease of the actual charge of the bentonite developed below  $\text{pH} \approx 7.5$ , which can be due to the decrease of the lattice charge. High amount of newly formed variable charge constituents (silicon oxides) in acid treated bentonite causes a sharp increase in the actual charge above  $\text{pH} \approx 7.5$ , tending to exceed the original mineral charge above  $\text{pH} \approx 9$ . Alkali treatment less affects the lattice charge of the bentonite, however the input of variable charge surfaces increases the actual charge at high pH values. Possibly positive charging of these surfaces causes a decrease of the actual charge at lower pH values. For kaolin and zeolite changes of the actual charge after all but extreme acid and alkali treatments are less pronounced. The illite is markedly affected only by the acid treatment of extreme concentration. 1 mole  $\text{dm}^{-3}$  and 5 mole  $\text{dm}^{-3}$  NaOH treated kaolin and 5 mole  $\text{dm}^{-3}$  NaOH treated zeolite a positive actual charge appears below pH c.a. 4.3 and c.a. 3.7, respectively. In vermiculite the lattice charge seems to decrease consecutively with increase of both treatments concentrations with the exception of 01H sample. In the latter case acid treatment of the smallest concentration may dissolve some charge-blocking species as e.g. Al-polycations present in the interlayers. The variable charge on vermiculite seems to occur only in acid treated samples, as far as the actual charge curves of alkali treated samples are roughly parallel to each other. The lack of the variable charge constituents in destruction products of the alkali treated vermiculite may indicate that these products are coarse and the finely dispersed ones were dissolved. A sharp increase of the actual charge is observed for the biotite after all treatments, opposite to the behavior of the other minerals. This should be due to the lattice and not to variable charge increase, because charge-pH curves after treatments are parallel also. The above phenomenon may be caused by a formation of expanded lattice smectite-like ( $14\text{\AA}$ ) structures in the studied biotite, as this was seen from the XRD spectra (Jozefaciuk and Bowanko 2002). The expanded spaces are available for exchange ions.

The actual charge results from the sum of permanent (lattice) charge and the variable charge. Acid treatment leads in general to a production of higher amounts of variable surface charge than the alkali treatment of the same concentration, which is presented in Fig. 84. This figure shows the ratio of the variable charge of the treated mineral to this of the control sample.

The acid treatment is more aggressive as this forms more variably charged destruction products. Vermiculite and zeolite produce the highest amounts of variable charge after acid treatment. Zeolite and kaolin are most affected by alkali treatment.

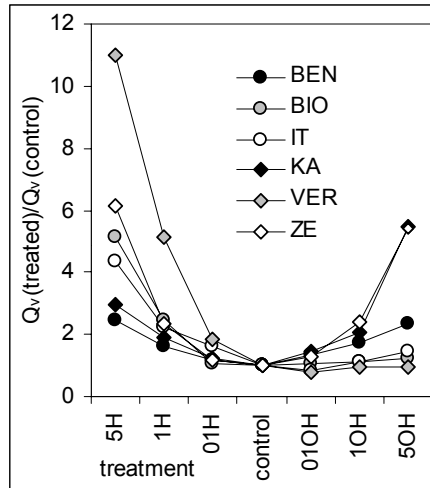


**Fig. 84.** Changes in the amount of variable charge under acid (H) and alkali (OH) treatment of selected soil minerals. On x-axis the treatment concentration is shown.

Effect of the treatments on the permanent charge is shown in Fig. 3, constructed similarly as the Fig. 85. As a measure of the permanent charge, the total charge developed at pH 6.5 is taken, because this is least dependent on pH.

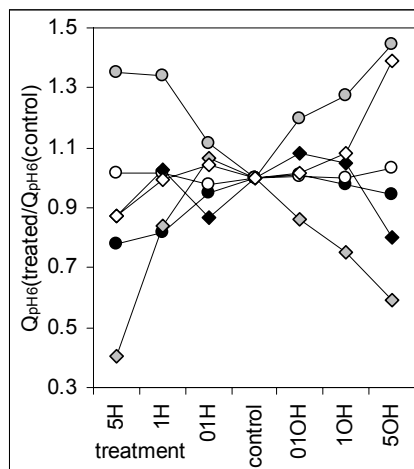


**Fig. 85.** Changes in the amount of permanent charge under acid (H) and alkali (OH) treatment of selected soil minerals. On x-axis the treatment concentration is shown.

Slight changes in permanent charge due to acid and alkali treatments are observed for illite. For other minerals but the biotite the lattice charge generally decreased. For biotite, an increase of the permanent charge after both treatments is observed. The decrease of the lattice charge may be connected with the destruction of the crystal lattice of the minerals (Rampazzo and Blum 1991, Warren *et al.* 1992). This should be a principal process at least under acid attack,

as far as, in contrast to the acidic treatments, the mineral lattice destruction is not evidenced by XRD spectra of alkali treated minerals (Jozefaciuk and Bowanko 2002). The increase of the permanent charge may be also connected with a removal of charge blocking species e.g. positively charged hydroxy-Al polymers present as surface coatings or located in interlayers (Keren, 1986) or the rearrangement of the mineral lattice (in the case of biotite).

After acid treatment an amount of slightly acidic surface functional groups increases for all minerals while an amount of stronger acidic groups decreases. However, Srasra and Trabelsi-Ayedi (2000) postulated generation of the strong acidic sites due to 3 M HCl boiling solution treatment of a glauconite. The partial dissolution of aluminum layers of the minerals (thus changing of the character of the edges) or Al and Fe oxide surface coatings, or impurities can be responsible for the decrease of the amount of surface groups of stronger acidic character. Note the decrease of the  $pK_{app} \approx 4$  peak in acid treated samples. The newly formed amorphous silica from the mineral lattice destruction may lead to an increase of the amount of slightly acidic surface groups after acid treatments. The isoelectric point of all kinds of silicon oxides is not higher than 3 (Parks, 1965). Its surface hydroxyls are not very reactive (Goates and Anderson, 1956) and so these compounds can develop high amounts of negative surface charge at high pH's (i.e. above 7.5 as observed in the present experiments).

Quite opposite tendencies in distributions of surface dissociation constants are found after alkaline treatment. Fraction of weakly acidic surface functional groups decreases in most of the minerals (silica dissolution) or increases only slightly. The amount of the surface groups of intermediate acidity, and particularly these forming  $pK_{app} \approx 4$  peaks, rises sharply with increasing concentration of alkali treatment. The mineral dissolution patterns (Jozefaciuk and Bowanko 2002), and especially high silicon dissolution in alkaline media, can indicate that strong alkali action removes outer silica sheets from mineral lattices leading to an exposure of aluminum (hydroxylated) layers thus increasing the positive surface charging at low pH's. A possibility that the rise of  $pK_{app} \approx 4$  peak reflects accumulation of iron oxides precipitated after destruction of mineral lattices due to low Fe solubility in alkaline media seems less probable because of no evidence of lattice destruction from XRD spectra. However, these spectra may remain unchanged if congruent dissolution of the lattice takes place. Iron oxides can accumulate also if finest mineral particles are dissolved. The disappearance of finest particles after alkali (and acid) treatment was observed visually in vermiculite and biotite which have the largest particles.

Average values of surface dissociation constants differ not much between soil minerals. The highest surface acidity is found for bentonite and illite and the lowest for zeolite. Figure 86 shows changes of average  $pK_{app}$  values under acid

and alkali treatments. An increase in  $pK_{app}$  after acid treatment indicates the weakening of overall surface acidity (or increase in proton binding forces). The decrease in surface acidity indicates that the minerals become less reactive towards charged and polar compounds and that the reaction products become more hydrophobic, which was also frequently observed from the decrease in water vapor adsorption energy (Jozefaciuk and Bowanko, 2002). The opposite phenomena occur after alkali treatment. Generally, the surfaces of the reaction products bind protons with less forces thus more polar surfaces are formed.

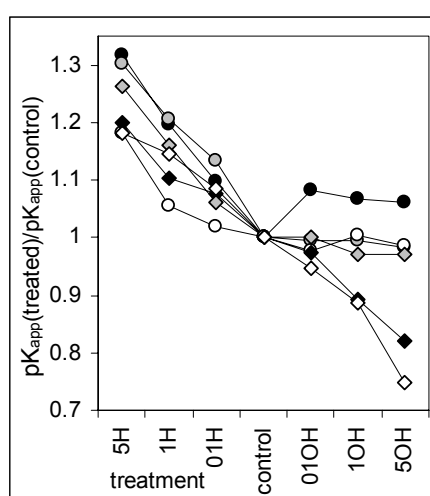


**Fig. 86.** Changes in average values of surface dissociation constants under acid (H) and alkali (OH) treatment of selected soil minerals. On x-axis the treatment concentration is shown.

Basing on surface areas measured from water vapor adsorption isotherms (Jozefaciuk and Bowanko, 2002) and the surface charge, variable and permanent surface charge densities of soil minerals can be calculated. The highest surface density of the permanent charge is observed for biotite. For bentonite, vermiculite and zeolite this is more than 2 times lower and for illite around 1.5 times lower. The lowest permanent charge density is found for kaolin. The highest variable charge density characterizes surface of the zeolite. Slightly lower values are noted for biotite, illite and kaolin. Due to its high surface area, rather low variable charge density occurs on bentonite and this is the smallest for vermiculite.

As compared to the original minerals, the variable charge density (Fig. 87) increases in general after both acid and alkali treatments. This may be due to the formation of amorphous phases of high variable charge as well as to hydration of mineral surfaces via breaking of Al-O-Al or Si-O-Si bonds and producing of ionizable hydroxyls. Changes of external surface build-up from silica to alumina in alkali treatments may be also responsible for increase in surface charge density,

as occurring principally on the same geometrical surface. However, the permanent surface charge density (net charge at pH=6.5 divided by the surface area) generally decreases indicating apparently that newly formed surfaces have no lattice charge (Fig. 88). Simultaneous decrease in the lattice charge makes the above effect more pronounced.

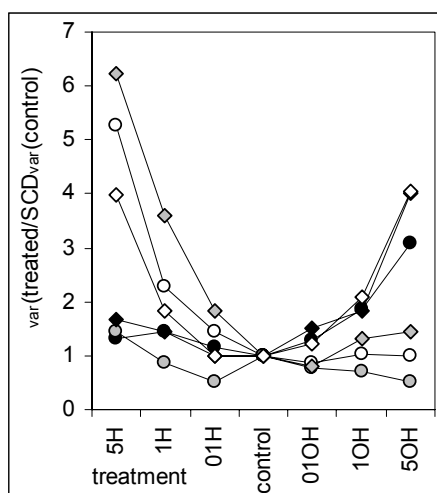


**Fig. 87.** Changes in variable surface charge density under acid (H) and alkali (OH) treatment of selected soil minerals. On x-axis the treatment concentration is shown.

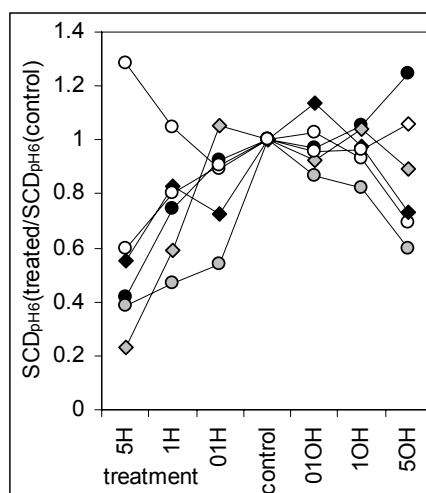


**Fig. 88.** Changes in permanent surface charge density under acid (H) and alkali (OH) treatment of selected soil minerals. On x-axis the treatment concentration is shown.

Both acidification and alkalization processes seriously affect surface charge properties of the minerals. Acid and alkali actions on minerals lead to different products. Various minerals react on acid and alkali with different intensities which is also observed under natural conditions (Frank and Gebhard 1991, Righi *et al.*, 1995). After acid attack formation of amorphous silica from the mineral lattice destruction and/or dissolution of aluminum layers (or coatings) seem to be responsible for the increase in variable charge of weak acidity in the reaction products. Occurrence of higher amount of variable charge of stronger acidity in alkali treated minerals was most probably connected with a depletion of outer silica sheets from mineral lattices leaving exposed alumina layers or with an accumulation of iron (hydr)oxides. Weakly acidic surfaces of the acid treated minerals would possibly better catalyze reaction of nonpolar compounds in nonpolar media whereas polar reactions can be better catalyzed by alkali treated

minerals. Production of higher amounts of variable charge in soil mineral phases may partially counteract the decrease in soil CEC due to changes in soil reaction.

Changes in surface charge properties are sensitive indicators of acidification and alkalization processes in soils. The amount of variable charge in exemplary soils after acid and alkali treatments is illustrated in Fig. 89. This figure shows the ratio of the variable charge after the treatments to this of the initial soils.

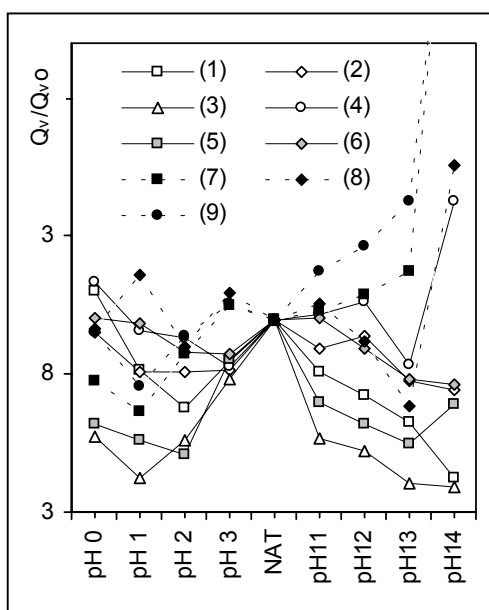


**Fig. 89.** Exemplary changes in the amount of variable charge under changes in soil pH in laboratory conditions. Dashed lines – clay rich soils, solid lines – clay poor soils.

The decrease of the variable charge in the acid and alkali treated soils (a drop in buffering properties and/or base neutralization capacity) is easy to explain by a dissolution of any variable charged soil component(s). An increase in the base consumption indicates a formation of new variable charge surfaces. These surfaces may occur e.g. on new soil components, being products of the destruction of crystalline mineral phases. The increase in variable charge of organic matter via breaking of multivalent cation complexes either by their replacement by protons at low pH's or by precipitation of hydroxides at high pH's may occur as well. Entering of aluminum into clay minerals interlayers during acidification may block a part of the permanent charge. This charge is unblocked by Al neutralization during subsequent titration that is equivalent to an apparent increase of the variable charge. As illustrated in Fig. 3, the amount of the variable charge decreases in general during acid treatments down to pH 2 or pH 1 ones, indicating that dissolution processes of variable charge components prevail over new-formation ones.

Further acidification generally leads to an increase in variable charge, indicating that formation of new variable charge components dominate. Changes in the variable charge under acid treatments should be attributed rather to mineral soil constituents, as far as during the acid treatments small changes in the organic matter content are noted. Alkalization leads to the decrease of variable charge of clay poor soils and one clay rich soil (No. 1), which seems to be due mostly to soil organic matter depletion. Organic matter carries most of variable charge in clay poor soils. Soil No. 1 contains high amount of organic matter thus its removal may govern the overall decrease in variable charge, as well. Other clay rich soils in general show the opposite trends, which indicates a new formation of mineral variable charge surfaces under alkaline conditions.

As compared to the natural soils, a relative number of functional groups of weakly acidic character ( $pK_{app} > 7$ ) increase with the acid treatment concentration increase. The increase in weakly acidic surfaces can reflect silica oxides accumulation. The isoelectric point of all kinds of silica oxide is not higher than 3 (Parks, 1965). Its surface hydroxyls are not very reactive (Goates and Anderson, 1956) and so these compounds can develop high amounts of negative surface charge at high pH's (i.e. above 7.5 as observed in the present experiments). Most probably, an entering of aluminum ions into the interlamellar spaces of clay minerals (leading also to the variable charge increase) did not occur during the acid treated soils. This phenomenon should lead to an increase in strong acidity, as this can be deduced from the studies of Sun Kou et al. (2000) who observed a dramatical increase in strong acidity after Al pillaring of a montmorillonite.

Changes in the relative amounts of surface functional groups in clay poor soils after alkali treatments exhibit generally similar trends as in acid treatments, however a decrease of strongly acidic groups is more pronounced. Strongly (carboxylic) and weakly (phenolic) acidic groups dominate in soil organic matter and the amount of moderately acidic groups is low thus the  $pK_{app}$  distribution function is U-shaped (Nederlof et al. 1993). The alkali-soluble fraction of organic matter has more fulvic character than the insoluble OM-fraction (Wilczynski et al. 1993) thus having higher charge per unit mass and more acidic character. Removal of soluble organic matter may explain that the fraction of strongly acidic groups remaining in the solid phase after alkali treatment is reduced to large extent. For clay rich soils the alkali treatment cause a significant increase in strongly acidic groups and a decrease in weakly acidic groups. The decrease of weakly acidic groups may reflect silica oxides dissolution (note high Si dissolution in alkaline media). During alkali treatments the amount of  $pK_{app} = 4.5$  groups in clay and iron rich soils increases sharply. If these groups occur on aluminum oxides, the  $pK_{app} = 4.5$  peak should decrease since aluminum oxides are alkali-soluble. However, cleaning of oxide surfaces from adsorbed organic matter can

lead to an increase of  $pK_{app}=4.5$  peak. The production of alkali insoluble iron oxides under alkaline dissolution of soil minerals may be also responsible for the observed behavior of  $pK_{app} = 4.5$  sites. Taking into account high amount of silica dissolved in alkaline media, one can postulate an additional mechanism leading to the increase of  $pK_{app} = 4.5$  sites: alkaline dissolution of the outer silica sheets of clay mineral lattices leaving aluminum oxide layers. Such surfaces should have high variable charge of rather high acidity, similar to aluminum oxides.

The weakening of the acidic character of the surfaces of the studied soils after acidic treatment is clearly seen from the increase of  $pK_{app,av}$  with the decrease of soil pH, shown in Fig. 90. Similar effects are noted after alkalization of clay poor soils (Nos 2, 3, 5, 6) and the opposite for the clay rich ones (Nos 1, 4, 7, 8, 9).

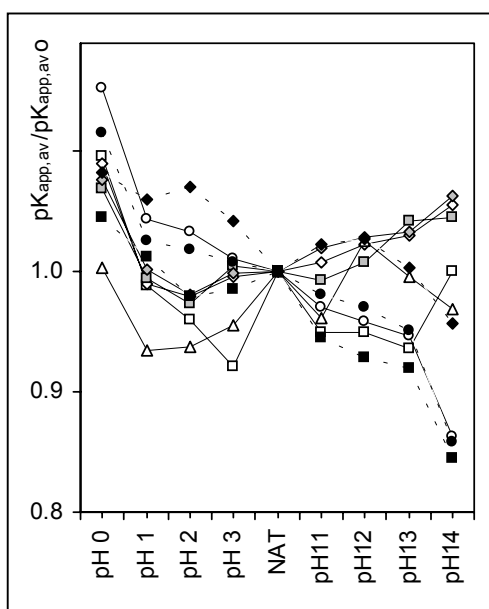


**Fig. 90.** Exemplary changes in the average value of surface dissociation constant under changes in soil pH in laboratory conditions. Dashed lines – clay rich soils, solid lines – clay poor soils.

Changes in soil variable charge properties in acidic and alkaline environments are composite effects of removal, formation and alteration of organic and mineral soil components.

## CHAPTER 7.

### FRactal CHARACTER OF SOIL

Z. SOKOŁOWSKA, G. JÓZEFACIUK

Fractal geometry has emerged as an analytical and mathematical tool for the description of complex structures, such as those, which have been found in a vast majority of porous media (Brakensiek et al. 1992, Perfect and Kay 1995). This geometry assumes that objects under study have similar features at different resolutions. The term "fractal" comes from a Latin word "*fractus*", which also means "flawed" or "fractional". According to a mathematical definition the fractal dimension of a given object is the formal fractional dimension of a space to which this object belongs. For example, if the fractal dimension of an object is 1.4, then the digit 1 means that this object is a "zig-zag" type branched line on a plane and the number 0.4 informs how "effectively" this line fills two-dimensional plane.

The theory of fractals is becoming more widely used for describing the structure of disordered media and the processes occurring in them (Mandelbrot, 1982; Pfeifer and Obert, 1990). Among the most frequently encountered examples of natural disordered media are soils. As a rule, these materials have a very complex, irregular structure, practically impossible to describe by the conventional methods of Euclidean geometry. One is thus compelled to seek new methods for describing the structure of soils and the application of fractals opens new possibilities for a more complete description of their structure and the processes that take place in them (Perfect and Kay, 1995; Anderson et al., 1998; Pachepsky et al., 2000).

An object displays fractal behavior if the general morphology of its irregularities depends on the magnification at which the object is observed. Fractals demonstrate specific dependencies of measurable properties on the scale measurements. The original definition of fractals regards them as geometrical constructs, i.e. as sets of points with a particular geometry, in a given space. The basic property of fractal objects is that they are geometrically similar to their parts.

The soil systems consist of solid (mass) and pore spaces. Solid may have fractal surfaces, i.e. boundaries separating mass and pore spaces are fractals. However, several physical properties of systems may depend not only on fractal character of surfaces, but also on the scaling behavior of the entire mass and the entire pore spaces. If mass and surface scale alike, the system is called a mass

fractal. If pore space and surface scale alike, it is called a pore fractal. Finally, if only the surface is fractal, the system is called a surface fractal.

Applications of fractals in soil science can be grouped into three broad categories (Perfect and Kay, 1995; Anderson et al., 1998): (i) description of soil physical properties; (ii) modeling soil physical processes; and (iii) qualification of soil spatial variability. In general, fractal models provide a framework within which several multidisciplinary studies of soil can be conducted complex relation between different soil processes can be understood, several examples of the application of fractal approaches in soil science are given in recent book, edited by Pachepsky et al. (2000).

Many methods have been developed to obtain surface fractal dimensions of adsorbents on the basis of different experiments, e.g. adsorption, mercury porosimetry, scanning electron microscopy, and neutron scattering measurements. Among those, the methods based on analysis of adsorption isotherms play important role, since they require only one complete adsorption isotherm for a given adsorbent to calculate the surface fractal dimension (Avnir and Jaroniec, 1989; Ehrburger-Dolle, 1999; Tatlier and Erdem-Senatar, 1999). A simple method of calculation of the fractal dimension from single adsorption isotherm was developed by Avnir and Jaroniec (1989). This method, elaborated later by Pfeifer and Cole (1990), emerges now as a straightforward standard approach for surface fractal dimension evaluation.

The evaluation of the mass fractal dimension can be done, for example, from scattering (e.g. small-angle neutron) experiments (Schmidt, 1989) and from analysis of the experimental data on particle size or aggregate size distributions (Ohiai et al., 1992; Rasiah et al., 1993; Kozak et al., 1996, Yongfu and Songyu, 1999). The knowledge of mass fractal dimension is important for predicting permeability and porosity of soils (Perfect, 1999; Bird et al., 2000).

Adsorption and mercury intrusion data lead to evaluation of the exponents, which can be interpreted as surface fractal dimensions (Neimark 1990, 1992). Obviously, nitrogen, water and mercury molecules "probe" different parts of the surface and consequently, resulting values of the exponents are different. Moreover, water retention curves, when interpreted in terms of the so-called "pore-solid-fractal" (PSF) model lead to another fractal dimension, which, in fact, can be treated as the mass fractal dimension.

For a wide class of geometrical fractals, the dependencies of their geometric measures on the resolution have the form of a power law  $A \propto B^D$ , where  $A$  is a measure of the features under study, and  $B$  is the resolution. The exponent  $D$  reflects the irregularity of the features. Therefore  $D$  characterizes the effective geometry for a given process, and not necessarily the geometry. This conclusion of the fractal approach bears on all methods used to characterize a porous solid. The

geometrical irregularities and roughness of surface have an essential influence on the value of the fractal dimension  $D$ , which for solid surfaces may vary from 2 to 3. The lower limiting value of 2 corresponds to a perfectly regular smooth surface, whereas the upper limiting value of 3 relates to the maximum allowed surface complexity.

Several simple relationships have been proposed as a means of evaluating the fractal dimension from various type experiments such as gas adsorption measurements, mercury porosimetry, water retention, particle and aggregate size distribution, scanning electron microscopy, particle size measurements, and so on. Adsorption and mercury intrusion data are used to evaluate the surface fractal dimensions. Nitrogen, water and mercury molecules are sensitive to different parts of the surface and, consequently, resulting values of the exponents (fractal dimensions) are different. Analysis of particle size distribution can provide information how the is distributed in a three-dimensional space, i.e. they give the mass fractal dimension. The discrepancy between the results emerging from different experimental methods may be due to an incomplete model of the processes from which fractal dimensions are derived. Also, it is important to apply very precise experimental techniques to measure the data from which the fractal dimension is subsequently computed. Despite of a big progress, there still exist controversies concerning the methodology of the fractal dimension evaluation. Moreover, there are also undertaken several questions about practical value of fractal scaling. Therefore, the problems of recognition of soil fractality and reliability of the methods used for its determination should still be the subject of further studies.

## FRactal Character of Soil Surface

Adsorption isotherms can be used to evaluate the values of the surface fractal dimensions. This is performed by employing a well-established method, based on the Frenkel-Hill-Halsey (FHH) equation. According to this approach, the experimentally measured data,  $N$ , versus the relative pressure,  $x$ , are approximated by using the equation (Neimark, 1990; Jaroniec, 1995, Jaroniec and Kruk 1997):

$$\ln N = -(1/m) \ln(-\ln(x)) + C, \quad (29)$$

where  $C$  is a constant and the parameter  $m$  is related to the surface fractal dimension of the sample. The determination of the surface fractal dimension,  $D_s$ , requires knowledge of the adsorption regime. The magnitude of the parameter  $1/m$  distinguishes two possible adsorption regimes, namely when  $1/m < 1/3$ , the adsorption is occurs within van der Waals regime and the surface fractal dimension is then  $D_s = 3(1 - 1/m)$ . Alternatively, for  $1/m > 1/3$  the adsorption is governed by the capillary condensation mechanism for and  $D_s = 3 - 1/m$ .

Equation (29) should be applied to the experimental data measured within multilayer adsorption region, i.e. for relatively high relative pressures (Neimark, 1990). Within this region the effects of energetic surface heterogeneity play negligible role, because the surface molecule interactions are screened by the already adsorbed particles.

Because of different chemical character of water and nitrogen molecules, the values of the fractal dimension obtained for those adsorbates are different. The surface fractal dimensions resulting from water vapor adsorption are lower than those estimated from nitrogen adsorption isotherms. Similar relationship between the values of the surface fractal dimension, evaluated from nitrogen and from water vapor adsorption data has been already observed for soils (Sokołowska et al., 2000; Hajnos et al., 2000, Slawinski et al. 2002), and also in the case of cement materials (Niklasson, 1993). However, a caution should be exercised in interpreting values of fractal dimensions obtained from water vapor adsorption because of specific interactions of water molecule with soils, leading to absorption and dissolution of water by soils constituents. Thus, the surface fractal dimensions evaluated from nitrogen adsorption data provide more reliable information about geometric heterogeneity of the surface of soils.

Surface fractal dimensions (D) obtained from nitrogen and water adsorption data for a range of mineral soils are compared in Fig. 63. Usually higher fractal dimensions are calculated from nitrogen adsorption isotherms.

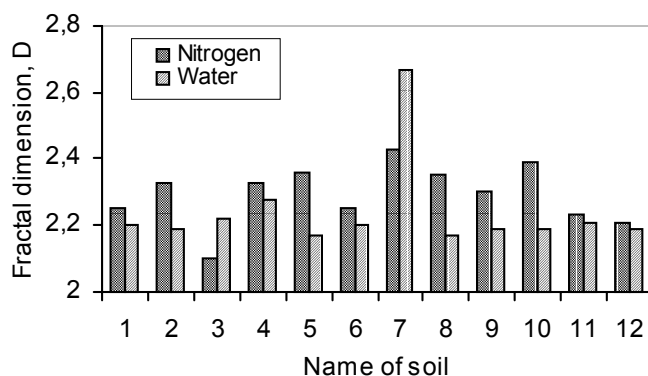


**Fig. 63.** Surface fractal dimension (D) obtained from nitrogen and water adsorption data for mineral soils formed from: sand (1), loam (2), clay (3), silt (4), loess (5), for brown soils formed from loam (8) and sand (11), for podzolic soils formed from loam (9) and sand (12), for black earth formed from loam (10), and for alluvial soils (6) and mucks (7)

## FRactal Character of Pore System

The pore system of many soils can be self-similar at different scales of observation. The schematic illustration of the cross section of various pore types is presented in Fig. 64. The nonfractal pores are not self-similar and the ideal fractal pores are self-similar at any scale of observation. As a rule, the fractal behavior of soil porosity occurs in a limited range of pore dimensions, called upper and lower cutoffs (Pachepsky et al., 1995). However, fractal dimensions should be addressed with great care to particular features of the pore structure (Crawford and Matsui, 1996), so these values could be treated more as comparative parameters.

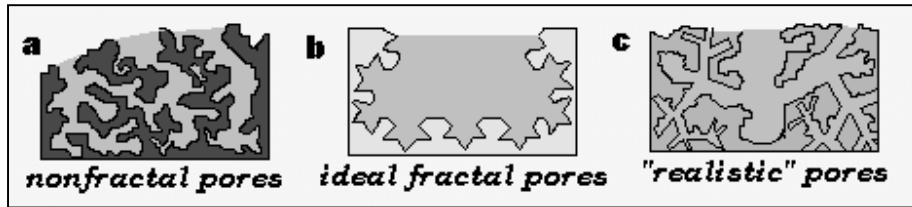


Fig. 64. Cross sections of pores of various self-similarity.

The basic relationship of the method used for surface fractal dimension calculation is based on the equation (Pfeifer and Obert, 1989, Perfect and Kay, 1995):

$$S(\varepsilon) \propto \varepsilon^{2-D}, \quad (30)$$

where  $\varepsilon$  is the size of the gauges covering the surface and  $S(\varepsilon)$  is the surface area. In the approach proposed by Neimark (1992) the role of a gauge is played by an average radius of curvature of the meniscus at the mercury-sample interface,  $r$ , when mercury is forced into the sample at the pressure  $p$ . The average radius of the curvature of the mercury meniscus is related to the pressure by Washburn - type relation:

$$p = C_1 / r, \quad (31)$$

where  $C_1$  is a constant. The surface area of the interface can be calculated from the Rootare and Prenzlou (1967) relation:

$$S_1 = C_2 \int_0^V p dV', \quad (32)$$

where  $V$  is the volume of pores of equivalent radius  $r$  and  $C_2$  is a constant. The area  $S_1$  is interpreted as that which would be measured by balls of radius  $r$ . Assuming that  $S_1 = S$  and taking into account Eqns (30-32) we get:

$$D_{Hg} = 2 + \frac{d \log \int_0^V p dV'}{d \log p}, \quad (33)$$

where the symbol  $D_{Hg}$  has been invoked to distinguish the values of the surface fractal dimension obtained from porosimetric data.

The latter equation is equivalent to:

$$dV(R)/dR \propto R^{2 D_{Hg}}. \quad (34)$$

Thus knowing the pore radii distributions, the mesopore surface fractal dimension can be evaluated from the slopes of the linear parts of the log-log plots of the above equation from the following dependence (Pachepsky et al. 1995):

$$D_{Hg} = 2 - \text{slope} = 2 - d \log[dV(R)/dR]/d \log R. \quad (35)$$

Figure 65 shows the plots of the above dependence corresponding to pores of different self similarity.

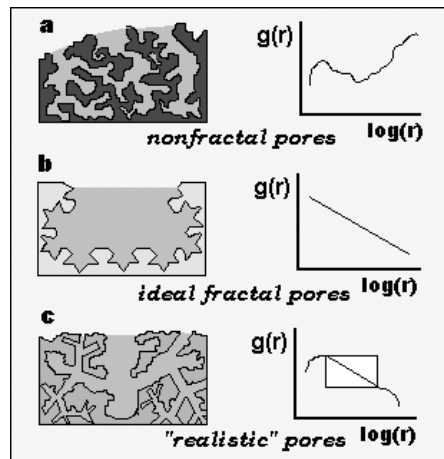


**Fig. 65.** Pores of various self-similarity with corresponding fractal plots.

The  $D_{Hg}$  values calculated using mercury intrusion data are frequently higher than 3, which are theoretically restricted values. Possibly, pores of larger voids connected by narrower necks (similarly as e.g. spaces between spherical grains) are involved. Therefore, a larger pore volume (voids) is attributed to a given pore radius than is formally possible to calculate  $D_{Hg} = 3$  in a cylindrical pore model. Thus,  $dV/dR$  is also higher and leads to higher  $D_{Hg}$ .

## FRACTALITY OF GRAIN-SIZE DISTRIBUTION

Several physical properties of soil systems may depend not only on fractal character of pores and surfaces, but also on the scaling behavior of the entire mass. The knowledge of mass fractal dimension is important for predicting permeability and porosity of soils (Perfect, 1999; Bird et al., 2000). The evaluation of the mass fractal dimension can be done, for example, from scattering (e.g. small-angle neutron) experiments (Schmidt, 1989) and from analysis of the experimental data on particle size or aggregate size distributions (Rasiah et al., 1993; Kozak et al., 1996, Yongfu and Songyu, 1999). The latter approach is presented further.

The number  $n$  of objects with a characteristic linear dimension greater than  $z$  is given by:

$$n(z) \propto z^{-D_m}. \quad (36)$$

The validity of Eq. (36) for the size distribution of fragments is treated as evidence that the fragmentation mechanism is scale invariant (Turcotte, 1986). The exponent  $D_m$  is recognized as fractal dimension of fragment-size distribution.

Several computational techniques have been proposed to evaluate  $D_m$  from particle-size distribution data (Tyler and Wheatcraft, 1992; Rasiah et al., 1993; Perfect and Kay, 1995). A modified approach developed by Kozak et al. (1996) is based on the equation:

$$\frac{M(z_{i-1} > z > z_i)}{c_i \rho_i k} = \frac{D}{3-D} (z_{i-1}^{3-D} - z_i^{3-D}) \text{ for } D \neq 3, \\ \text{and } = 3 \ln(z_{i-1}/z_i) \text{ for } D=3 \quad (37)$$

where  $M(z_{i-1} > z > z_i)$  is the mass of the fraction of sizes  $z_{i-1} > z > z_i$ , and  $c_i$  and  $\rho_i$  are constants, related to shape and density of the  $i$ -th fraction, respectively. Both these quantities are usually assumed invariant for the whole range of grain sizes. The parameters of Eq. (37) are evaluated by minimizing the lack-of-fit mean square:

$$s^2 = \sum_{i=1}^{n_c} \frac{l_i [M^{calc}(z_{i-1} > z > z_i) - M^{meas}(z_{i-1} > z > z_i)]^2}{n_c - K}, \quad (38)$$

where the superscripts *calc* and *meas* denote masses of fractions obtained from eq. (38) and from experiment, respectively,  $K$  is the number of unknown parameters,  $n_c$  is the number of size classes and  $l_i$  is the number of replications of each class. The exponent  $D_m$  of the particle-size distribution provides information about the cumulative distribution of the mass. Details on computational procedure were given by Kozak et. al. (1996).

Correlations between the surface fractal dimensions and the mass fractal dimension for mineral soils are shown in Fig. 66. A good linear correlation exists between the values of  $D$  obtained from the mercury porosimetry data and the values of  $D_m$  evaluated from the particle size distribution.

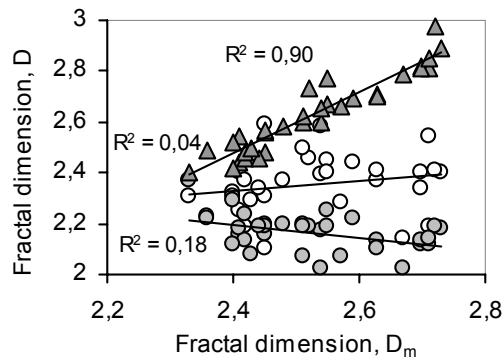


**Fig. 66.** Surface fractal dimension ( $D$ ) obtained from various experimental data for mineral soils versus the mass fractal dimension ( $D_m$ ) obtained from particle size distribution. Triangles denote the values of  $D$  from mercury intrusion measurements, white circles - from water adsorption data and black circles from nitrogen adsorption measurement. The values of the square of the correlation coefficient,  $R^2$  are given in the figure.

However, the plot in Fig. 67 presents the results for organic soils. One can see that for organic soils the values of the fractal dimension estimated from adsorption nitrogen data are lower and more differentiated for different soils samples than those obtained from the data of water adsorption and water retention.

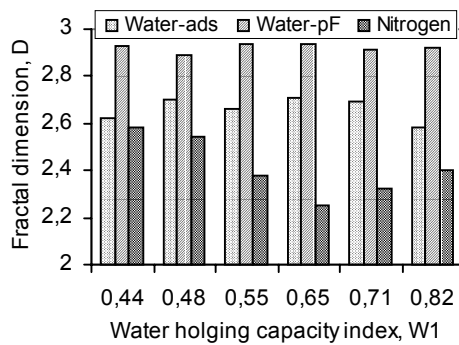


**Fig. 67.** Dependence between the values of  $D$  (from water adsorption, water retention data (pF) and from nitrogen adsorption) and the water holding capacity index, ( $W_1$ ), which characterizes the secondary state of muck transformation.

The discrepancy between the results emerging from different experimental methods may be due to an incomplete model of the processes from which fractal dimensions are derived. Also, it is important to apply very precise experimental techniques to measure the data from which the fractal dimension is subsequently computed. Despite of a big progress, there still exist controversies concerning the methodology of the fractal dimension evaluation. Moreover, there are also undertaken several questions about practical value of fractal scaling. Therefore, the problems of recognition of soil fractality and reliability of the methods used for its determination should still be the subject of further studies.

### FRACTALS IN SOILS AND SOIL PROCESSES

Both fractal dimensions and the ranges of fractal scaling differ between different soils. Jozefaciuk et al. (2001) studied effects of different soil cultivation practices (no tillage, ploughing, disking and the two last treatments combined with loosening) on surface properties of a brown forest soil. Surface fractal dimension had changed very slightly, indicating that general geometrical structure of the fine pore system remained unaltered despite changes in other physico-chemical properties of the soil. Fractal dimension changes at soil compaction (Lipiec et al. 1998) and depends on organic matter content (Raychev et al., 2003).

Fractal dimensions change under changes in soil reaction. The mesopore fractal dimension calculated from mercury intrusion data decrease after acid treatment showing a smoothing of the material porous surface. Alkaline treatment affects the mesopore fractal dimension to a lower extent. A slight rise of the mesopore fractal dimension was noted in most cases. Despite the occurrence of rather well defined tendencies of the changes in macropore volumes and radii, the fractal dimensions of macropore surface change in both directions (Fig. 68), indicating either an increase or a decrease of the complexity of the pore surfaces.

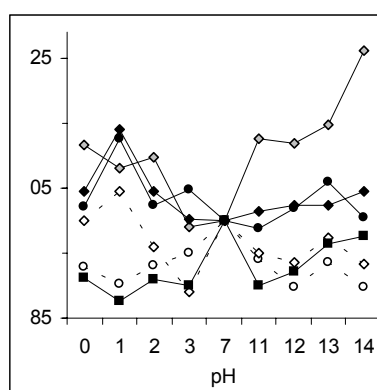


**Fig. 68.** Changes of MIP fractal dimension of a range of soils under pH changes in a laboratory experiment.

In general, for a given soil, both acid and alkali treatments lead to changes of the macropore surface fractal dimension in the same direction i.e. the  $D_s$  values either decrease or increase after both treatments. This can be due to different mechanisms of soil material dissolution in different soils or a preferential dissolution of some soil components. For instance, the dissolution of amorphous material of high degree of dispersion or cementing agents should lead to the decrease of pore surface complexity ( $D_s$  decrease) while the partial dissolution of soil particles and the resulting increase of their degree of dispersion may lead to an increase in the fractal dimension. The reorganization of the aggregate structure may cause changes in pore construction reflected in changes of fractal dimensions in any direction. The prevailing mechanism has a dominant effect on soil fractal behavior.

A smoothing of the surface roughness under two extremely low pH is clearly indicated by the decrease of fractal dimensions  $D$  calculated from water vapor adsorption isotherms (Fig. 69). Most probably, this is connected with a removal of amorphous soil components and surface coatings. It is worth noting that amorphous silica oxides that are produced by acidic destruction of clay mineral lattices also have a low fractal dimensions. The extreme alkali treatment leads in general to a slight increase of the fractal dimension.

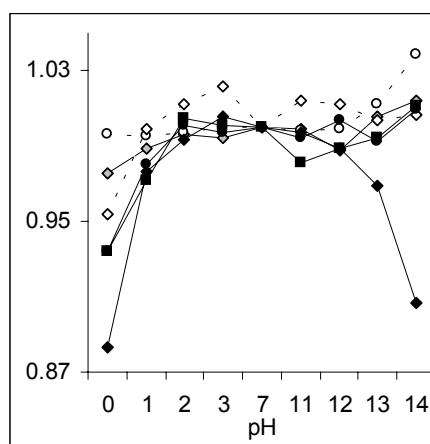


**Fig. 69.** Changes of water vapor adsorption fractal dimension of a range of soils under pH changes in a laboratory experiment.

Removal of organic matter from soil clay fraction leads to a decrease in the fractal dimension calculated from water vapor adsorption data. Thus, the organic matter removal makes clay surfaces smoother. Soil OM seems to have rougher surface than clay minerals. Exemplary fractal plots of a clay fraction separated from a black alluvial soil (Jab) and from a typical brown soil (Tar) before and after organic matter removal (-OM) are shown in Fig. 70.

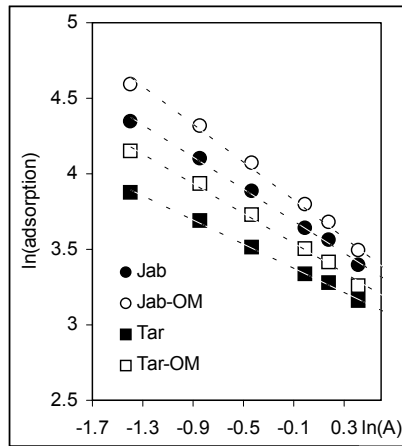


**Fig. 70.** Exemplary fractal plots for soil clay fractions before and after removal of organic matter

Further removal of iron oxides and aluminum oxides leads to consecutive decrease in fractal dimension that is illustrated in Fig. 71 for a range of soil clays.

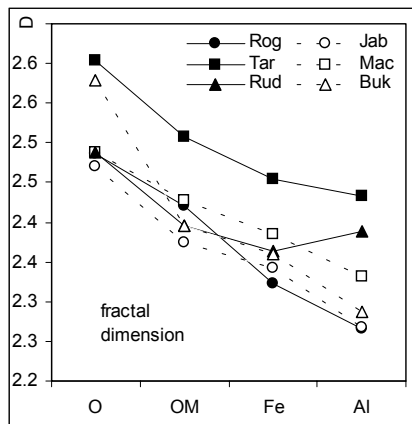


**Fig. 71.** Changes in fractal dimensions determined from water vapor adsorption after removal of organic matter (OM), iron (Fe) and aluminum (Al) compounds from soil clay fraction.

While all clay components are present, the surface of original clays are rough. The removal procedures make clay surfaces consecutively smoother. Finally the clay surfaces may approach properties of a mixture of pure clay minerals thus the differences among particular clays may result mainly from their mineral composition.

Addition of cyclodextrins to soil minerals and soils influences their fractal build-up. Fractal character of the surface alters as evidenced by the ln-ln plots of

adsorption vs. adsorption potential. The ranges of the fractal scaling (linearity intervals) are different for different minerals and these do not change significantly after RAMEB addition. The slope of the linear part of these plots is highest for RAMEB indicating that the water sorption process by RAMEB surface exhibits apparently fractal scaling with a very low fractal dimension. The fractal dimensions ( $D$ ) for the minerals do not change markedly with RAMEB addition that is shown in Fig. 72. A slight increase in micropore fractal dimension at high RAMEB contents. This increase indicates a rise in changes in surface roughness or micropore complexity. Note that the micropore fractal dimension of the RAMEB is much lower than for the minerals.

This figure illustrates also changes in fractal dimensions ( $D_s$ ) of mesopore surface, calculated using mercury intrusion porosimetry data. In general the linearity ranges of  $dV/dR$  vs.  $R$  log-log plots are found for all the samples, as this was observed also for the micropores. For the RAMEB, two linearity ranges of similar slopes can be distinguished. These slopes are lower than for the minerals, indicating the RAMEB fractal dimension is smallest. The linearity ranges for the initial minerals occur for pore radii from 0.35 to 0.01  $\mu\text{m}$  for BEN, 0.45 to 0.02  $\mu\text{m}$  for IT and 0.71 to 0.14  $\mu\text{m}$  for KA and in general these become narrower with RAMEB addition increase (which is particularly seen for IT) and shift towards smaller pore radii (which is particularly seen for BEN).

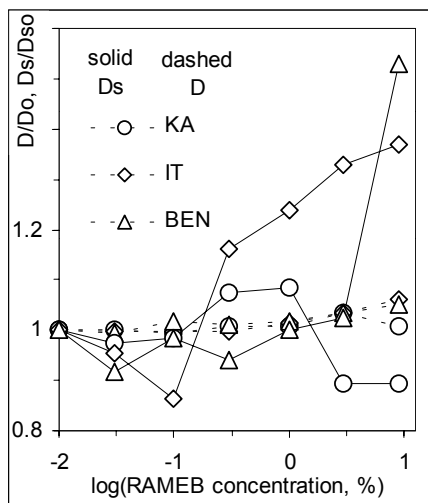


**Fig. 72.** Changes in fractal dimensions determined from water vapor adsorption ( $D$ ) and from mercury intrusion porosimetry ( $D_s$ ) of selected soil minerals under RAMEB treatment. The y-axis shows the ratio of fractal dimension of the mineral + RAMEB to this of the control mineral.

The fractal dimension  $D_s$  of BEN and IT decreases at low RAMEB additions and rises at higher RAMEB doses. For KA, the  $D_s$  decreases again at higher

RAMEB doses. For all of the minerals, the decrease of  $D_s$  may be related to filling of the smallest pores and pore walls coverage by RAMEB, both leading to smoothing of pore surfaces. As a possible explanation of the  $D_s$  increase one may consider the accumulation of cyclodextrins at the necks of the mesopores. This leads to a decrease of the radii of the necks while the volumes of the voids remain large. This is apparently consistent with the observed decrease of the scaling range and its shift towards smaller mesopore radii. At higher RAMEB doses the KA mesopores can become closed or filled with CD.

Surface fractality of soils alter under addition of RAMEB, as well that is illustrated in Fig. 73. The fractal scaling intervals do not change significantly. The micropore fractal dimension of exemplary soils drops slightly at minimum RAMEB dose and next increases. For sandy soils this decreases again at high RAMEB contents. This trend may be explained as follows: initially RAMEB covers the most complex parts of original soil surfaces, next a rearrangement of the micropore structure or grouping of the RAMEB as “surface islands” increases surface complexity and finally (as observed for sandy soils) the excess of RAMEB tend to exhibit its own properties.

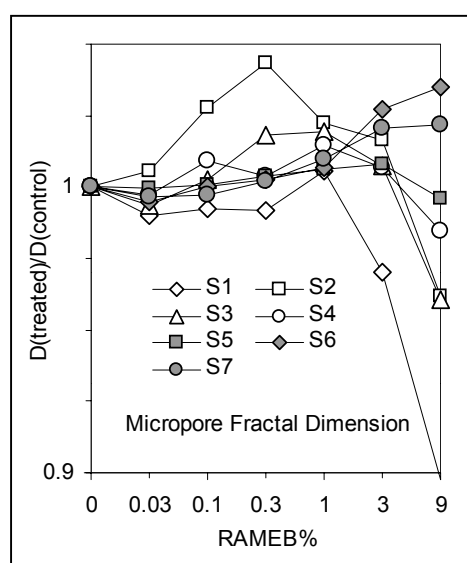


**Fig. 73.** Changes of micropore fractal dimension of exemplary soils under RAMEB treatment. On y-axis the ratio of fractal dimension of the soil + RAMEB to this of the control soil is shown.

The water volume absorbed by swelling clay minerals is related to its surface fractality (Xu 2003). The surface fractal dimension of swelling clay minerals can be estimated from the correlation of the normalized water volume by the volume of swelling clay minerals to vertical overburden pressure. The surface fractal dimension of Wyoming bentonite obtained from the swelling tests is 2.64. Its surface fractal dimension determined from the swelling tests nearly equals to that obtained from the nitrogen adsorption isotherms, and is larger than that measured using the mercury intrusion porosimetry.

## CHAPTER 6.

### SOIL POROSITY

*M. HAJNOS, R. ŚWIEBODA, G. JÓZEFACIUK*

Porosity is one of more important parameters characterizing porous bodies. The solid phase of a given body may be either nonporous (cast, monolyte) or may contain pores - spaces filled by liquid or gas phases. The pores may be open and/or closed, may have different shape, may be available or nonavailable from the surface of the body, may have very different sizes. So, the porosity is defined as the occurrence of internal spaces in solid body (Czachor 1997).

A measure of the porosity is a volumetric ratio of all free spaces to the bulk of the body. The latter value is called absolute porosity ( $\text{m}^3/\text{m}^3$ ). The other definition, relative porosity ( $\text{m}^3 \text{ m}^{-3}$ ), is a ratio of a volume of available (open) pores only to the bulk volume of the body (Swieboda and Kocjan 2004).

Both porosity values may be expressed also as percentage or, which is frequently used, as volume of pores in a mass unit of the body ( $\text{m}^3 \text{ kg}^{-1}$ ).

Porous structures may be formed in several ways:

- connection of smaller nonporous units (grains) into larger aggregates. The porous structure is thus formed from internal spaces between the grains and the grains themselves form the structure skeleton.
- removal of some part of the solid from monolytic body (e.g. leaching, dissolution). Such materials have a sponge structure.
- both processes together.

For most porous materials one can distinguish the intergranular porosity (between the grains) which is called bed porosity and intragranular porosity (inside the individual grains). Solid bodies may have also a geometrically irregular surface, which is difficult to distinguish from “real” pores. The pore is thus defined by a convention as the surface cavity having larger depth than the half of its average size (e.g. the radius for cylindrical pore), that is illustrated in Fig. 43.

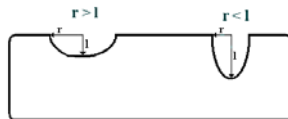


**Fig. 43.** Scheme demonstrating the differences between pores and the surface irregularity

The pores may be classified according to different criteria:

According to their availability from outside (Fig. 44) one distinguishes:

Unavailable pores (totally closed, isolated) – having any connection with surface of the solid body (e.g. occluded gas or liquid bubbles in rocks). Such pores are not detected by most porosimetric methods, however they influence among others the measurements of solid phase density, shear stresses under high pressures and may be responsible for a collapse of a solid under high external forces.

Available pores – connected with the surface either indirectly or via other pores (channels). These pores are subdivided on several groups:

- pores available from one side (one-side open),
- pores available from two sides (two-side open),
- connected pores,
- nets or clusters – systems of interconnected pores (channels, voids, cavities).

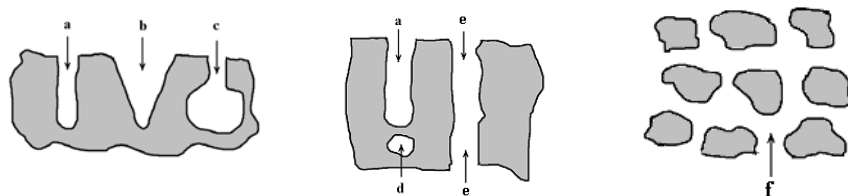


**Fig. 44.** Pore types. One-side open pores: cylindrical - a, conical - b, bottle - c. Unavailable pore- d. Two-side open pore - e. Pore net - f.

The shape of natural pores is usually nonuniform. Their complicated build-up for calculation purposes is usually approximated by selected geometrical models. Among many models (slit-like, ink-bottle, conical, globular etc.) the most frequently used is a cylindrical pore model.

According to the dimension of pores, that is connected with the method of their measurement, several pore classifications are introduced.

From point of view of capillary condensation process, Dubinin proposed the following classification:

- macropores – more than 200 nm in radius; in such pores no capillary condensation occurs but they may be important in diffusion transport of molecules,
- mesopores - 2 - 200 nm in radius; in these pores capillary condensation takes place,
- micropores – less than 2 nm in radius; in these pores no capillary condensation occurs, but a volumetric filling with adsorbate vapor (Dubinin – Radushkevich theory).

A popular soil science classification (Luxmoore) is based on water retention (pF curve) in soils and is related to plant water availability. One distinguishes capillary and noncapillary (aeration) pores. The boundary between the above is 20  $\mu\text{m}$  in diameter (pF = 2.2). In pores larger than 20  $\mu\text{m}$  (macropores) the water is passed through with gravitational force.

Less than 20  $\mu\text{m}$  pores are divided on criteria of water availability for plants:

- storing easily available water,  $d = 20 - 3 \mu\text{m}$  (pF = 2.2 - 3),
- storing difficult available water,  $d = 3 - 0.2 \mu\text{m}$  (pF = 3 - 4.2),
- storing unavailable water, microcapillary pores,  $d < 0.2 \mu\text{m}$  (pF > 4.2).

Smart classified pores according to image resolution:

- for an eye - larger than 200  $\mu\text{m}$ ,
- for microphotography – larger than 6  $\mu\text{m}$ ,
- for optical microscopy – larger than 0.2  $\mu\text{m}$ .

Greenland had distinguished:

- bonding pores (<5 nm), important for connecting primary soil aggregates,
- residual pores (5 - 500 nm), important for soil reactions on molecular level,
- water storage pores (0.5 - 50  $\mu\text{m}$ ), storing water available for soil organisms,
- transmission pores (50 - 500  $\mu\text{m}$ ), important for water movement and roots penetration.

These nonuniform classification systems lead to misinterpretations of porosity. Therefore the International Union of Pure and Applied Chemistry (IUPAC) recommends use of the following terms:

- micropores – of radii less than 2.0 nm,
- mesopores - between 2,0 and 50 nm,
- macropores – larger than 50 nm.

Various pore size classification systems are summarized in Fig. 45.

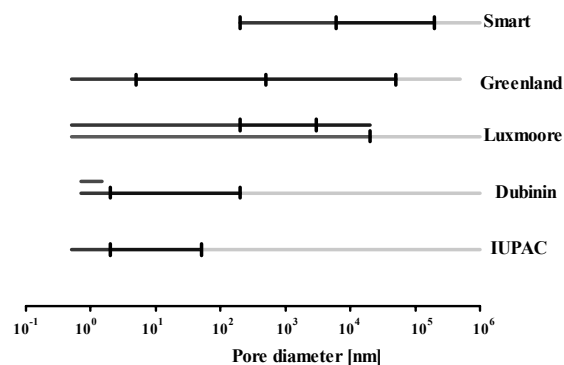


**Fig. 45.** Various classifications according to pore sizes (explanations in the text).

## MEASUREMENT OF POROSITY

Total (absolute and/or relative) porosity may be estimated from measurements of the bedvolume (or bulk density) and the solid phase density. The open pores volume may be estimated pycnometrically basing on Boyle-Mariotte gas law. Total porosity value is of less importance for characteristic of porous materials because provides no information on pore dimensions and number. The same total porosity can result from small number of large pores and large number of small ones despite both above materials have quite different properties. More important pore characteristic is than a function relating pore volume and dimensions within defined pore size class (pore size distribution).

The pore size distribution is determined using so called direct and indirect methods (Lawrence 1977, Sing 1982).

Direct methods are usually used for investigation of larger than 30  $\mu\text{m}$  pores and indirect methods for studying of smaller pores. Direct methods are based on an analyze of cross sections of porous bodies: nontransparent sections in reflected light (Fig. 46) and transparent ones in transmitted light microscopy. Soil cross sections are useful for determination of pore shapes. Image analyze of XRD and NMR scanning photographs is used, as well.

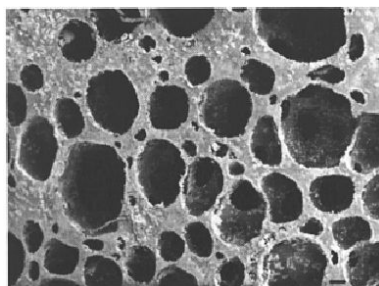


*Fig. 46. The example of the microscopic picture for pore analysis in the direct method.*

Indirect methods determine pore size distributions basing on measurements of other physicochemical parameters related to pore sizes and volumes as for example gas, vapor or liquid volume and pressure present within and over the sample of porous body in equilibrium. Most frequently used indirect porosimetric methods are nitrogen or water vapor desorption, mercury intrusion and water retention techniques (Hernandez 2000; Hajnos 1998; Roquerol et al., 1994).

The desorption isotherm is a function relating the amount of adsorbed gas (vapor) to its equilibrium pressure during the pressure decrease at a constant temperature. While measurement of the isotherms for nitrogen at liquid nitrogen tem-

perature requires advanced instrumental techniques, the water vapor desorption isotherm can be measured at a room temperature using a simple vacuum chamber method. The samples are placed as rather thin layers (few mm) in weighing vessels and closed in the vacuum chamber. The relative water vapor pressure,  $p/p_0$ , in the chamber is controlled by sulfuric acid solutions of stepwise increasing concentrations ( $p/p_0$  decrease). The amount of water present in the sample at a given  $p/p_0$ ,  $a$ (kg/kg), is measured by weighing after at least 48h of equilibration. The dry mass of the samples is estimated after completing the measurements, after 24h oven drying at 378K. The  $a$  value is related to the pore volume. Because below  $p/p_0 = 0.35$  surface adsorption processes dominate, the pore volume  $v$  is taken as the volume of adsorbed water at the given  $p/p_0$  value minus that at  $p/p_0 = 0.35$ .

Mercury porosimetry (MIP) is based on forcing mercury to the sample at high pressures (Konstankiewicz and Stawinski 1976, Volzone and Hipendinger 1997). Because mercury does not adhere to most of solids (contact angle  $> 90$  degs), it enters the pores only when an external pressure ( $p_m$ ) is applied (for example water of contact angle close to 0 degs enters the pores spontaneously). The higher the pressure, the mercury is forced to narrower pores. The pores should be empty at the beginning and so the sample is outgassed at a vacuum prior to the mercury intrusion. The mercury intrusion porosimetry apparatus registers the volume  $V$  of the mercury forced into the sample against the intrusion pressure.

The measurement is performed as following: 1. Placing sample in dilatometer, 2. Evacuating sample for 30 - 60 min to remove air, 3. Filling with mercury, 4. Applying pressure for meso and fine pores. The idea of the mercury intrusion measurements is briefly illustrated in Fig. 47.

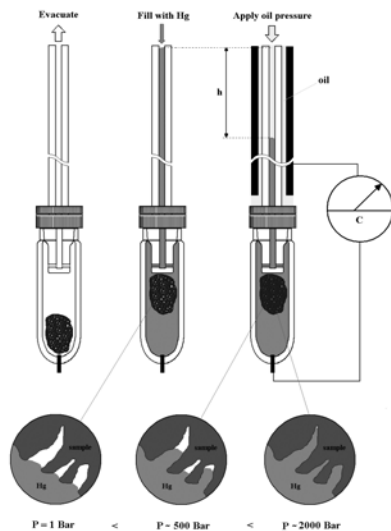


**Fig. 47.** An idea of mercury intrusion porosimetry.

Water retention curves are estimated basing on measurements of soil moisture at defined suction pressure of water (water potential, pF) in the soil bed. For measurements at low water potentials the suction plate method is applied (Richards 1949). Water retention at high water potentials is measured using the pressure-chamber method (Walczak 1984, Kutilek and Nielssen 1994).

The gas or vapor condensed in a pore or liquid filling the pore form a lens-shaped surface, called meniscus. The pressure difference across the meniscus (inside and outside the pore),  $\Delta P$ , is related with the curvature of the meniscus  $r$  (and so the pore dimension) according to Young-Laplace equation:

$$\Delta P = \frac{2\gamma}{r} \quad (21)$$

where  $\gamma$  is a surface tension of the liquid (condensate) present in a pore.

The curvature of the meniscus is dependent somehow with the pore dimension. One relates these two values using any convenient pore model, which is selected either operationally or basing on a knowledge of the sample structure. As far as the model pore shape may not reflect the real pore shape, the pore dimensions calculated using models are called equivalent dimensions. The pore size distributions coming from indirect measuring methods do not include closed, nonavailable pores.

Using desorption isotherms, the pore radius  $r$  can be related to the desorption pressure  $p$  by the Kelvin equation for the hemispherical meniscus with zero water/solid contact angle (Oscik, 1979):

$$r = 2M \sigma_w \cos\alpha_w / \rho R T \ln(p_o/p), \quad (22)$$

where  $M$  is molecular mass of water,  $\sigma_w$  is water surface tension,  $\alpha_w$  is a water-solid contact angle (assumed here to be zero),  $\rho$  is density of water,  $R$  is the universal gas constant and  $T$  is the temperature of the measurements.

Using mercury intrusion porosimetry, the pore radius  $r$  is related to the mercury intrusion pressure  $P$  by Washburn equation:

$$r = -2\sigma_M \cos\alpha_M / P, \quad (23)$$

where  $\sigma_M$  is mercury surface tension,  $\alpha_M$  is mercury – solid contact angle (for soils this is usually taken as 141,3 degs).

Using water retention (pF) curves the pore radius is related to water pressure head  $H$  by the equation:

$$r = 2\sigma \cos\alpha / H \quad (24)$$

Due to intrinsic features and limitations of the above methods, the ranges of (equivalent – cylindrical model) pores detected by them are:

- from water vapor desorption isotherms: 1.6 to 60 nm,
- from mercury intrusion porosimetry: 3.7 to 7500 nm,
- from water retention (pF) curves: 95 to 150000 nm.

that is illustrated in Fig. 48.

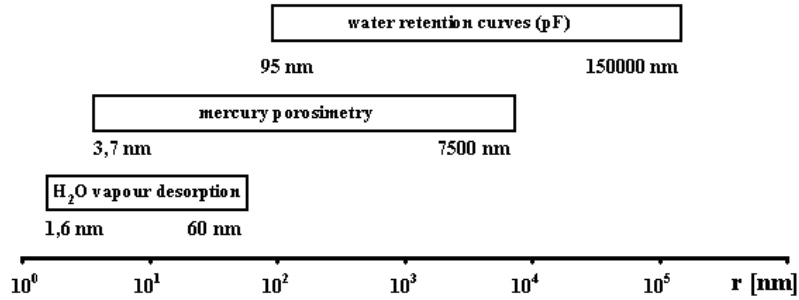


*Fig. 48. The ranges of pores detected by the above methods.*

The volume of the pores (i.e. amount of a liquid accumulated in the pores) at a given radius,  $v(r)$ , can be treated as a sum of pore volumes,  $v_i(r_i)$ , of the radii  $r_i \leq r$ ,

$$v(r) = \sum_{i=1}^n v_i(r_i). \quad (25)$$

Dividing the above equation by the total pore volume,  $v_t$ , the scaled pore volume vs. radius curve,  $\Xi(r)$ , is a sum of fractions of particular pores,  $f(r_i)$ :

$$\Xi(r) = v(r)/v_t = \sum_{i=1}^n v_i(r_i)/v_t = \sum_{i=1}^n f(r_i) = 1 \quad (26)$$

The pore fraction in a given range of pore sizes can be calculated as:

$$f(r_{i,av}) = [\Xi(r_{i+1}) - \Xi(r_i)], \quad (27)$$

where  $r_{i,av}$  denotes the arithmetic mean of  $r_{i+1}$  and  $r_i$ . Knowing the latter values one easily constructs a pore size distribution function i.e. pore fraction vs. pore radius dependence.

The average pore radii,  $r_{av}$ , in the measuring range can be calculated as:

$$r_{av} = \sum_{i=1}^n r_i f(r_i) \quad (28)$$

Contrary to the desorption, the MIP results strongly depend on the state of the sample used (i.e. powder or aggregate), giving much higher readings for loose samples because of detecting the pores between sample grains and the walls of the measuring chamber (Jozefaciuk et al., 1998). Therefore, if possible, the measurements should be done on soil aggregates. Exemplary dependencies of pore volumes on radii for powdered and aggregated soils obtained using two above methods are presented in Fig. 49.

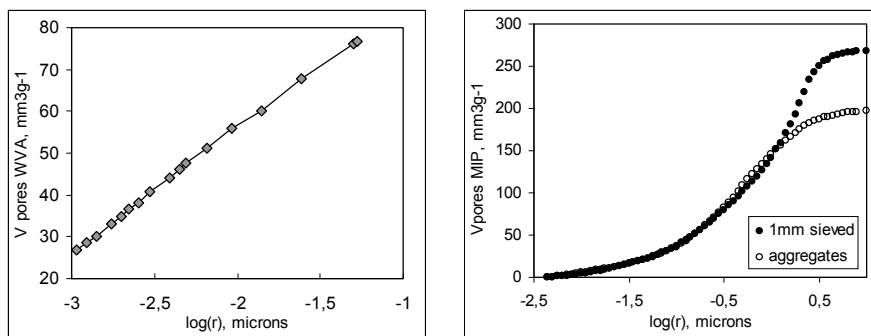


**Fig. 49.** Pore volume vs. radii dependencies for powdered and aggregated soils obtained from desorption isotherms (left curve independent of the sample state) and from mercury intrusion porosimetry (right two curves) Average data for 40 soil samples.

This is worth noting that the volumes of pores in the range of common pore radii (5-50 nm) for water adsorption and for mercury intrusion are different that shows that the numerical values of pore characteristics can be used separately for each method rather than as absolute values (Fig. 50).

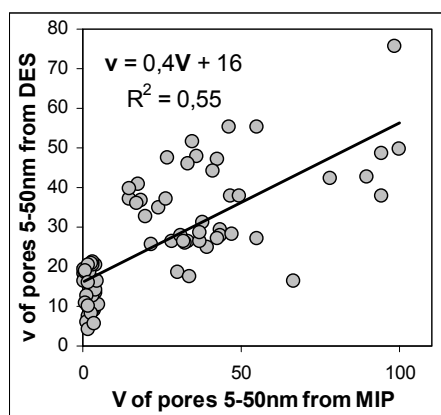


**Fig.50.** Dependence between pore volumes ( $\text{mm}^3\text{g}^{-1}$ ) measured in a common range of the desorption (DES) and mercury intrusion (MIP) methods.

## POROSITY IN SOILS AND SOIL PROCESSES

Porous structure of soils usually varies with soil depth as this is illustrated in Fig. 51. for a saline soil profile (Toth and Jozefaciuk 2002).

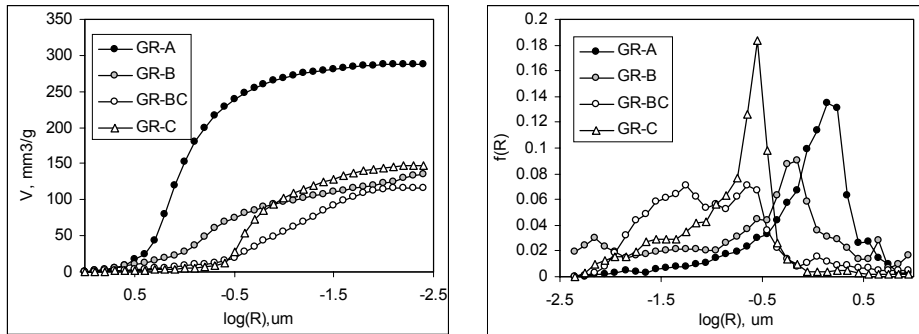


*Fig. 51. Pore volume vs. pore radius dependence (left) and pore size distribution functions (right) for exemplary soil profile. Data obtained using mercury intrusion technique.*

Soil organic matter markedly affects soil structure and pore properties. Fig. 52. shows pore volumes vs. pore radii dependencies for exemplary soil samples (CZ- chernozem and GF – gray forest soil) after addition of fulvic acid (FA) at different pH values. Fulvic acids affects mainly mesopores of larger sizes and cause a loosening of soil aggregate structure.

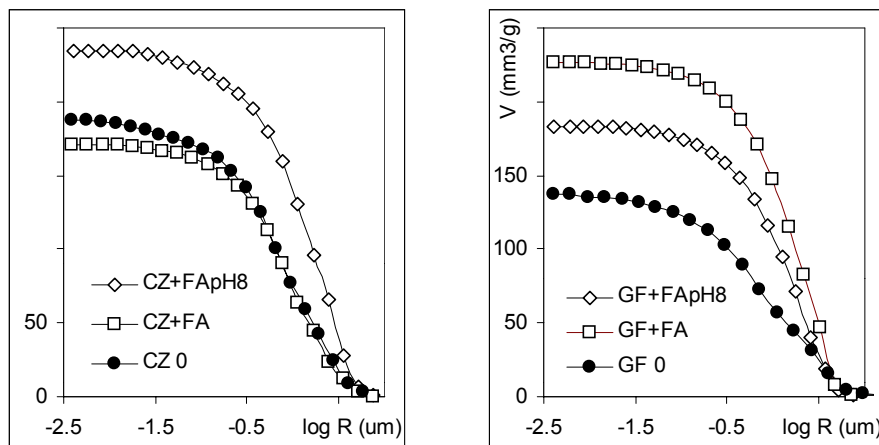


*Fig. 52. Pore volumes vs. pore radii dependencies for exemplary soil samples Abbreviations as in the text.*

Changes in soil pH and dissolved and exchange ions composition have significant influence on fine pore structure in soil via effects on its microaggregation status. This is due to changes in an amount and sign of soil variable charge thus to variation of electrostatic attraction and repulsion forces between soil charged particles. Also changes in the ionic strength of the soil solution and kind of dissolved ions may lead to aggregation or disaggregation of soil fine particles (Schultze-Hardy rule). The above effects are easily reversible by changing soil reaction. Various dissolution processes (organic matter, amorphous aluminum and iron oxides), destruction of the crystal lattice of the minerals and/or formation of precipitates and new phases in acidic and alkali environments lead to more permanent alteration of soil microstructure. In most of the literature on acid and alkali effect on soil structural properties, soils added with acid or alkali (in natural or artificial way) have been concerned. Thus the reported changes in soil structure are composite effects of alteration of soil solid phase, soil solution and exchangeable ions composition. Soil samples described later after acid or alkali treatments were transferred to calcium homoionic forms to abort the effects of solution pH and composition on microstructure.

For clay poor soils, usually, with the increase of the concentration of both acid and alkali treatment, the micropore volumes consecutively decreases that is presented in Fig. 53, showing the relative changes of the micropore volume vs. treatment pH. In the acidic range this decrease is most probably governed by a dissolution of amorphous soil components, while under alkaline treatment, leaching of soil organic matter should play a more important role. The depletion of organic material is much higher under alkali than under acid treatment, while acid is more aggressive in dissolving mineral components. The relative decrease of micropore volume is higher in the alkaline range. Different behavior is observed for the clay rich soils at the treatments with maximal concentrations of the reagents. Here the increase of the micropore volume increases, what is particularly obvious for the acid treated soils. Here the formation of amorphous silica from destructed clay mineral lattices can prevail over dissolution of amorphous soil phases.

Acid and alkali treatments have frequently opposite influence on the fractions of micropores of various sizes, that is shown in Fig. 54. As this may be expected, the effect of both treatments on the largest micropore fraction is least.

Relative changes in micropore radii in acid and/or alkali treatment pH, calculated from desorption isotherms are presented in Fig. 55. Similarly as in Fig. 53., on y-axis the ratio of the given parameter of the treated sample to the untreated one is given.

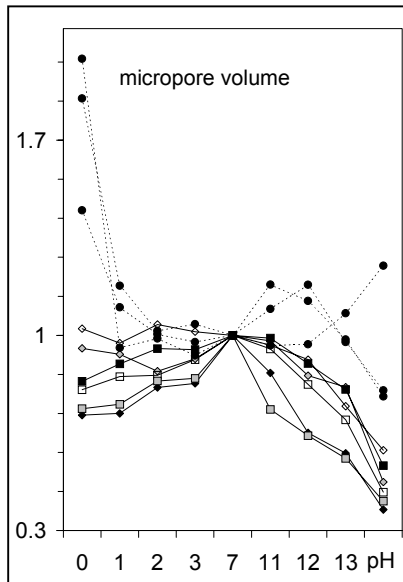


**Fig. 53.** Effect of acid and alkali treatment pH on changes in micropore volume of exemplary soils. The dashed line denote clay rich soils. On the y-axis the ratio of micropore volume of the treated sample to this of the initial sample is presented. Similar way of presentation of the results are maintained in the next

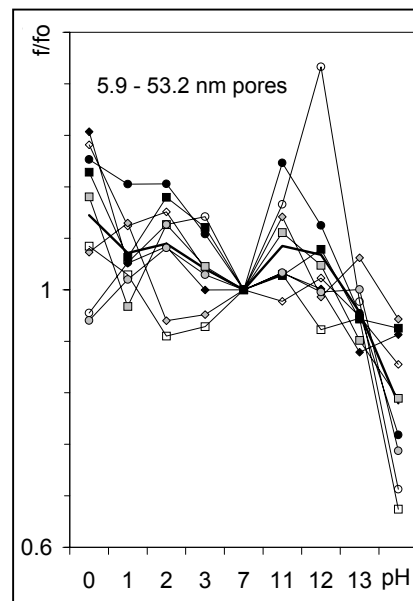
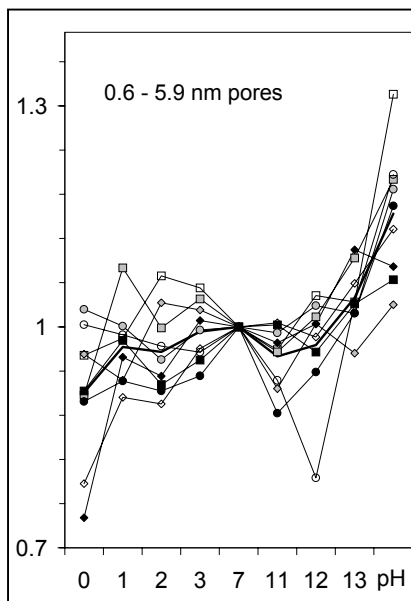


**Fig. 54.** Effect of the treatment pH on fractions of small (left) and medium (right) micropores. (Data from water vapor desorption isotherms)

As a consequence of changes in micropore fractions, the average micropore radius undergoes alterations, as well. This appears that acid treatment leads to its increase whereas alkali treatment gives opposite effect.

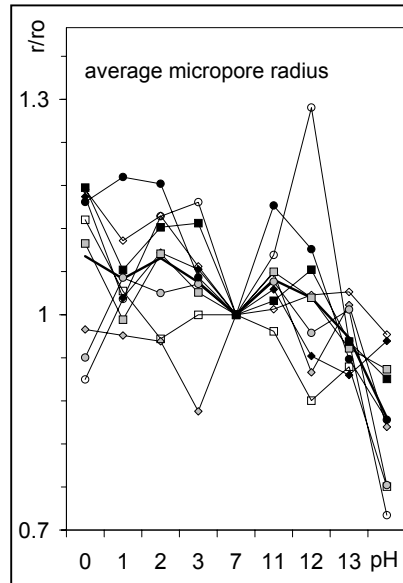


*Fig. 55. Effect of the treatment pH on average radius of pores measured from water vapor desorption isotherms.*

As measured from mercury intrusion porosimetry, the mesopore structure undergo significant changes with both acid and alkali treatments. As seen in Fig. 56, both mesopore volumes and radii increase in general under both treatments.

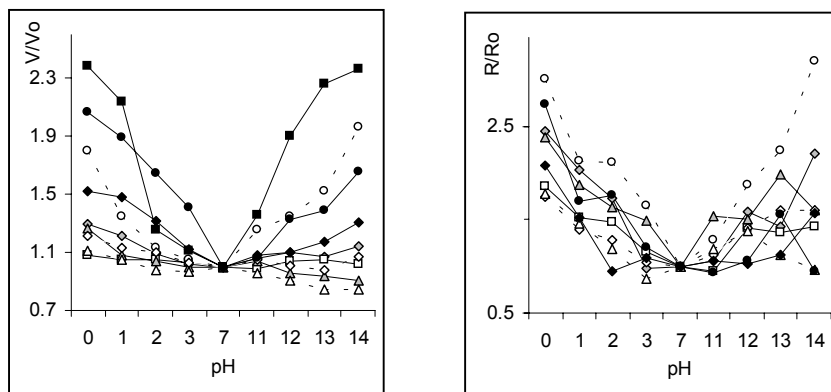


*Fig. 56. Effect of acid and alkali treatment pH on relative changes in mesopore volume (left) and mesopore radius (right) of exemplary soils.*

The increase of the mesopore volume and radius can be explained by the dissolution of amorphous and very finely dispersed solid soil components, having very high degree of dispersion and fine porosity. In alkaline media this can reflect the loss of soil organic matter. Mesopore size distributions functions shows a shift of the dominant pore peaks in the direction of larger pore radii in all soils and formation of new pores of large radii is observed for aggregates of the clay rich soils. The above changes indicate marked loosening of the soil aggregate structure most probably connected with the rearrangement of the aggregate build-up due to a removal of the cementing agents.

The total amount of the retained water is higher in soils of higher total porosity and lower bulk density, because more space is available for water. Addition of the peat to the soil increases its water retention, which can be important particularly in urban areas where the present infrastructure favours the rainwater outflow and diminishes its retention. Freezing-thawing cycles affect soil pore structure to the less extent. The above processes are illustrated in Fig. 57 for a loessial soil (C-control soil, CP – soil with added 6% of peat, FT - the latter soil after 4 freezing-thawing cycles). This figure shows soil moisture vs. water potential dependencies, that can be directly translated to porosity.

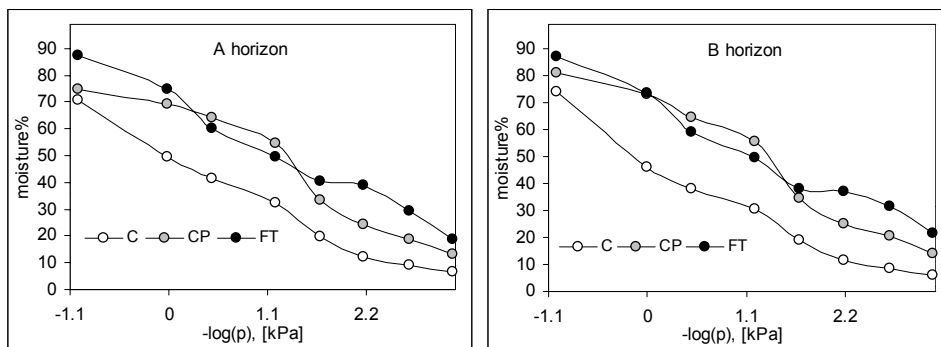


**Fig. 57.** Soil moisture vs. water potential dependencies for exemplary soil after peat addition and freezing-thawing cycles.

Remarkable role of organic matter in formation of structural properties of soils is illustrated in Fig. 58 on the example of acidic sandy forest soils. These soils, poor in clay minerals, exhibit very clear dependencies of pore characteristics on organic matter. Quantity of soil organic matter governs amounts of pores in all pore ranges and influences soil bulk density, which is a direct consequence of the soil pore system build-up.

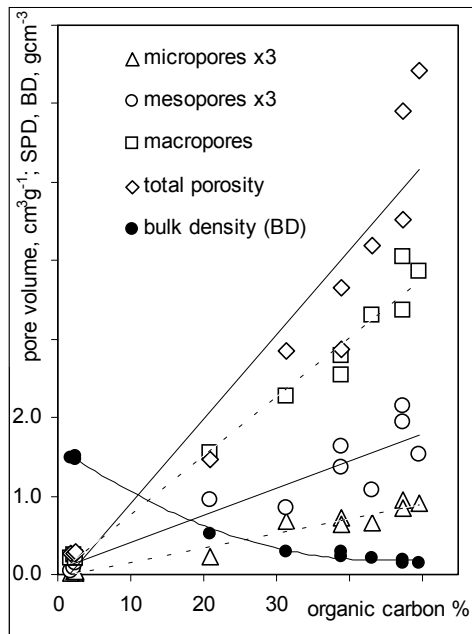


**Fig. 58.** Dependence of pore volumes and bulk density on the organic matter content for acidic sandy forest soils. Note: to better illustrate micro- and mesopore values, they are enlarged by a factor of 3.

Pore size in soils is important for biological life development. The pore neck diameters intervals correspond to pore necks that are considered inaccessible to bacteria (<0.3  $\mu\text{m}$ ), in which bacteria are protected from predation (0.3-3  $\mu\text{m}$ ), where protozoa can access their prey (3-30  $\mu\text{m}$ ), and where nematodes can access their prey (30-100  $\mu\text{m}$ ).

The clay content effect is attributed to the partial filling of micro- and mesopores by clays.

The drying and wetting cycles which occurred during the cultivation period lead to pore volumes redistribution which should be attributed to shrinking and swelling processes: water menisci produce forces between soil particles or micro-aggregates leading to aggregation increase during drying events and shrinking and swelling processes leading to micro-crack growth during wetting.

The total volume of the fine pores (measured from desorption isotherms) significantly decreases due to mechanical tillage, while the volume of the coarser pores (measured using MIP) increases. The changes in pore volumes are accompanied by changes of pore radii in the same direction. The decrease of fine pore radii may still be connected with organic matter oxidation and the removal of organic particles gluing smaller pores in mechanically tilled soils. Some rearrangement of soil structure on the level of microns, caused possibly by mechani-

cal disruption/reconstruction processes of soil aggregates, could result in increase of pore radii and volumes after mechanical tillage. A higher amount of very coarse (water conductivity) pores in no tilled soils as compared to mechanically tilled soils has been reported by many authors (Azooz et al., 1996; Douglas et al., 1981).

Soil pore system is markedly affected by biological life development. As an example mercury intrusion curves and pore size distribution functions of some soils before and after inoculation with a mixture of bacteria and fungi are shown in Fig. 59.

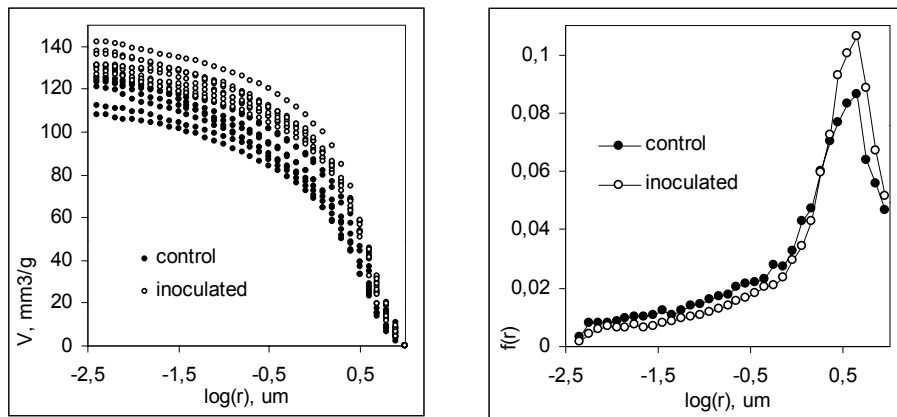


**Fig. 59.** Mercury intrusion curves (left side) and average pore size distribution functions (right side) of the soils inoculated with bacteria-fungi mixture.

The mercury intrusion curves show an increase of porosity of the inoculated soils in comparison to the control samples. From pore size distribution functions one can see that the increase of the relative amount of large pores occurred due to the bacteria-fungi activity.

Pore parameters are sensitive against addition of various compounds to soils that is illustrated on an example of the randomly – methylated cyclodextrins. Changes in micropore volumes of soils vs. RAMEB addition are illustrated in Fig. 60. Although RAMEB micropore volume ( $630 \text{ mm}^3 \text{ g}^{-1}$ ) is much higher than that of the soils, for clay reach-soils this hardly changes after RAMEB treatment. For clay-poor soils the micropore volume increases at higher RAMEB doses.

In general, small changes in pore size distributions measured from water vapor desorption isotherms (micropores) are noted for clay-rich soils at lower than maximum RAMEB doses, for which the fraction of large micropores (few tens of nanometers) increases on the expense of smaller micropores. In clay-poor soils

the fraction of large micropores starts to increase markedly at 1% RAMEB load. However, small changes in micropore size distribution of oil-contaminated clay poor soil were observed under all RAMEB concentrations applied suggesting that until significant portion of the added RAMEB reacts with the oil, the micropore sizes may not alter markedly. Moreover, this soil has very large micropores, which can be least sensitive on size changes. Small micropores in this soil are probably filled with the oil.

Changes in average micropore radius of the exemplary soils due to RAMEB addition are illustrated in Fig. 60. In general, an increase in the average micropore radius with increasing RAMEB load is seen. For soils having initial micropore radius lower than that of the RAMEB, one may explain the micropore radius increase as a simple effect of RAMEB addition. However, if the micropore radius of the initial soil is larger, the increase of micropore radius may be connected with filling of smaller pores by RAMEB, and/or by gluing their walls together. As a direct consequence of the smallest changes in micropore size distributions, changes in average micropore radius for oil polluted (S2) soil are the lowest.

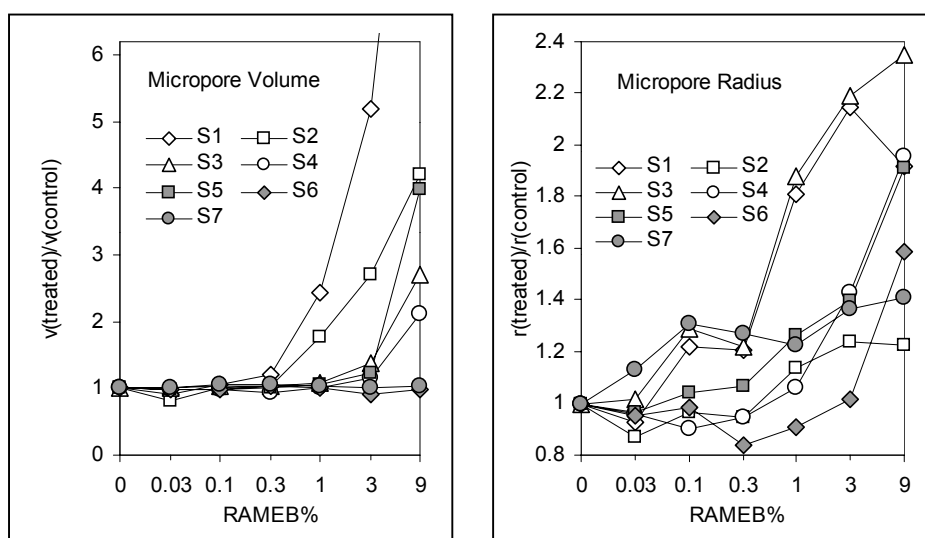


**Fig. 60.** Changes of micropore volumes (left) and average micropore radius (right) of selected soils under RAMEB treatment. The y-axis shows the ratio of the micropore volume of the soil + RAMEB to this of the control soil.

Addition of the cyclodextrin alters the larger pore build-up, as well as this can be observed from mercury intrusion porosimetry measurements (mesoporosity).

The mesopore volume of the RAMEB is lower than this of all but S1 and S2 soils. The oil-polluted S2 soil has very low mesopore volume ( $15 \text{ mm}^3 \text{ g}^{-1}$ ), even lower than the most sandy soil S1, suggesting that oil can fill the mesopores. The mesopore volume of all but S5 soils decreases after RAMEB addition, indicating that the aggregate structure of these soils becomes generally more compacted and/or the mesopores are filled with RAMEB (Fig. 61). The structure compaction and closing mesopores after RAMEB treatments may alter soil water capacity and ventilation. For S5 soil an increase in mesopore volumes is observed, which may be connected with a rearrangement of soil particles within aggregate network. Similar increase in mesopore volumes was observed for aggregates of pure illite.

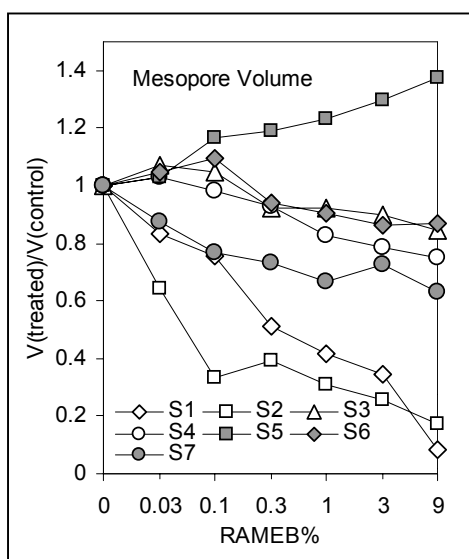


**Fig. 61.** Changes of mesopore volumes of selected soils under RAMEB treatment. The y-axis shows the ratio of the micropore volume of the soil + RAMEB to this of the control soil.

Mesopore size distribution functions (data not presented) have a single-peak shape for all but S2 and S6 soils. The maximum of this peak (i.e. largest fraction of pores) occurs at the pore radius  $R = 10 \mu\text{m}$  for S1,  $0.2 \mu\text{m}$  for S3 and S4,  $8 \mu\text{m}$  for S5, and  $1.6 \mu\text{m}$  for S7. Two broad peaks are found for S2 (at  $5$  and  $0.01 \mu\text{m}$ ) and two narrow peaks for S6 (at  $1$  and  $0.008 \mu\text{m}$ ). In general, RAMEB addition did not markedly change mesopore size distributions for all but two most sandy soils, S1 and S2. For S1 soil, the narrow peak at  $10 \mu\text{m}$  markedly broadened at 9% RAMEB addition thus resembling the pore size distribution function of the RAMEB itself; probably all mesopores in this soil were filled with 9% RAMEB. In the oil-contaminated S2 soil, fine ( $0.1 \mu\text{m}$ ) mesopores decreased sharply with increasing RAMEB concentration, and vanished completely at 1% RAMEB

addition. Similar decrease in fine (0.008  $\mu\text{m}$ ) mesopores occurred also for S6, however part of these pores remained at all RAMEB loads.

Average mesopore radii for most of the soils tend to increase with RAMEB dose (Fig. 62) that can reflect gluing of finer mesopore walls by the cyclodextrin. For two most sandy soils S1 and S2, the mesopore radius sharply decreases at 9% RAMEB: most mesopores are filled-up and properties of the RAMEB start to dominate. The increase in mesopore radius due to the RAMEB addition is the largest in oil-contaminated S2 soil that may be connected with rearrangement of organic matter architecture (this soil is very rich in organic material) and partially with entering RAMEB cavities by oil thus emptying the pores and cleaning their walls from oil layers.

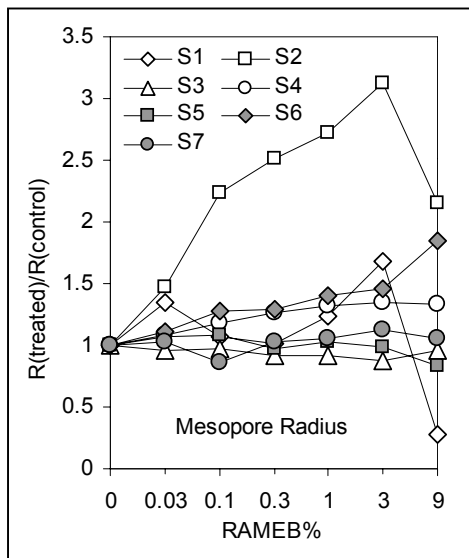


**Fig. 62.** Changes of average mesopore radius of selected soils under RAMEB treatment. The y-axis shows the ratio of the micropore volume of the soil + RAMEB to this of the control soil.

## CHAPTER 5.

### ADSORPTION ENERGY AND SURFACE HETEROGENEITY

Z. SOKOŁOWSKA, G. JÓZEFACIUK

Soil surface is extremely complex due to diversified mineral, organic and ionic composition of soil constituents. From energetic point of view, surface heterogeneity can be characterized by an adsorption energy distribution function. This function, showing amounts (fractions) of surface sites of different adsorption energies is estimated assuming that different surface sites bind adsorbate molecules with different forces (and energies) thus influencing adsorption pathways. Knowing that at the equilibrium the free energy is constant throughout the system, the energy of water vapor at a given relative vapor pressure is associated with adsorption energy on a given site, while the number of given adsorption sites is estimated from the amount adsorbed. From the distribution function one can easily derive an average adsorption energy that characterizes global energetic character of the surface (Cerofolini 1974).

Among various models used to find adsorption energy distribution function  $f(E)$ , (Ballard et al. 1997, Jaroniec et al. 1976, Jaroniec and Brauer 1986, Rudzinski et al. 1982) probably the simplest and reasonably accurate one is to model a complex surface as a combination of energetically homogeneous patches (or randomly distributed sites) having distinct energies. The schematic view of surface sites distribution on idealized and "natural surfaces is presented in Fig. 31.

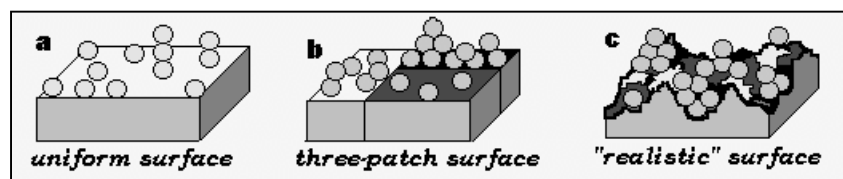


*Fig. 31. Surface sites distributions on idealized and "natural" surfaces .*

The total water vapor adsorption at a given pressure,  $a(p)$ , is expressed as a sum of local adsorptions  $a_i$  on different sites of energies  $E_i=(E_{a,i}-E_c)$ , where  $E_{a,i}$  is the adsorption energy of  $i$ -th site:

$$a(p) = \sum_{i=1}^n a_i(p, E_i), \quad (16)$$

where  $n$  is the assumed number of sites. Thus the total adsorption isotherm,  $\Theta(p)$ , is a sum of adsorptions on all sites,  $\Theta_i(p, E_i)$ , weighted by their fractions,  $f(E_i)$ :

$$\Theta(p) = a(p)/a_m = \sum_{i=1}^n a_i(p, E_i)/a_{m,i}(a_{m,i}/a_m) = \sum_{i=1}^n \Theta_i(p, E_i)f(E_i), \quad (17)$$

where  $a_{m,i}$  is the monolayer capacity of sites kind  $i$  and values of  $f(E_i)$  fulfill normalization condition:

$$\sum_{i=1}^n f(E_i) = 1. \quad (18)$$

The easiest way to solve Eq. (4) and find site fractions values,  $f(E_i)$ , goes through a condensation approximation, CA, (Harris 1968, 1969). This method is based on the replacement of the true local isotherm by a step-function. Every pressure value becomes associated with the corresponding value of the adsorption energy that provides the adsorption equal to one-half of the adsorption at infinite energy. Various models for description of local adsorption effects are used throughout the literature (Pachepsky et al 1995, Polubesova et al., 1997). Among the most convenient one applies the BET and the Aranovich (1992) models. The latter model provides direct relation of energy adsorption and energy of the gaseous adsorbent (both values are equal). Following the CA definition and using the Aranovich equation for describing local adsorption, the final CA formula is:

$$f(E_i) = [(1-x_{i+1})^{1/2} \Theta_{i+1}(E_{i+1}) - (1-x_i)^{1/2} \Theta_i(E_i)] / (E_{i+1} - E_i), \quad (19)$$

where  $E = -RT \ln(p_0/p)$ .

A schematic view on the results of analysis of the adsorption isotherms in terms of adsorption energy distribution functions for the idealized and “realistic” surfaces presented above is illustrated in Fig. 32.

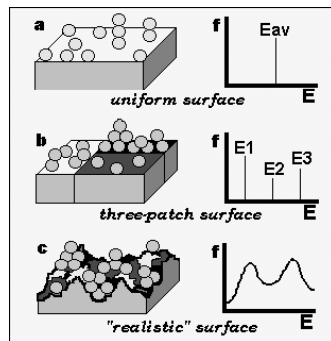


**Fig. 32.** Surface sites distributions on idealized and “natural” surfaces and corresponding adsorption energy distribution functions .

Having calculated  $f(E_i)$  values, the average water vapor adsorption energy of the whole adsorbent,  $E_{av}$ , can be calculated as:

$$E_{av} = \sum_{i=1}^n E_i f(E_i). \quad (20)$$

The adsorption energy values are usually expressed as dimensionless energies in the units of  $RT$  ( $E/RT$ ). To convert these dimensionless energies on SI units one shall use the following dependence  $E_a [\text{kJ mol}^{-1}] = -44 + 2.48E/RT$ , where  $-44 \text{ kJ mol}^{-1}$  is the condensation energy of water vapor and  $2.48 \text{ kJ mol}^{-1} = RT$  for  $T = 298 \text{ K}$ . The dimensionless energy equal to 0 holds for energy adsorption equal to the condensation energy of the vapor. To avoid infinities, the maximum adsorption energy should be placed. The maximum energy value in the condensation approximation should relate to the minimum value of the  $p/p_0$  applied. However, this value can be considered only as a first estimate of the maximum energy, because of the lack of experimental data at lower than minimum relative pressure. Therefore somewhat higher maximum energy is selected arbitrarily. If there are no sites with higher adsorption energies then the corresponding values of  $f(E)$  should be close or equal to zero. Condensation approximation allows for the detection of adsorbing sites differing not less than by 1 dimensionless energy unit. Because condensation approximation used for evaluation of energy distribution functions is considered to be precise only at 0 K (Rudzinski and Everett, 1991) one can suspect that the nitrogen adsorption distribution is more realistic because of low temperature of measurements. However, the energy distribution function characterizes the adsorbent-adsorbate system thus reflecting also different polarity of adsorbate molecules. Anyway, both adsorption energy distributions and especially this of the water vapor should be used rather for comparison between particular minerals and treatments and not as absolute surface characteristics.

## ADSORPTION ENERGY IN SOILS AND SOIL PROCESSES

Exemplary adsorption energy distribution functions for some soil minerals (Jozefaciuk and Bowanko 2002) calculated from nitrogen and water vapor adsorption are presented in Fig. 33. The nitrogen adsorption energy distribution functions of bentonite and zeolite have dominant high-energy peaks ( $-8$  to  $-6 E/RT$  range) showing that nitrogen adsorption is highly energetic. In water vapor adsorption energy distribution functions of these minerals lower energy peaks ( $-4$  to  $-2 E/RT$  range) dominate indicating that water molecules undergo adsorption with lower energies, which is consistent with the latter conclusion. The adsorption of nitrogen on biotite, illite and vermiculite is low energetic:  $0$  to  $-2 E/RT$  peak dominates and with increasing energy adsorption, consecutively smaller site fraction occurs. In water vapor energy distribution function of biotite,  $-6$  to  $-4 E/RT$

sites dominate. The shape of this function for illite is a mirror reflection of its nitrogen adsorption distribution function. For vermiculite both water and nitrogen adsorption energy distributions are similar, however very low fraction of high energy ( $-8$  to  $-4$   $E/RT$ ) sites occurs for water adsorption. Nitrogen adsorption distribution function for kaolin is bimodal with two peaks of  $-6$  to  $-4$  and  $-2$  to  $0$   $E/RT$  sites, whereas water adsorption reveals higher inputs of lower energy peaks.

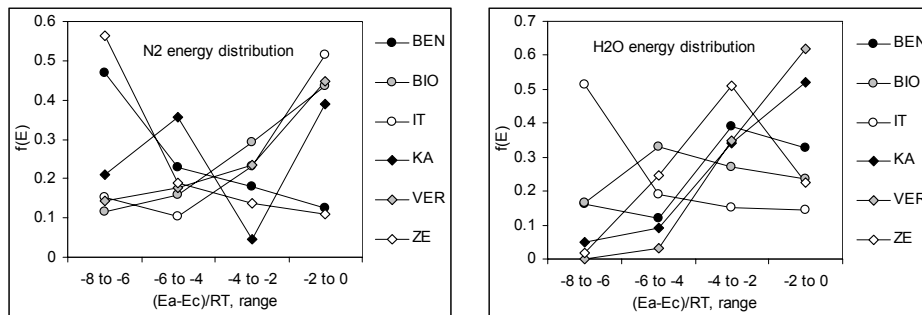


**Fig. 33.** Exemplary adsorption energy distribution functions for some soil minerals calculated from nitrogen (left) and water vapor(right) adsorption isotherms

Exemplary adsorption energy distribution functions for soils calculated from water vapor adsorption isotherms are presented in Fig. 34.

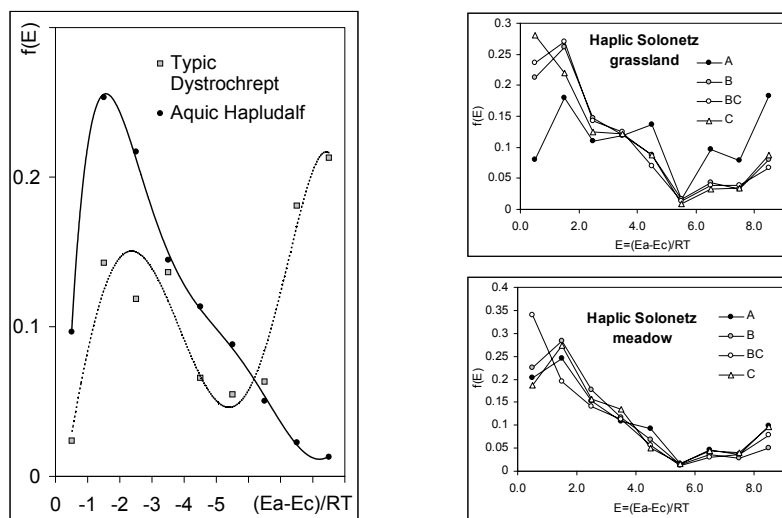


**Fig. 34.** Exemplary water vapor adsorption energy distribution functions for different soils (soils on left- upper A horizons, on right – whole profiles).

The typical adsorption energy distribution functions for brown and podzolic soils are similar to this illustrated for Typic Dystrachrept (Poland, Lublin region). The distribution functions are of a two-peak character, showing the presence of two dominant surface sites of high and of low adsorption energies. The surfaces of clay rich yellow-red soils (Korea) are low energetic with one-peak located at low adsorption energies. Energy distribution functions can differ or not with the depth of the soil as this is illustrated for salt affected soil profiles.

High energy centers can arise from high amount of polar, hydrophilic groups on mineral or organic surfaces. Low energy centers, except of their occurrence on less polar and hydrophobic groups of soil constituents, can be due to the effect exchange ions. Monovalent sodium cations bind water with lower energy than the divalent ones such as Ca and Mg. The energy distribution function of organic matter of humic character is usually skewed in direction of lower energies what can be concluded from Sokolowska et al. (1993, 1997), which reflects high amounts of less polar or apolar groups. Fulvic organic matter in has more polar character than humic organic matter.

Average adsorption energy markedly changes under acid and alkali conditions that for selected soil minerals is illustrated in Fig. 35.

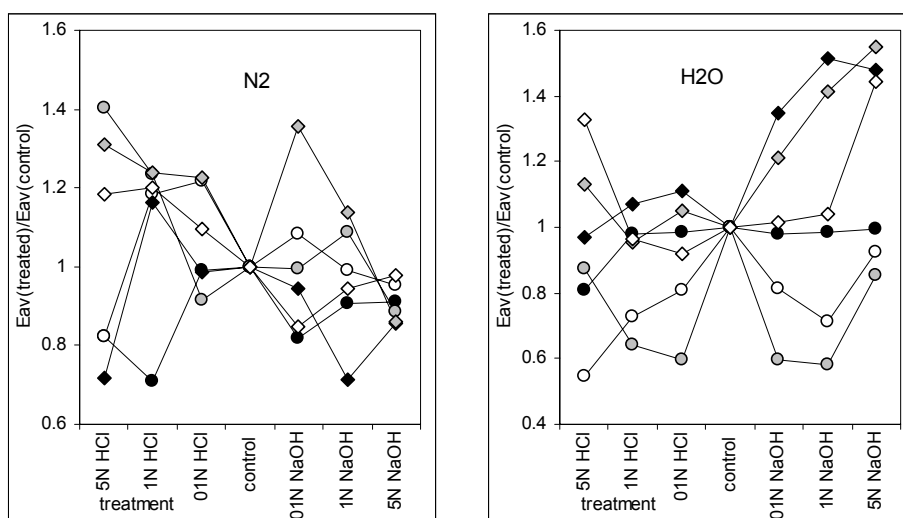


**Fig. 35.** Relative changes in average adsorption energy of selected soil minerals under acid and alkali conditions (laboratory experiment). Abbreviations as in Fig. 33.

With the increase of acid treatment concentration the average water adsorption energy increases for biotite and zeolite and decreases for bentonite, illite and kaolin, whereas that of the nitrogen increases in most cases. The increase in ad-

sorption energy may be due to the formation of cracks and voids on the attacked surfaces. The decrease in adsorption energy may be due to the removal of surface impurities. Silicon oxides, products of mineral lattice destruction, have also low adsorption energy (Gregg and Sing, 1967). Changes of the nitrogen adsorption energies under alkali treatment appear to follow the opposite direction than the water adsorption energies, which can reflect different polarity of the adsorbates and different forces involved in their interactions with surfaces.

Changes in nitrogen and water adsorption energy distribution functions under acid and alkali conditions appear to exhibit no common tendencies for all minerals that is illustrated in Fig. 36. for selected energetic sites (0-2 and 2-4 E/RT).

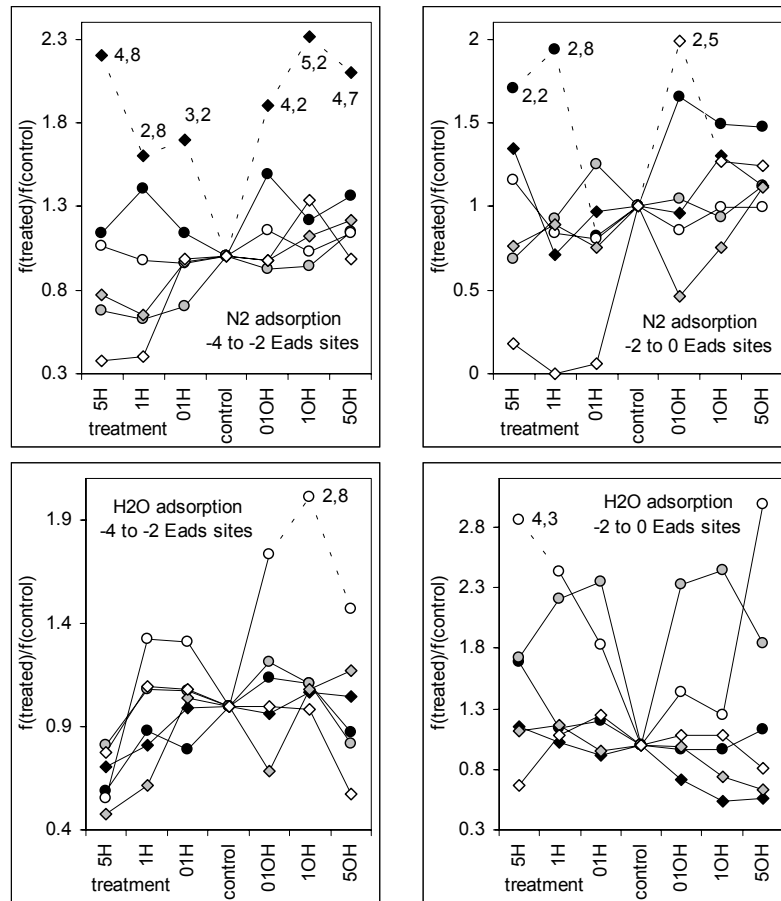


**Fig. 36.** Relative changes in fractions in various adsorption sites of selected soil minerals under acid and alkali conditions (laboratory experiment). Abbreviations as in Fig. 33.

Under acidification, soil minerals should be generally less polar than under with alkaline conditions, due to formation of low energetic silica from mineral lattice destruction. Minerals in alkaline media should be more polar due to eventual formation of finely dispersed and highly energetic Mg or Fe oxide precipitates and/or removal of outer silica sheets from mineral lattices leaving alumina sheets, more polar than silica. Together with producing chemically different surface groups and energetic centers in individual minerals, acid and alkali attack may change the geometrical surface features, which can affect the adsorption energies and site distribution functions. Chemically identical surfaces may exhibit different adsorption energies depending on their shape e.g. by overlapping of force field between fine pore walls thus increasing adsorption potential. Different directions and/or intensities in changes in surface/micropore structure for individual minerals may cause lacking of general patterns in the behavior of distinct adsorption sites observed for the minerals.

More uniform changes in average adsorption energy are observed in soils due to changes in soil reaction that is illustrated in Fig. 37 for various soils.

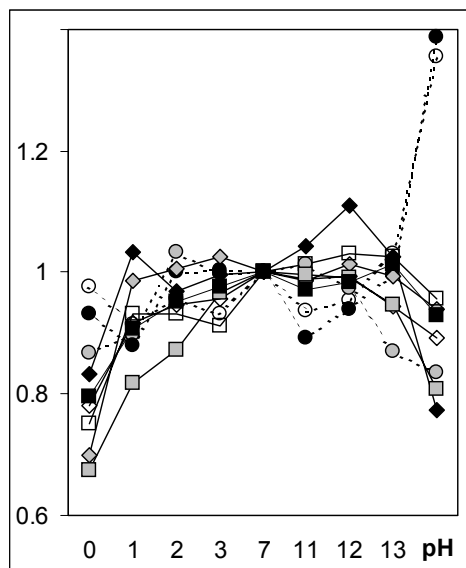


**Fig. 37.** Relative changes in average adsorption energy of selected soil minerals under acid and alkali conditions in a laboratory experiment. Dashed lines – clay rich soils, solid lines – clay poor soils

The average adsorption energy of soils decreases in general with the rise of the concentration of both treatments, however a slight initial increase is observed for a few soils. The decrease of the adsorption energy under acid treatment may be addressed to new silica oxide surfaces, having large but low energetic surface. However, under alkaline treatment the silica oxides are better soluble. The ad-

sorption energy decrease under alkaline conditions may be connected with the fact that during the consecutive removal of organic matter the remaining organic material has more hydrophobic character and less adsorption energy (Jozefaciuk et al., 1996). For two of the illustrated soils, the marked increase of average adsorption energy occurs at the highest concentration of the added base. These two soils are rich in iron oxides, which are resistant in alkaline environment. Cleaning of iron oxide surfaces and their peptization in alkali may be due to both surface area and adsorption energy increasing.

The observed changes in average adsorption energy vs. pH are caused by variations in the surface energetic build-up, which is characterized by adsorption energy distribution functions. Similarly as for the minerals, surface adsorption centers of various energies change in various direction during soil acidification and alkalization processes that is illustrated in Fig. 38.

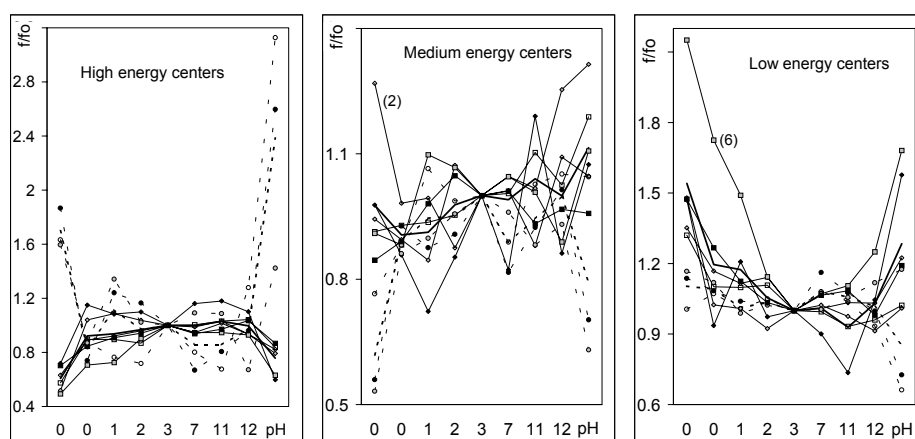


**Fig. 38.** Changes in surface adsorption centers of various energies during changes in soil pH in a laboratory experiment. Solid lines – clay poor soils, dashed lines – clay rich soils.

The fractions of high energy centers decrease under both treatments for clay poor soils, however for clay rich soils a slight initial increase is observed. For clay rich soils the marked increase of the amount of high energy sites occurs after the treatments with the highest concentrations of the reagents. However, taking into account the very low input of these sites in initial soils even as high rise in their relative amount does not change the overall shape of the distribution function. The fraction of the medium energy centers decrease in general under acid treatment, what is more pronounced for clay rich soils. The alkaline treatment causes in general the increase of medium energy sites amount for clay poor soils and its decrease for clay rich soils. Both treatments lead to the increase of low energy

centers for all but two soils, for which the alkaline treatment causes the decrease of low energy sites. This is difficult to attribute various energy sites to the presence of particular soil components. However the increase of the low energy centers in acid treatment is due most probably to the forming of silica oxides and in alkali treatment this can be due to the exposure of more hydrophobic organic surfaces.

Adsorption energy and its distribution are good indicators of the effect of tillage on soils. Mechanical tillage treatments lead to a significant decrease of water vapor adsorption energy in comparison to no tilled soil (Jozefaciuk et al. 2001). The decrease in average adsorption energy (average data from 7 points) in the following order: NT no tillage (-3,66) > D+L disking + loosening (-3,49) > P+L ploughing + loosening (-3,46) > D disking (-3,38) > P ploughing (-3,37).

Changes in adsorption energy distribution functions at the above tillage treatments are illustrated in Fig. 39.

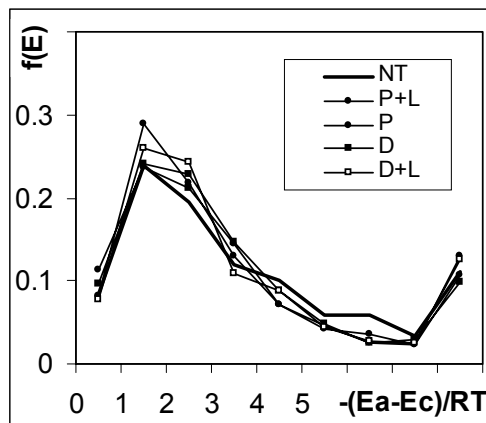


**Fig. 39.** Adsorption energy distribution functions at various tillage treatments (abbreviations in the text).

The shape of this function is similar for all tillage treatments: low energetic adsorption centers of  $E=-(Ea-Ec)/RT$  around 2-3 dominate and a smaller fraction of high energetic centers occurs at a scaled energy equal to 8.5 units. For tilled soils an increase of the fraction of low energetic adsorption centers (0-4 scaled energy range) and a decrease of medium energy centers (5-8 E range) occurs.

The decrease in average adsorption energy indicates that water binding forces become lower. Therefore soil water may be more available for plants, despite its amount decrease which can be concluded from decrease in surface area.

Lower adsorption energy in saline and sodic soils as compared to not salt affected soils may be due to lower hydration energy of sodium than the other ions (Toth and Jozefaciuk 2002).

In saline soils a clear relation of the average adsorption energy and soil sodium adsorption ratio is noted that is illustrated in Fig. 40. for a range of Hungarian salt affected soils. Average adsorption energy decreases logarithmically with the increase of sodium adsorption ratio.

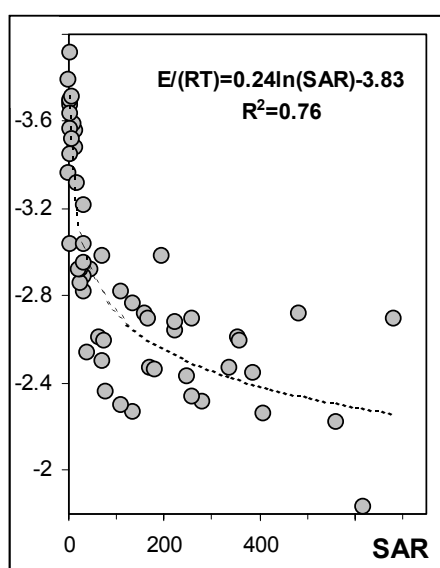


*Fig. 40. Relation of the average adsorption energy and sodium adsorption ratio(SAR) for a range of Hungarian salt-affected soils.*

Cyclodextrins, polysaccharides increasingly used in soil decontamination from organic hydrophobic compounds alter the energetics of water interactions with soil as this can be deduced from water vapor adsorption patterns. The water vapor sorption in RAMEB is a low energy process, which can be seen from the water vapor sorption energy distribution function. The highest amount of low energy sites is present. Fractions of high- and medium-energy sites are small. The shape of this function reflects that water molecules interact with cyclodextrins practically only via hydrogen bonds, with energies close to water-water interactions (condensation energy).  $\beta$ -Cyclodextrin crystallizes with 6.5 water molecules in the internal cavity, involved in a well-defined network of hydrogen bonds. The sorption energy of the internal waters should be low also. However, for the minerals enriched with CD, an increase of higher energy centers and a decrease of the lower energy ones with RAMEB concentration increase is ob-

served. Strong interactions of the RAMEB and minerals apparently affect the average adsorption energy patterns (Fig. 41) as well. Instead of an adsorption energy decrease, as could be expected because of the very low water vapor sorption energy of the RAMEB, the adsorption energy of the minerals increases after RAMEB addition, consistent with the changes in adsorption energy distribution functions described above. The decrease of the average adsorption energy for kaolin (KA) is noted at the extreme RAMEB content, which can be related to the overload of RAMEB.

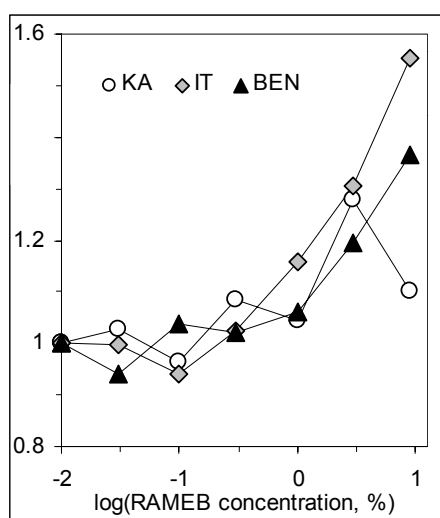


**Fig. 41.** Effect of different doses of randomly methylated  $\beta$ -cyclodextrin on adsorption energy of soil minerals. KA – kaolin, IT – illite, BEN – bentonite.

Despite water vapor sorption on RAMEB is low energetic, for soils at low RAMEB doses an increase in the relative amount of higher energy centers and a decrease of the lower energy centers is observed also, reflecting strong interactions of RAMEB and soil constituents. This tendency extended towards high RAMEB doses for clay-rich soils, while for clay-poor soils low energy centers started to dominate above c.a. 1% RAMEB dose.

Changes in energy distribution patterns affect average adsorption energy values what is illustrated in Fig. 42. Instead of adsorption energy decrease, as expected because of very low water vapor sorption energy of the RAMEB, the adsorption energy of all soils increases at low RAMEB concentrations. For clay-rich soils this tendency holds in all RAMEB concentration range. For clay-medium soils at 9% RAMEB the adsorption energy starts to decrease. Similarly, for clay-poor soils, the initial increase in average adsorption energy is followed by its drop at higher RAMEB doses, which can be related to the overload of RAMEB.

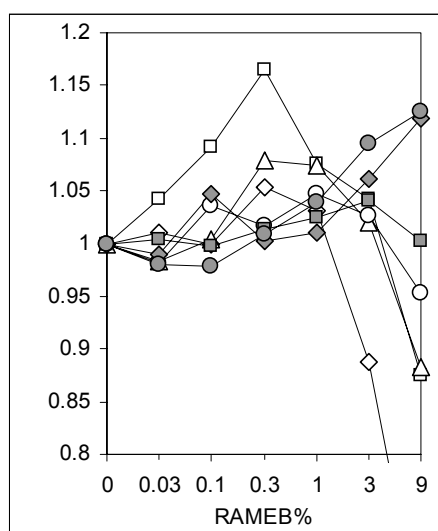


**Fig. 42.** Effect of different doses of randomly methylated  $\beta$ -cyclodextrin on water vapor adsorption energy of soils. Rhombs: sandy soils, triangles: soils of low clay content, squares: clay rich soils.

The adsorption energy increase indicates that the overall water binding forces become higher after cyclodextrin treatments that may reduce the amount of water available for soil biota. However, the increase in interaction energy of polar water molecules with RAMEB treated soils show that the soil surface tends to be less hydrophobic that may result in enhanced desorption of nonpolar contaminants and their inclusion into the cyclodextrin.

Average adsorption energy is appears to be correlated with many soil properties, as this is shown in Table 4.

**Table 4.** Correlation coefficients of linear regression between the average adsorption energy ( $H_2O$  and  $N_2$ ) and selected properties of mineral soils (482 samples)

	Fraction %		OM %	CEC	Exchangeable cations, $cmol\ kg^{-1}$				
	<0,02	<0,002			Hh	Ca	Mg	K	Na
Loesial soils									
$E(N_2)$	0,275	0,397	<b>-0,655</b>	0,271	<b>-0,541</b>	0,269	0,321	-0,367	0,119
$E(H_2O)$	<b>-0,532</b>	<b>-0,830</b>	0,594	<b>-0,840</b>	<b>0,591</b>	<b>-0,826</b>	<b>-0,861</b>	0,180	-0,443
Clayey soils									
$E(N_2)$	0,470	<b>0,676</b>	0,171	0,269	-0,047	0,079	<b>0,653</b>	0,389	0,407
$E(H_2O)$	-0,341	<b>-0,532</b>	-0,068	-0,268	-0,126	-0,118	<b>-0,549</b>	-0,372	-0,256
Silty soils									
$E(N_2)$	<b>0,582</b>	<b>0,502</b>	-0,351	0,243	-0,070	0,214	0,458	0,079	0,108
$E(H_2O)$	-0,274	-0,306	0,211	-0,204	0,394	-0,201	-0,233	0,183	-0,148

**Table 4.** Continued

	Fraction %		OM %	CEC	Exchangeable cations, cmol kg <sup>-1</sup>				
	<0,02	<0,002			Hh	Ca	Mg	K	Na
Loamy soils									
<i>E</i> (N <sub>2</sub> )	<b>0,610</b>	<b>0,594</b>	-0,115	0,485	0,082	0,428	<b>0,560</b>	0,034	0,427
<i>E</i> (H <sub>2</sub> O)	<b>-0,544</b>	<b>-0,565</b>	0,014	<b>-0,538</b>	0,100	<b>-0,519</b>	-0,431	0,056	-0,383
Sandy soils									
<i>E</i> (N <sub>2</sub> )									
<i>E</i> (H <sub>2</sub> O)	-0,127	-0,186	-0,151	-0,092	0,048	-0,074	-0,306	0,061	0,014
Brown loamy soils									
<i>E</i> (N <sub>2</sub> )	<b>0,627</b>	<b>0,567</b>	-0,349	0,471	0,391	<b>0,604</b>	0,088	0,424	0,480
<i>E</i> (H <sub>2</sub> O)	<b>-0,614</b>	<b>-0,600</b>	0,433	-0,236	<b>-0,549</b>	-0,464	-0,174	-0,399	<b>-0,581</b>
Loamy podzols									
<i>E</i> (N <sub>2</sub> )	<b>0,772</b>	<b>0,724</b>	-0,144	<b>0,566</b>	0,110	<b>0,503</b>	<b>0,770</b>	-0,017	0,442
<i>E</i> (H <sub>2</sub> O)	<b>-0,625</b>	<b>-0,654</b>	0,123	<b>-0,513</b>	0,112	-0,484	<b>-0,542</b>	0,262	-0,426
Loamy black earths									
<i>E</i> (N <sub>2</sub> )	<b>-0,805</b>	<b>-0,751</b>	<b>0,699</b>	<b>-0,805</b>	0,483	<b>-0,731</b>	<b>-0,778</b>	0,277	<b>-0,558</b>
<i>E</i> (H <sub>2</sub> O)	0,449	0,401	-0,486	<b>0,532</b>	-0,174	<b>0,509</b>	<b>0,505</b>	-0,045	-0,109

Average adsorption energy, as well as energy distribution functions may be good indicators of the intensity of many soil processes (Sapozhnikov 1985).

## CHAPTER 4.

### SOIL SURFACE AREA

Z. SOKOŁOWSKA, G. JÓZEFACIUK

Surface area is recognised to play complementary part to porosity in adsorption phenomena for a vast range of solids.

Different kind of the surface area may be found in soils (Petersen et al. 1996). The *geometric* surface area is calculated, knowing shapes and dimensions of representative soil particles. *The internal surface area* is the surface inter walls of the microcapillares (the term "internal surface" is usually restricted in its application to those cavities, which have an opening to exterior of the grains). *The external surface area* is defined as the sum of geometric and internal surface area. *The interlayer surface area* - the surface of interlayer walls of minerals type as montmorillonite. *The total surface area* is the sum of the external, internal and the surface area of organic matter (Dechnik and Stawinski 1973).

The specific surface area of a soil sample is combined surface area of all the particles in the sample as determined by some experimental technique and expressed per unit mass of the sample. As its definition implies, term *specific surface area* is an operational concept.

The numerical value found for a given soil depends which experimental method has been used. There are two principal reasons for this very important characteristic. First, the properties of the solid surfaces in soil can often be altered during preparation of the sample for a surface measurement. Secondly, if a surface reaction is involved in the measurement of the specific surface area, the data obtained reflect only the characteristics of the surface functional groups that participate in the reaction, and provides only information about the solid surfaces that were reactive under the condition of the measurement.

#### ***Methods of measure of surface area***

The principal physical methods for measuring specific surface areas of soils are electron microscopy and X-ray diffraction.

The most of methods are based on measurement of adsorption of polar and nonpolar gases or vaporous. The adsorbable compounds used to determine specific surface area are chosen on the basis of their molecular properties. Nitrogen is commonly used as the adsorbate because it interacts weakly with a broad array of

surface functional groups and therefore permits for the determination of exposed area of soil. The limitation on the use of this adsorbate is stereochemical. Relatively large radius of N<sub>2</sub> molecule prevents it from interacting with the surface functional groups occluded in very small void spaces. Polar adsorbates are water vapor, ethylene glycol or ethylene glycol monoethyl. Typical non polar adsorbates are nitrogen, argon, krypton.

In the present paper we shall consider the application of the physical adsorption of gases for the estimation of the specific surface area of soils. The starting point is the adsorption isotherm, and the problem reduces to determination of the specific surface area, or the *monolayer capacity* of the adsorbent from the isotherm by mathematical analysis. The monolayer capacity is defined as the quantity of an adsorbate which can be accommodated in a completely filled, single layer of molecules on the surface of the solid. The surface area,  $S$ , is directly proportional to the monolayer capacity  $N_m$ , and the relationship between these two quantities is given by the equation:  $S = N_m \times \omega$ , where  $\omega$  is the area occupied per molecule of the adsorbate in a completely filled monolayer. To find the value of  $N_m$  from an isotherm it is necessary to interpret the isotherm in a quantitative manner. A number of different theories have been proposed for the interpretation of adsorption data. The best known and probably the most frequently used theory, is that proposed by Brunauer, Emmett and Teller (BET). It leads to the equation called *the BET equation*, which has proved remarkably successful in the calculation of specific surface from the isotherms of the type II.

#### ***Calculation the specific surface area from adsorption data***

The surface area of soil samples was evaluated from adsorption-desorption isotherms in the BET range of relative water vapor pressure, using the Brunauer-Emmett-Teller (BET) method. The first step in the application of the BET method is to obtain the monolayer capacity ( $N_m$ ) from the BET plot in the range of relative pressures  $0 < p/p_0 < 0,35$ :

$$\frac{x}{N(1-x)} = \frac{1}{C_{BET} N_m} + \frac{(C_{BET} - 1)}{C_{BET} N_m} x \quad (12)$$

where  $x = p/p_0$  is the relative pressure of water vapor,  $N$  is the amount of adsorbed water vapor, and  $C_{BET}$  is a constant.

According to this, when  $x/N(1-x)$  is plotted against  $p/p_0$  a straight line should result with slope  $s = (C_{BET} - 1)/N_m C_{BET}$  and intercept  $i = 1/N_m C_{BET}$ . Solution of the two simultaneous equations gives  $N_m$  and  $C_{BET} - N_m = 1/(s+i)$  and  $C_{BET} = (s/i)+1$ .

The above described procedures of calculating surface areas from Langmuir and BET plots are illustrated in Fig. 21.

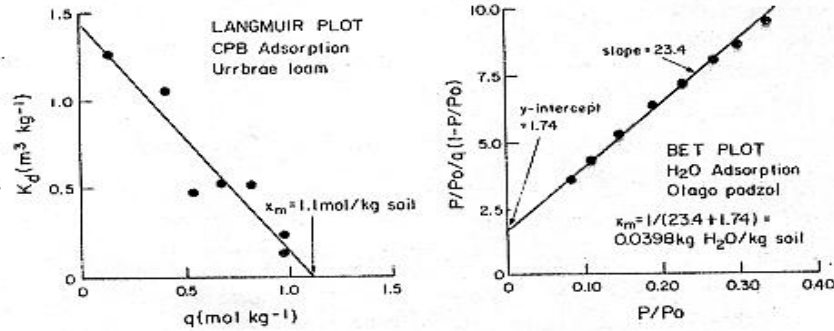


Fig. 21. The calculate of the value  $N_m$  (monolayer capacity) from Langmuir and BET plot

The second step is to calculate the surface area from the dependence:

$$S = N_m \times M^L \times L \times \omega, \quad (13)$$

where  $L$  is the Avogadro number ( $6.02 \times 10^{23}$  molecules per mole),  $M$  is the molecular weight of water (gram per mole) and  $\omega$  is the molecule cross-sectional area ( $10.8 \times 10^{-20}$  m<sup>2</sup> for water molecule). If  $N_m$  is expressed in grams of adsorbate (water) per gram of solid the specific surface area  $S$  (m<sup>2</sup>g<sup>-1</sup>) is estimated from the monolayer capacity as:

$$S = 3612 \times N_m. \quad (14)$$

In order to use of any of these formulae, it is necessary to know the value of the molecule cross-sectional area,  $\omega$ . Emmett and Brunauer proposed that  $\omega$  be calculated from the density  $\rho$  of the adsorbate in the ordinary liquid or solid form. This leads to the formula:

$$\omega = f(M/\rho N)^{2/3} \times 10^{16} \quad (15)$$

where  $M$  is molecular weight of adsorbate,  $N$  is Avogadro's constant,  $f$  is a packing factor and  $\rho$  is the mass density of bulk liquid. With hexagonal close packing at density of bulk liquid phase the value of  $f$  is 1.091 and if  $\rho$  is expressed in kilograms per cubic meter  $\omega$  is expressed in square nanometers. For nitrogen as adsorbate at  $-195^\circ$  the value  $\omega = 0.162$  nm<sup>2</sup> ( $16.2 \text{ \AA}^2$ ). Adsorption of water vapor is complicated in that it is highly specific and it appears that the application of BET equation to water isotherms, in many cases, has no real validity. Early work indicated that the value of the molecule cross-sectional area is  $10.6 \text{ \AA}^2$  ( $0106 \text{ nm}^2$ ). The work of Harkins and Jura showed that it was necessary to adjust  $14.8 \text{ \AA}^2$ .

## SURFACE AREA IN SOILS AND SOIL PROCESSES

Surface area is highly sensitive indicator of various processes occurring in soils: organic matter accumulation, leaching and oxidation, soil acidification, alkalization, silica accumulation, wetting-drying cycles and many others. Surface area is well correlated with many soil properties, as this is shown in Table 1.

**Table 1.** Correlation coefficients of linear regression between the specific surface area (H<sub>2</sub>O and N<sub>2</sub>) and selected properties of mineral soils (482 samples)

	Fraction		OM	CEC	Exchangeable cations				
	<0.02	<0.002			Hhydr.	Ca	Mg	K	Na
soils formed from loess									
S(N <sub>2</sub> )	0.419	<b>0.705</b>	<b>-0.550</b>	<b>0.589</b>	<b>-0.555</b>	<b>0.570</b>	<b>0.646</b>	-0.197	0.263
S(H <sub>2</sub> O)	<b>0.701</b>	<b>0.976</b>	0.395	<b>0.936</b>	-0.309	<b>0.906</b>	<b>0.920</b>	0.098	<b>0.738</b>
soils formed from clay									
S(N <sub>2</sub> )	<b>0.720</b>	<b>0.656</b>	<b>-0.503</b>	<b>0.542</b>	0.062	0.400	<b>0.641</b>	0.312	<b>0.553</b>
S(H <sub>2</sub> O)	<b>0.627</b>	<b>0.832</b>	-0.068	<b>0.579</b>	-0.178	0.357	<b>0.891</b>	<b>0.666</b>	0.480
soils formed from silt									
S(N <sub>2</sub> )	<b>0.547</b>	<b>0.679</b>	-0.251	0.067	0.268	0.007	<b>0.612</b>	0.030	-0.125
S(H <sub>2</sub> O)	<b>0.696</b>	<b>0.875</b>	<b>0.865</b>	<b>0.535</b>	0.084	0.478	<b>0.901</b>	0.303	0.270
soils formed from loam									
S(N <sub>2</sub> )	<b>0.805</b>	<b>0.792</b>	-0.332	<b>0.666</b>	-0.011	<b>0.606</b>	<b>0.712</b>	0.019	0.479
S(H <sub>2</sub> O)	<b>0.936</b>	<b>0.902</b>	0.018	<b>0.667</b>	0.203	<b>0.568</b>	<b>0.838</b>	0.171	<b>0.559</b>
soils formed from sand									
S(N <sub>2</sub> )	<b>0.561</b>	<b>0.641</b>	0.491	0.425	0.278	0.404	<b>0.521</b>	0.191	0.049
S(H <sub>2</sub> O)	<b>0.589</b>	<b>0.770</b>	<b>0.607</b>	<b>0.700</b>	0.358	<b>0.655</b>	<b>0.751</b>	0.252	0.146
brown soils formed from loam									
S(N <sub>2</sub> )	<b>0.732</b>	<b>0.677</b>	-0.422	0.430	<b>0.538</b>	<b>0.653</b>	0.153	0.464	<b>0.615</b>
S(H <sub>2</sub> O)	<b>0.937</b>	<b>0.824</b>	-0.168	<b>0.579</b>	<b>0.537</b>	<b>0.829</b>	0.357	<b>0.637</b>	<b>0.667</b>
podzolic soils formed from loam									
S(N <sub>2</sub> )	<b>0.827</b>	<b>0.872</b>	-0.255	<b>0.727</b>	-0.116	<b>0.687</b>	<b>0.790</b>	-0.216	<b>0.528</b>
S(H <sub>2</sub> O)	<b>0.931</b>	<b>0.954</b>	0.078	<b>0.624</b>	0.238	<b>0.548</b>	<b>0.902</b>	-0.048	<b>0.535</b>
black earth formed from loam									
S(N <sub>2</sub> )	<b>0.940</b>	<b>0.949</b>	<b>-0.530</b>	<b>0.826</b>	-0.147	<b>0.710</b>	<b>0.947</b>	0.319	0.395
S(H <sub>2</sub> O)	<b>0.943</b>	<b>0.973</b>	-0.399	<b>0.669</b>	0.088	0.491	<b>0.925</b>	0.388	0.267
brown soils formed from sand									
S(H <sub>2</sub> O)	<b>0.591</b>	<b>0.769</b>	<b>0.594</b>	0.461	0.160	0.452	<b>0.517</b>	0.163	0.151
podzolic soils formed from									
S(H <sub>2</sub> O)	<b>0.542</b>	<b>0.876</b>	<b>0.777</b>	<b>0.620</b>	<b>0.879</b>	0.398	<b>0.940</b>	0.263	-0.055

Fraction = particle fraction of defined size, OM = organic matter content, CEC = cation exchange capacity. Significant correlations are written in bold.

In general, surface area of soils from organic farming is significantly higher than that obtained for that same soils originating from conventional cultivation (Sokolowska et al. 1999) as this is shown in Table 2.

**Table 2.** The BET surface area ( $\text{m}^2\text{g}^{-1}$ ) for soil with different crop and sampling time

Crop	Sampling period								
	II III		I II III			I II III			
	1996		1997			1998			
Barley, organic farming	24.7	20.4	16.3	14.6	16.5	23.7	23.0	18.4	
Barley, conventional	18.9	17.4	13.0	11.6	10.8	13.3	21.2	15.5	
Winter wheat, organic farming	25.3	17.7	25.6	20.3	21.3	17.7	21.7	16.2	
Winter wheat, conventional	13.7	8.2	13.0	12.4	8.5	14.2	12.3	15.1	
Red clover, organic farming	n.d	13.3	17.8	11.8	12.3	13.2	13.2	14.5	

Abbreviations: I - seedlings; II - stem elongation stage; III - after harvest;

Cereal species do not influence significantly the soil specific surface area. Note that similar results were found for conventional cultivation system. Specific surface area for red clover was almost the same as that evaluated for cereals in the conventional cultivation system (Table 3).

**Table 3.** Average surface area ( $S_{\text{aver.}}$ ) and its standard deviation ( $\sigma$ ) from adsorption measurements

Cropping system and method of cultivation	$S_{\text{aver.}} [\text{m}^2\text{g}^{-1}]$	$\sigma$
Barley organic farming	19.7	3.8
Barley conventional farming	15.2	3.7
Winter wheat organic farming	18.3	5.7
Winter wheat conventional	12.2	2.5
Red clover organic farming	13.7	2.0
Barley + winter wheat organic farming	20.2	3.6
Barley + winter wheat conventional farming	13.7	3.4

Abbreviations: I - seedlings; II - stem elongation stage; III - after harvest;

The sampling period does not practically influence adsorption of water vapor and the obtained surface areas. The amount of adsorbed water vapor on the soil samples depends on the method of the soil cultivation.

Mechanical tillage treatments lead to a significant decrease of surface area in comparison to no tilled soil (Jozefaciuk et al. 2001). The decrease in surface areas

(average data from 7 sampling points) in the order: no tillage ( $64,4 \text{ m}^2\text{g}^{-1}$ ) > ploughing + loosening ( $59 \text{ m}^2\text{g}^{-1}$ ) > disking ( $54,3 \text{ m}^2\text{g}^{-1}$ ) > disking + loosening ( $44,9 \text{ m}^2\text{g}^{-1}$ ) > ploughing ( $42,8 \text{ m}^2\text{g}^{-1}$ ).

Surface areas of soil minerals are different. Usually the literature data refer to the surface area of the minerals calculated using the BET model. The Aranovich model gives surface areas around 25% larger. Throughout the literature the lowest surface areas are reported for kaolinites: from 5 to 25 (nitrogen) and 10 to 30  $\text{m}^2\text{g}^{-1}$  (water). Surface areas of illites from 50 to 200, of zeolites from 100 to 400 and for vermiculites up to 700  $\text{m}^2\text{g}^{-1}$  are found (Newman 1987 Moise et al. 2001, Volzone et al. 1999). For smectites 110-550  $\text{m}^2\text{g}^{-1}$  surface areas are found from water adsorption and 80-180  $\text{m}^2\text{g}^{-1}$  from nitrogen adsorption, however as low nitrogen surface area as 14  $\text{m}^2\text{g}^{-1}$  was found in a montmorillonite extracted from Kuzmice bentonite (Czech Republic) by Tombacz et al (1998). Extremely high surface areas of smectites, around 800  $\text{m}^2\text{g}^{-1}$  are measured using ethylene glycol monoethyl ether (EGME) sorption, being close to the value determined from the crystallographic cell dimensions and weight (Van Olphen 1997).

Frequently the nitrogen surface area has been interpreted as the “external” surface, and the water surface area as the “total” one, including the external and internal (interlayer) surfaces. In most cases the total surface area exceeding the external one is measured. For soil minerals the water surface area is higher than the nitrogen surface area: for bentonite and zeolite about 10 times, for vermiculite more than 25 times, whereas for the other minerals around 2-3 times.

Acid or alkaline environments modify surface areas of soils and their constituents (Jovanovic and Janackovic 1991; Jozefaciuk 1998). HCl treatment of two bentonites lead up to 5-fold increase of the surface area of the raw materials (Christidis *et al.*, 1997). Dekany *et al.* (1999) observed that as the amount of iron and aluminum extracted from the acid treated sepiolite increased, the specific surface area of the sample increased also. Srasra and Trabelsi-Ayedi (2000) reacted a glauconite with boiling 3 mole  $\text{dm}^{-3}$  HCl solution finding that the specific surface increased with the activation time. Natural phillipsite treated with orthophosphoric acid increased the surface area with increasing concentrations of the acid (Notario *et al.*, 1995). A palygorskite was treated with 1.0, 3.0, 5.0 and 7.0 mole  $\text{dm}^{-3}$  solutions of HCl for 1 hour under reflux by Suarez Barrios *et al.* (1995). An important increase in the specific surface area was observed during the treatments, reaching a maximum in the sample treated with 5.0 mole  $\text{dm}^{-3}$  HCl. Sepiolite and palygorskite activated at different concentrations with solutions of boiling HCl under reflux conditions by Myriam (1998) showed the maximum increase in specific surface area at 3 mole  $\text{dm}^{-3}$  HCl for sepiolite and at 9 mole  $\text{dm}^{-3}$  HCl for palygorskite. For the increase in specific surface area cleaning and disaggregation of the particles and the increase in the number of micropores were

responsible. Suárez Barrios *et al.* (2001) studied the HCl activation of a saponite. Both the external and the internal surface areas of the most intensively treated sample (2.5% HCl for 24h) was doubled with respect to that of natural mineral. Balci (1999) found that the BET surface area of a sepiolite increased from 150 m<sup>2</sup>g<sup>-1</sup> up to >500 m<sup>2</sup>g<sup>-1</sup> after acid treatment. Sucha *et al.* (2001) found an increase in total surface area in a weathering profile developed on the top surface of a K-bentonite containing mixed-layer illite due to dissolution of illite-smectite and appearance of smectite as a separate phase. However, similar profile of Al-Mg montmorillonite showed a decrease in total surface area accompanied by montmorillonite dissolution, decrease in Mg content and precipitation of amorphous SiO<sub>2</sub>.

Rassineux *et al.* (2001) observed a decrease of the total surface area of a Wyoming-type bentonite treated with pH 13.5 solutions at 35 and 60°C for periods of 1 to 730 days.

Changes in the surface area of some selected soil minerals during acid and alkali treatments are shown in Fig. 22. In this figure the ratio of the surface area of the treated mineral to the surface area of the control sample is given. Note that parts of the curves depicting extreme changes (dashed lines) are not proportional to the others and the shifted points are labeled with their real values. Except of the nitrogen surface area for acid treated illite and alkali treated bentonite, and vermiculite, the surface areas of the minerals discussed increased generally with both acid and alkaline treatments. However, in a few cases the surface area drops after the lowest treatment concentration. This may be due to the removal of the minerals impurities e.g. amorphous and/or very finely dispersed crystalline solids having very high surface areas. The acid treatment affects surface areas more than the alkaline treatment. The nitrogen surface areas are more sensitive on the treatments. For example at the highest acid treatment the nitrogen surface area of vermiculite increased up to 35 times whereas the water surface area increased less than twice. The highest increase of the water surface area after both acid and alkali treatments occurred for the biotite, which may reflect the adsorption in newly formed expanded layers. The rise of the surface area under acid treatment may be caused by production of finely dispersed silicon oxides from destruction of mineral lattices, removal of amorphous aluminum or silica components plugging surface pores or interlamellar spaces, formation of the surface cracks and voids. Under alkaline conditions similar processes may occur together with an accumulation of iron and magnesium hydroxides (calcium hydroxides were most probably dissolved during the washing step). High value of surface area is important for catalytic activity of acid activated clays. The alkaline treatment producing high surface areas may possibly be used in production of the mineral catalysts, as well.

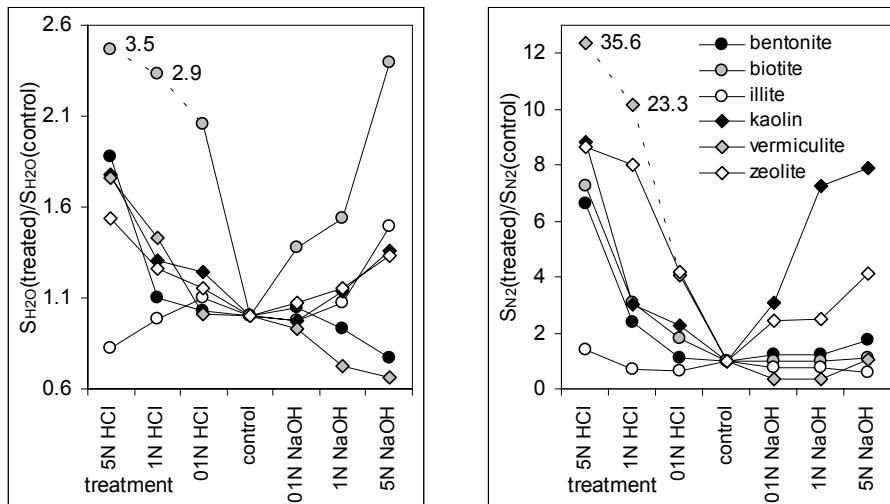


**Fig. 22.** Relative changes in surface areas due to acid and alkali treatments. Abbreviations within the figure. On y-axis the ratio of the control sample surface to the treated one is given. The points which are shifted against y-axis are labeled with their real values.

With the exception of alkali treated biotite and illite, the increase of the concentration of both treatments lead to a smaller increase of the water surface area than the nitrogen surface area, which is explicitly presented in Fig. 23 showing the ratio of these two values.

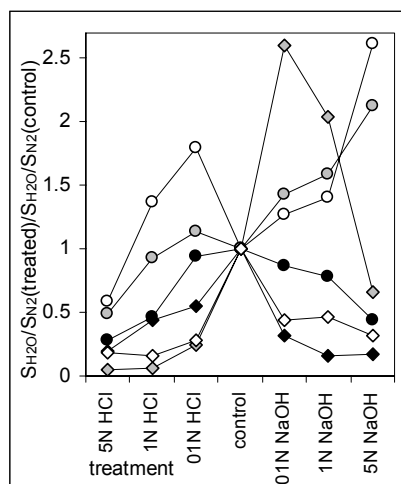


**Fig. 23.** Relative changes in ratio of water surface area to nitrogen surface area due to acid and alkali treatments. Abbreviations and notes as in Fig. 22.

That the increase of both nitrogen and water surface areas is not parallel may be caused by opening of  $N_2$  inaccessible spaces, as well as by a formation of new adsorbents on which nitrogen adsorption is higher than water. These can include various silicon oxides having higher nitrogen than water surface area (Gregg and Sing, 1967). An occurrence of silicon oxides after alkali treatment seems less probable. Short-term alkali treatment (hot sodium hydroxide) is supposed to clean mineral surfaces from silicon oxides, which is frequently applied as one of the pretreatment steps for mineralogical XRD analysis (Kunze and Jackson, 1965). Silicon compounds are more soluble under alkaline conditions than e.g. iron or magnesium, thus under the long term treatment the latter phases (if appear) may affect changes in surface areas.

The specific surface area of the clay poor soils decreases consecutively with the rise of the concentration of both acid and alkaline treatments, what is presented in Fig. 24 (solid lines). However, for clay rich soils (dashed lines), the initial decrease of the surface area at lower acid and/or base concentration is followed by its increase at the higher concentrations.

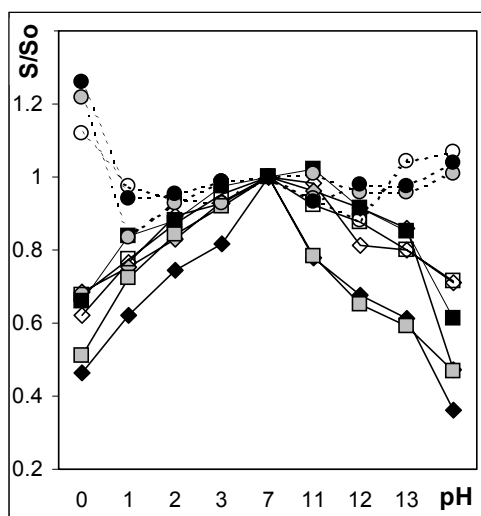


**Fig. 24.** Effect of pH (laboratory conditions) on specific surface area of exemplary soils.

The drop of the surface area is most probably connected with the dissolution of amorphous and very finely dispersed microporous soil solid phase components, having very high surface areas, as well as with the lost of soil organic matter. The rise of the surface area of clay rich soils at least under most extreme acidic treatment may be connected with the acid activation of the minerals and

production of amorphous silica oxides from destruction of mineral lattices. The above processes may prevail over the dissolution ones. Under alkaline conditions similar processes may occur also, however different may be involved, as well.

Extremely high surface areas has soil organic matter (Chiou et al. 1990). Humic acids may have surface areas up to  $1000 \text{ m}^2\text{g}^{-1}$  and fulvic acids up to  $2000 \text{ m}^2\text{g}^{-1}$ . Surface areas of a few hundreds  $\text{m}^2\text{g}^{-1}$  are common in peats, mucks and moorshes. Organic matter in saline soils has also very high surface area, over  $1000 \text{ m}^2\text{g}^{-1}$ . In general surface area of organic matter is larger in deeper soil profiles, wherein smaller organic particles are accumulated (Feller et al. 1992). Usually the removal of organic matter from soils leads to surface area decrease, however sometimes the increase of surface area of mineral soils has been noted, most probably due to opening of the fine pores previously plugged by organic material (Sokolowska et al. 1993).

Marked changes in surface area of soil organic matter occur due to sample pretreatment prior to its measurement. As an example one may see how the surface area depends on the heating temperature and/or on the time of drying that is illustrated in Figs 25 and 26, respectively.

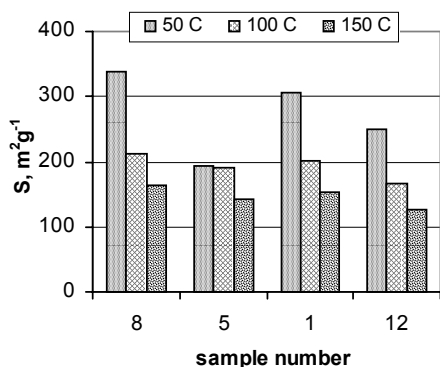


*Fig. 25. Dependence of surface area of different peat samples on the heating temperature.*

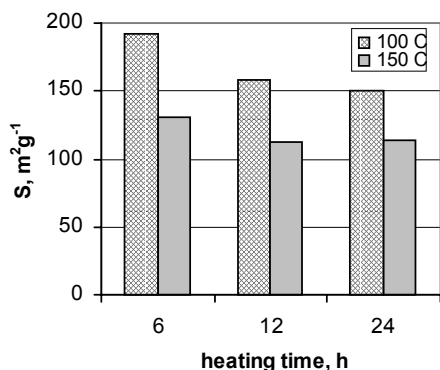


*Fig. 26. Dependence of surface area of different peat samples on the heating time.*

Jozefaciuk et al. (2001, 2003) studied effect of cyclodextrins, polysaccharides increasingly used in soil decontamination from organic hydrophobic compounds, on soil and clay minerals physicochemical properties using water vapor adsorption-desorption technique. As compared to clay minerals, pure randomly methylated  $\beta$ -cyclodextrin (RAMEB) had very large surface area. When increasing amounts of RAMEB were added to the minerals, the surface area decreased. RAMEB increased surface area in sandy soils and decreased in clayey soils. The above mentioned dependencies are illustrated in Figs 27 and 28.

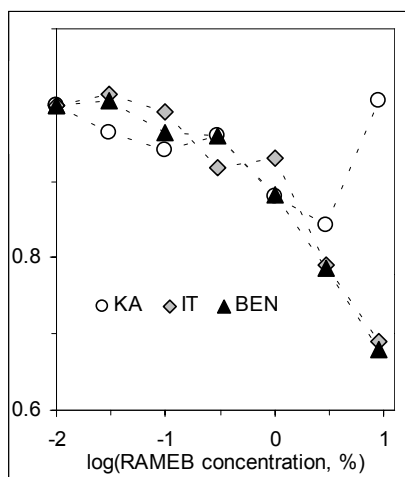


**Fig. 27.** Effect of different doses of randomly methylated  $\beta$ -cyclodextrin on surface area of selected soil minerals

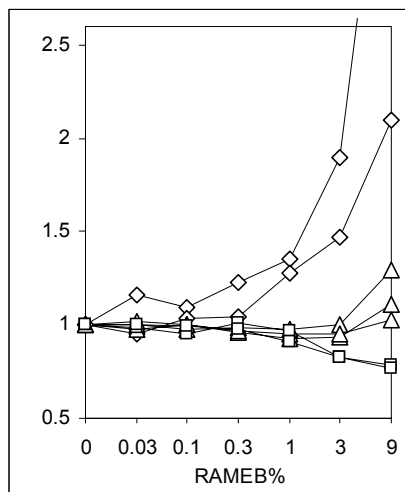


**Fig. 28.** Effect of different doses of randomly methylated  $\beta$ -cyclodextrin on surface area of soils. Rhombs: sandy soils, triangles: soils of low clay content, squares: clay rich soils.

Long-term studies of surface area of soils revealed its usability in diagnosis of soil quality, as this is correlated with clay and organic matter content, cation

exchange capacity, water holding capacity and other factors governing soil fertility. Therefore, for practical applications, maps of water vapor and nitrogen surface areas of Polish arable soils were constructed (Stawinski et al. 2000). An examples of such maps are presented in Figs 29 and 30.

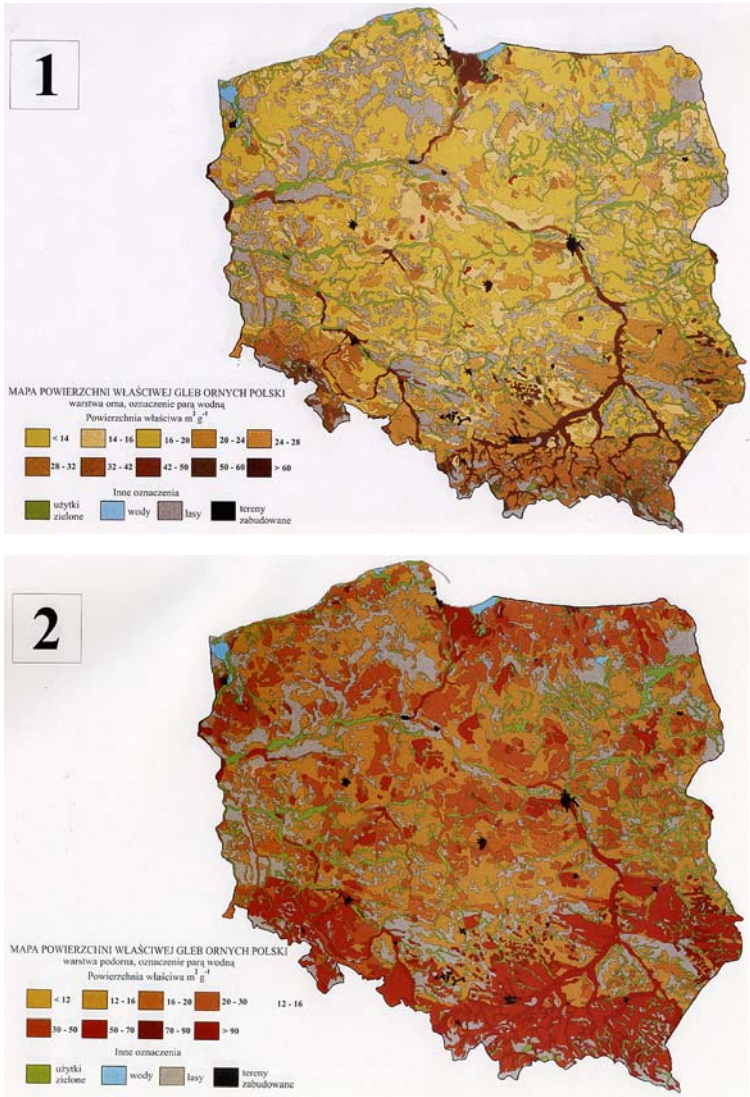


**Fig. 29.** Exemplary maps of water vapor surface areas of Polish arable soils (upper map: surface horizons, lower map: subsurface horizons).

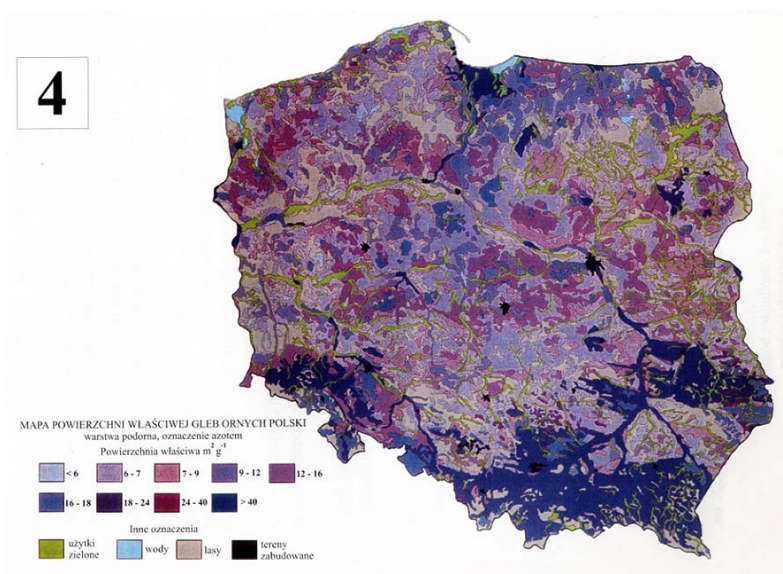
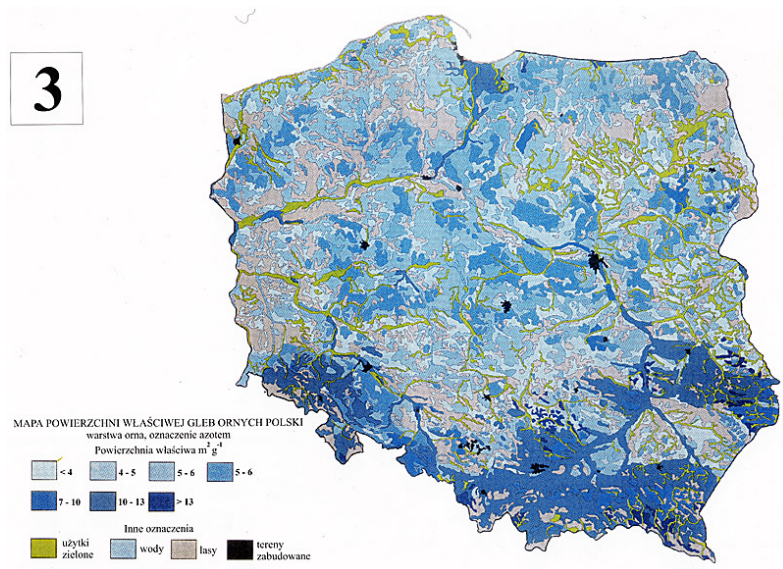


*Fig. 30. Exemplary map of nitrogen surface areas of Polish arable soils. Surface horizons (above) and subsurface horizons (below).*

## CHAPTER 3.

### ADSORPTION OF GASES OR VAPORS ON SOLIDS

Z. SOKOŁOWSKA, G. JÓZEFACIUK, G. BOWANKO

The term *adsorption* appears to have been introduced by Kayser in 1881 to connote the condensation of gases on free surfaces, in contradistinction to gaseous *absorption* where the gas molecules penetrate into the mass of the absorbing solid. The term *sorption* proposed by McBain in 1909, embraces both types of phenomena, adsorption and absorption. When a solid is exposed in a closed space to a gas or vapor at some definite pressure, the solid begins to adsorb the gas or vapor. The amount of gas adsorbed can be then calculated from the fall in pressure (by application of the gas law if the volumes of vessel and of the solid are known), or it can be determined directly as the increase in weight of the solid. The adsorption is a consequence of the field force at the surface of the solid (*the adsorbent*), which attracts the molecules of the gas or vapor (*the adsorbate*). The forces of attraction emanating from a solid may be of two main kinds, physical and chemical, and they give rise to physical adsorption and chemisorption, respectively:

- where the energy of adsorption is determined by weak Van der Waals forces (c.a.  $10 \text{ kJmol}^{-1}$ ) corresponding to the heat of the adsorbed fluid (Ar, He, CO, Kr,  $\text{N}_2$ ). In this case the adsorption process is a physical adsorption (or physisorption) and is always exothermic.
- where the energy of adsorption corresponds to the heat of reaction ( $80\text{-}300 \text{ kJmol}^{-1}$ ). The adsorption process is a chemical adsorption (or chemisorption) and need not necessarily be exothermic.

For physisorption a minimum in potential energy, between  $2\text{-}15 \text{ kJmol}^{-1}$ , exists at a distance corresponding to the Van der Waals radius (c.a.  $6\text{\AA}$ ). In the case of the chemisorption, however, the minimum occurs at a distance less than  $3\text{\AA}$  corresponding to the length of a covalent bond. Moreover, the minimum in potential energy is much better defined due to the greater bonding energy involved. With physical adsorption, the quantity of the fluid phase adsorbed decreases with increasing temperature. The quantity of gas adsorbed during chemisorption depends in an inversely proportional way on temperature. Moreover, with increasing pressure, up to a certain value, a plateau exists which corresponds to the volume of gas adsorbed as a monolayer.

## MEASUREMENT OF ADSORPTION

### *Static method*

The adsorption-desorption isotherms of a gas or a vapor are measured by *gravimetric method* as following: The solid is contacted with gas or vapor during a time necessary for equilibration. The time is dependent on the relative gas or vapor pressure and on the nature of solid. The amount of adsorbed gas or vapor is computed as the difference between the weight of the sample with gas (after adsorption) and the weight of initial sample of solid (before adsorption).

### *Dynamic method*

The method described above is static method. There is also a dynamic method of measuring of adsorption. It is used almost exclusively for determining the adsorption of gas mixtures, but can be employed just as well for pure gases also. The gas is filtered through a bed of adsorbent. The gas pressure ahead of the filter is kept constant. At the beginning of the filtration the gas pressure behind the filter is very small, practically the whole amount of gas reaching the bed is adsorb in it. This pressure gradually increases and finally becomes equal to that ahead of the bed, and the adsorbent becomes saturated with gas at the selected pressure.

### *Technique of measure adsorption isotherm according to Polish Standard PN-Z-19010-1 for measuring the surface area of soil*

Before the adsorption measurement the soil samples are dried in a vacuum chamber with the concentrated sulphuric acid until the weight of samples reached constant values. The soil sample of the weight equal approximately to 3g is put into the glass vessel and placed over sulphuric acid solution. The sample is equilibrated with water vapor during two days. The amount of adsorbed water vapor is computed as the difference between the weight of the sample with water and the dry sample (dried in an oven at 105°C). The relative water pressures are obtained from the density of sulphuric acid solutions. Five levels of relative pressure are usually selected in range of 0.034 to 0.352. The adsorption measurements are replicated three times keeping the temperature constant,  $T=20^{\circ}\text{C} \pm 0.5$ . The variation in replicated data are higher at lower vapor pressures (up to  $\pm 5\%$ ) than at higher vapor pressures (around  $\pm 1\%$ ).

### *Instrumental measurements of low temperature isotherms*

#### *Sample pretreatment*

To remove all species naturally present and adsorbed to the sample surface, i.e.  $\text{O}_2$ ,  $\text{H}_2\text{O}$ ,  $\text{CO}_2$ , organics, etc., the sample is heated gently under vacuum for a few hours or overnight. To avoid possible attached to contamination the outgassing circuit is kept separated from the analytical circuits. This operation is carried out using the outgassing stations and the furnaces located on the front of

the instrument. The conditions of vacuum and temperature may vary from sample to sample according to their different nature and characteristics therefore refer to the technical literature about specific pre-treatment conditions about samples. Generally it is possible to reassume that:

- organic materials are usually treated at temperature not exceeding 60-70°C,
- soil samples are usually treated at temperature 105°C,
- samples as alumina/silica are usually treated between 150 and 180°C,
- coals and active carbons are usually treated between 200 and 250°C,
- zeolites are usually treated at temperatures between 250-350°C.

The outgassing time, i.e. the time necessary to remove the humidity present in a given sample, can vary from 1 hour up to 15-16 hours according to the sample characteristics. In substance this time is a function of the “difficult” to remove completely the humidity from the samples. The sample must be placed into a burette properly chosen according to the characteristics of the sample.

#### ***Design of the apparatus***

The principal idea of the equipment used for low-temperature sorption measurements is illustrated in Fig. 11.

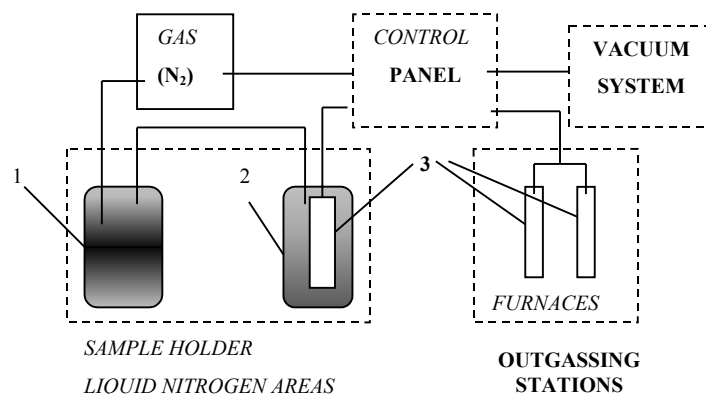


**Fig.11.** Idea of the low-temperature sorption equipment. 1. Liquid nitrogen standard reservoir; 2. Cooling Dewar vessel; 3. Sample burettes

In adsorption cycle the micro dose delivery system of the adsorbate (nitrogen) is connected to the adsorbent chamber. The chamber is filled with gas until the automatically chosen loading pressure is reached. After equilibration, the procedure is repeated stepwise at higher pressures. The amount of gas adsorbed is automatically measured knowing the amount of the gas dosed and the gas equilibrium pressure in the adsorbent chamber.

During desorption the chamber is connected with the vacuum system. The measuring gas is coming out from the sample holder (that is desorbing from the sample). After reaching an equilibrium the next amount of gas is desorbing from the sample holder.

## ADSORPTION ISOTHERM

At the boundaries between solids and gases an accumulation of the particles occurs. The amount adsorbed per gram of a solid depends on the equilibrium pressure  $p$ , the temperature  $T$ , and also on the nature of the gas and the solid:  $N=f(p, T, \text{gas, solid})$ . This function at a constant  $T$  is called the *adsorption isotherm* if  $p$  increases, and *desorption isotherm* - if  $p$  decreases. For a given gas adsorbed on a given solid, maintained at a fixed temperature, this equation simplifies to:  $N=f(p)_{T, \text{gas, solid}}$ , and if the gas is below its critical temperature the alternative isotherm equation is:  $N=f(p/p_0)_{T, \text{gas, solid}}$ , where  $p_0$  is the saturated vapor pressure of the gas. The adsorption,  $N$ , may be measured in any suitable units i.e. grams or milligrams, moles or millimoles, and  $\text{cm}^3$ .

The adsorption isotherm is the most popular expression of adsorption data. A complete adsorption isotherm covers the whole range of equilibrium pressures from very low pressures to the neighbourhood of the saturation pressure. Complete adsorption isotherms are common pointing by plotting along the abscissa the relative vapor pressure  $p/p_0$ . The isotherm naturally start at the origin of the coordinates and they end is at a nearly of the saturated vapor. No simple interpretation can be given to the main part of the curve. It is often supposed that at the higher relative pressures (at which adsorption hysteresis occurs) the adsorbed substance is capillary condensed, while at the lower  $p/p_0$  the surface of adsorbent is covered with a thin layer of gas molecules (Fig. 12.).

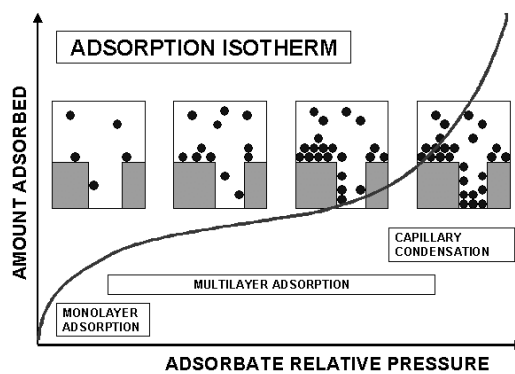


Fig. 12. Adsorption (desorption) isotherm.

The beginning part of the isotherm is used to obtain the surface area, and the end part to evaluate the pore structure in a solid body. The volume of liquid which is adsorbed at nearly saturated vapor by 1 gram of adsorbent is called the pore volume of the adsorbent.

**Types of adsorption isotherms**

In the literature of the subject there are recorded tens of thousands of adsorption isotherms, measured on a wide variety of solids. The majority of those isotherms, which result from the physical adsorption, may for convenience be grouped into five classes. This classification commonly referred as the Brunauer, Emmett and Teller (BET) classification. These types are shown in Fig. 13.

To the estimation of the surface area a kind of the soils mainly adsorption isotherm type II to be considered.

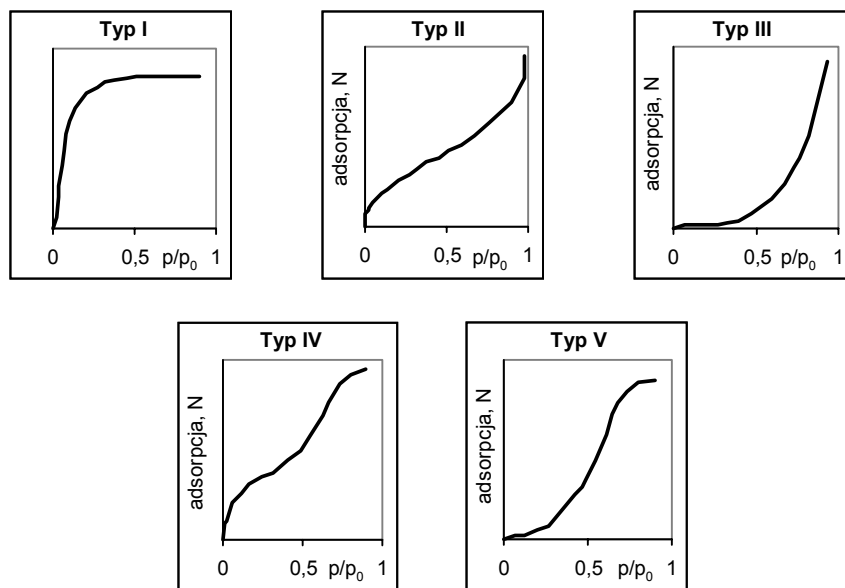


*Fig. 13. The types of adsorption isotherm in BET classification*

**Theory and equation of the adsorption isotherm**

In many instances an algebraic expression of the adsorption isotherm is more convenient than its graphic presentation. A few equations have been found to reproduce a large number of experimental isotherms.

The older one, commonly known as Freundlich isotherm:  $N = kp^{1/n}$ , where  $N$  is the amount of adsorbed gas,  $p$  is the pressure,  $k$  and  $1/n$  are constants. Many gases and vapors have  $1/n$  values between 0.3 and 0.5.

The other equation is known as Langmuir isotherm:  $N = (N_m kp)/(1 + kp)$ , where  $k$  is the constant. Langmuir regarded the surface of the solid as an array of adsorption sites, each site being capable of adsorbing one molecule, and all sites were characterized by the same adsorption energy, and the attractive interactions between adsorbed molecules could be ignored. The Langmuir equation described localised monolayer adsorption on the homogeneous surface of adsorbent.

Brunauer, Emmett and Teller approach the problem of adsorption kinetically. In 1938, they explicitly extended the Langmuir evaporation-condensation mechanism to second and higher molecular layers that is illustrated in Fig. 14.

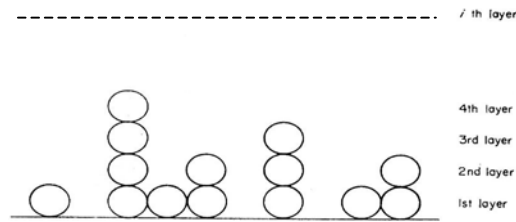


**Fig. 14.** The BET model for adsorption

The state of affairs when equilibrium is reached at any given pressure may be represented formally as varying numbers of molecules being condensed on any one site. The BET model assumes that the surface is energetically uniform i.e. that all adsorption sites are exactly equivalent. The model neglects horizontal interactions between the molecules within the adsorption layer, and takes into account only the vertical interactions, and postulates that the heat of adsorption in the higher layers is equal to the latent heat of condensation. The BET equation describes localised multilayer adsorption on the homogeneous surface of adsorbent:

$$N = \frac{N_m x C}{(1-x)[1+(C-1)x]} \quad (10)$$

where  $x = p/p_0$  relative pressure of water vapor,  $N$  amount of adsorbed water vapor, and  $C = \exp((E_a - E_c)/RT)$  is a constant related to the adsorption energy,  $E_a$  [J mol<sup>-1</sup>], and the condensation energy of water,  $E_c$  [J mol<sup>-1</sup>], and  $R$  [J mol<sup>-1</sup> K<sup>-1</sup>] is the universal gas constant.

The standard Brunauer-Emmett-Teller model is considered to be thermodynamically incorrect. The range of validity of BET equation does not always ex-

tend to relative pressure as high as 0.30 or 0.5. Mathematically similar Aranovich (1992) equation is thermodynamically correct and fits to the experimental adsorption data in a broader vapor pressure range (c.a.  $0.05 < p/p_0 < 0.8$ ). In contrast to the standard BET model, the Aranovich model allows for the presence of vacancies in the adsorbed layer. In linear form the Aranovich equation reads:

$$x/[N(1-x)^{1/2}] = 1/(N_m C) + x/N_m, \quad (11)$$

Many additional equations for the polymolecular adsorption isotherm have been published in the literature, for example the Dubinin-Radushkevich (DR), the Huttig or the Frenkel-Hasley-Hill (FHH) equation.

### ADSORPTION IN SOILS

For most of soils, clay minerals and organic matter the water vapor and nitrogen adsorption/desorption isotherms follow the II BET type dependence (Cases et al. 1997; Johansen and Dunning 1959) that is illustrated in Fig. 15. However, some peculiarities can be observed as well. Water vapor adsorption isotherms on biotite and vermiculite at low relative pressures ( $p/p_0 < 0.4$ ) resemble a combination of two Langmuir-type isotherms and the adsorption at medium relative pressures ( $0.4 < p/p_0 < 0.8$ ) is strongly limited (Jozefaciuk and Bowanko 2002).

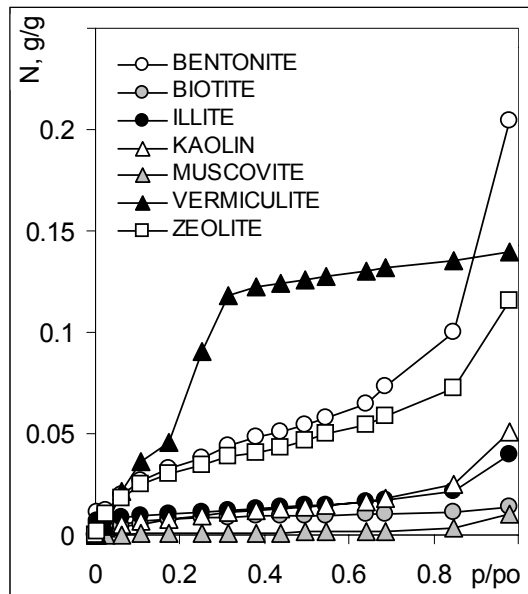
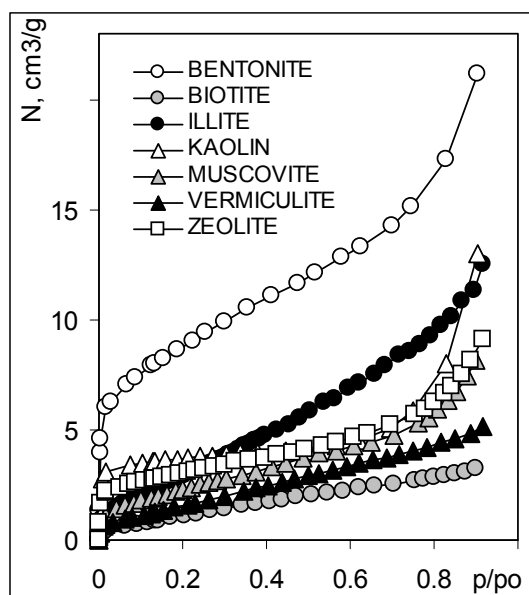


Fig. 15. Exemplary water vapor adsorption isotherms for selected soil minerals.

Exemplary low-temperature adsorption isotherms of nitrogen on soil minerals (Jozefaciuk and Bowanko 2002) are presented in Fig. 16.



*Fig. 16. Exemplary nitrogen adsorption isotherms for selected soil minerals.*

Large differences in adsorption of nitrogen and water vapor are observed in most cases. The nitrogen adsorption method requires prior evacuation and heating of the sample, which thins water films and brings the clay particles closer. The quasi-contact of the mineral plates (for morphological platy clays) can extend over a significant portion of the surface, which becomes inaccessible for nonpolar (nitrogen) molecules. If the clay contains expandible interlayers, these collapse on evacuation, giving the same effect. The molecular sieving is believed to differentiate the entrance of various size gas molecules into narrow spaces (Volzone et al., 1999) leading to differences in surface areas. The kinetic effects may diminish the adsorption of nitrogen to a great extent when entrances to larger spaces are of nitrogen molecule dimensions. To easily pass such narrow entrance, the thermal energy of the molecule should be similar to the energy barrier of the adsorption field among the entrance walls. At liquid nitrogen temperature the thermal energy is low and therefore the adsorption equilibrium may not be reached within a standard time of the measurement. Many restrictions hold also for interpretation of

water vapor adsorption isotherms, among which is different hydration of different surface cations, strong lateral interaction of polar water particles in adsorbed layer and/or different water content in interlayers of high charge density clays and in low charge density clays. Comprehensive discussions on nitrogen and water adsorption interpretation are presented by Gregg and Sing (1967), Newman (1985) and Low (1961).

Even more complicated situation occurs in soils. Except of the phenomena described above, severe changes in soil organic matter occur during sample pretreatment for  $N_2$  isotherms measurements. The organic material collapses and shrinks, internal spaces and micropores become closed that leads to much smaller adsorption of nitrogen than of water vapor. Therefore many scientists prefer to perform only water adsorption measurements, exemplary isotherms of which are shown in Fig. 17 (Jozefaciuk et al. 2000).

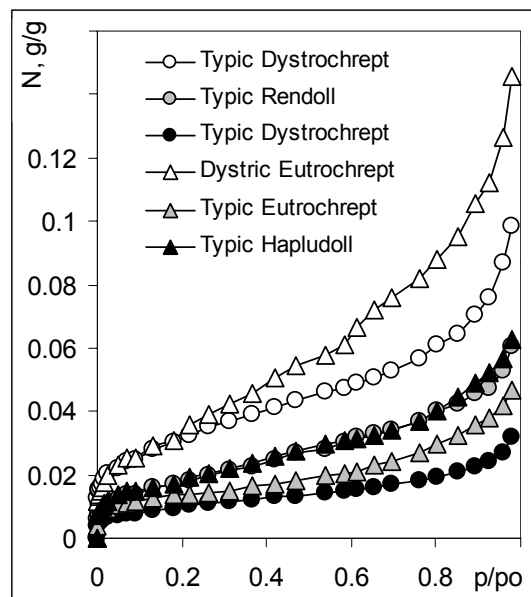


**Fig. 17.** Exemplary water vapor adsorption isotherms for selected soils.

Adsorption of water vapor on soil organic matter is very high (Wilczynski et al., 1993). In upper soil horizons the adsorption per unit mass of organic matter is usually lower than deeper horizons. In deeper horizons more mobile organic particles are accumulated. Small (fulvic) organic matter particles of high charge and polarity may adsorb more water than more hydrophobic, larger organic particles in upper horizons.

The adsorption isotherms for the same soils depend on many environmental and anthropogenic factors (Hoffmann et al. 1999). For example mechanical tillage treatments lead to a decrease of water vapor adsorption in comparison to no tilled soil in a whole relative pressure range. The decrease in adsorption in the following order: no tillage (NT) > ploughing + loosening (PL) > disking (D) > disking + loosening (DL) > ploughing (P) is observed that is illustrated in Fig. 18.

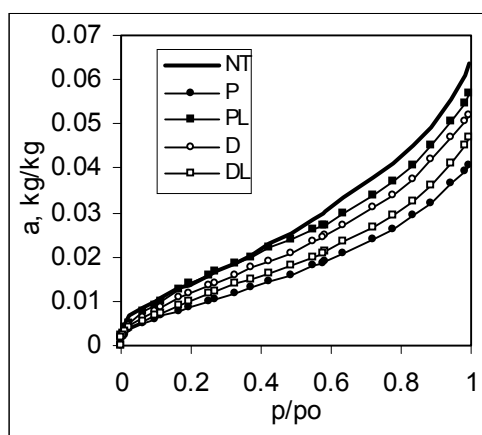


**Fig. 18.** Exemplary water vapor adsorption isotherms for an acidic brown soil under different tillage practices (data from 6<sup>th</sup> year of the experiment).

The effect of addition of chemicals to soils alters their adsorption properties. This will be illustrated on an example of a cyclodextrins, new compounds used in soil remediation (Jozefaciuk et al. 2001, 2003). Cyclodextrins and their derivatives remarkably increase the aqueous solubility and bioavailability of a great number of soil organic contaminants. Because of rapidly decreasing price, these compounds are more intensively used to intensify ex situ and in situ soil-washing technologies and to improve bioremediation. Randomly methylated  $\beta$ -cyclodextrin (RAMEB) is the most promising derivative to enhance the biodegradation of mineral and motor oil contamination in the soil and is effective in removal of explosives from contaminated soils of military areas.

The experimental desorption isotherms for the RAMEB enriched most abundant soil minerals are presented in Fig. 19. Very high amount of water is sorbed by RAMEB itself (few times more than for the minerals), so an increase in water sorption on minerals after RAMEB addition can be expected. However, the isotherms for RAMEB enriched minerals show lower adsorption as compared to the pure minerals for all but KA + 9% RAMEB samples.

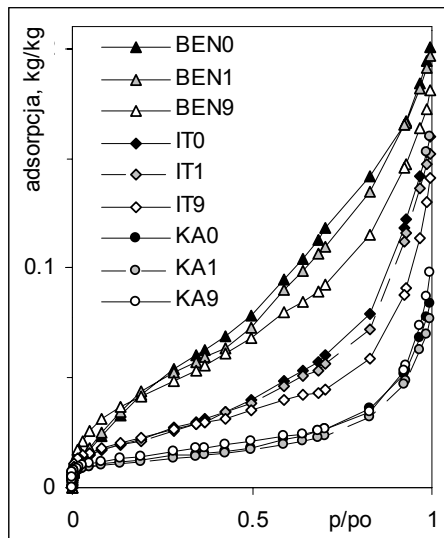


**Fig. 19.** Water vapor desorption isotherms RAMEB treated minerals. Abbreviations: BEN- bentonite, IT- illite, KA-kaolin. The number following the mineral abbreviation is the dose of RAMEB (%).

In soils, however, changes in adsorption isotherms depend on the clay content that is exemplary shown in Fig. 20. Soil S2 is a sandy soil, S5 is a loamy sand and S7 is clay rich.

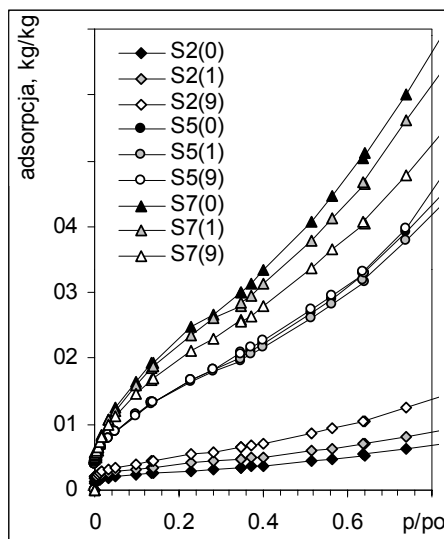


**Fig. 20.** Water vapor desorption isotherms RAMEB treated soils. The number following the mineral abbreviation is the dose of RAMEB (%).

Adsorption of water vapor on soils and minerals strongly depend on kind of exchangeable ions (Keenan 1951).

## CHAPTER 9.

### SURFACE FREE ENERGY AND WETTABILITY

*M. HAJNOS*

Any liquid can more or less spread on a solid surface that depends on the interparticle forces within and between both phases (Emmerson and Bond 1962). If the forces acting between liquid and solid are higher than these between the molecules of the liquid, the liquid moistens the solid, i.e. the solid is wettable. When interactions between the liquid molecules are higher than these between both phases, the solid is nonwetable and the drop of the liquid does not spread over the solid surface. A quantitative measure of the wettability is a solid-liquid contact angle, expressed usually in degrees, that is illustrated in Fig. 91.

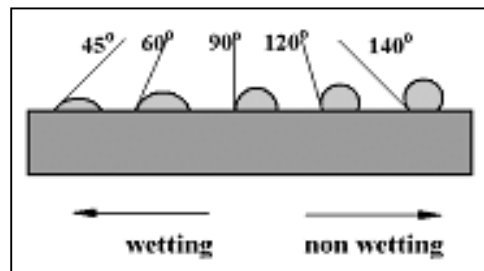


*Fig. 91. Wettability vs. contact angle*

As mentioned above, the contact angle depends on the force balance at the interface, as this is schematically illustrated in Fig 92.

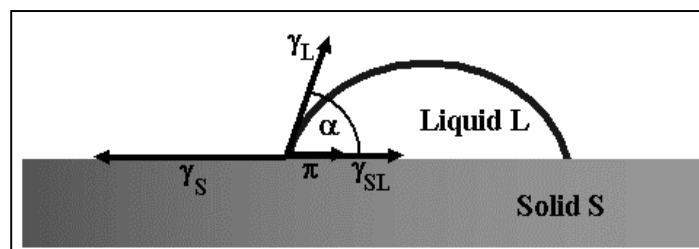


*Fig. 92. The force balance at the solid-liquid-air interface.*

This force balance can be described by a general Young equation (Fowkes, 1964):

$$\gamma_L \cos \alpha = \gamma_S - \gamma_{SL} - \pi, \quad (49)$$

where  $\alpha$  [deg] is the solid-liquid contact angle,  $\gamma_S$  [J m<sup>-2</sup>] is the surface free energy of the solid,  $\gamma_{SL}$  [J m<sup>-2</sup>] is the surface free energy of the solid-liquid interface and  $\gamma_L$  [J m<sup>-2</sup>] is the surface free energy of the liquid (surface tension) and  $\pi$  [J m<sup>-2</sup>] is a two-dimensional spreading pressure of the external liquid surface layer.

The wettability of a solid by a liquid may be regarded as a step process consisting of three stages: adhesion, immersion and final spreading of the liquid (Bennett and Zisman 1959). The possibility of spontaneous occurrence of the respective processes are determined by the surface free energies of the liquid, solid and solid-liquid interphase using the following conditions:

$$W_a = \gamma_S + \gamma_L - \gamma_{SL} = \gamma_L(1 - \cos \alpha) > 0, \quad (50)$$

where  $W_a$  [J m<sup>-2</sup>] is the work of adhesion,

$$W_i = \gamma_S - \gamma_{SL} = \gamma_L \cos \alpha > 0, \quad (51)$$

where  $W_i$  [J m<sup>-2</sup>] is the work of immersion, and

$$W_s = \gamma_L - \gamma_{SL} - \gamma_S = \gamma_L(\cos \alpha - 1) > 0, \quad (52)$$

where  $W_s$  [J m<sup>-2</sup>] is the work of spreading.

The contact angle of a liquid on a surface of a solid composed from a few individual components,  $\Theta_L$  [deg], is a function of the relative inputs of the surfaces of different natures to the total surface, which is described by the Cassie-Baxter equation (Jozefaciuk et al., 1993). For two components forming the composite surface this equation reads:

$$\cos \Theta_L = \sigma_1 \cos \Theta_{L,1} + \sigma_2 \cos \Theta_{L,2}, \quad (53)$$

where  $\sigma_1$  and  $\sigma_2$  are the parts of the surfaces of nature 1 and 2, and  $\Theta_{L,1}$  and  $\Theta_{L,2}$  are the liquid contact angles on surface 1 and 2, respectively. Knowing the contact angles on both components of the solid, from the above equation fractions of their surfaces in a composed surface can be estimated.

The pressure  $\pi$  of the liquid film formed on solid surface during wetting may be determined from the adsorption isotherm of the vapor of the liquid (Michel et al. 1998) on this solid using a Bangham-Razouk (Janczuk et al., 1991) equation:

$$\pi = RT/S \int_{p=p \min}^p a \ln(p), \quad (54)$$

where  $R$  [J mole<sup>-1</sup> K<sup>-1</sup>] is the universal gas constant,  $T$  [K] is the temperature of the measurements,  $S$  [m<sup>2</sup> g<sup>-1</sup>] is the surface area of the adsorbent,  $a$  [moles g<sup>-1</sup>] is

the amount adsorbed at a given adsorbate pressure  $p$  [Pa]. The lower integration limit  $p=p_{\min}$  holds for an assumed minimum adsorption pressure (a cut-off value to avoid infinite  $\ln(p)$  value) and the upper integration limit is this pressure at which water film of a defined thickness is present on the surface.

In general, the surface free energy can be regarded as a sum of two components, responsible for nonpolar  $\gamma^{LW}$  [ $J m^{-2}$ ] (Lifshitz-van der Waals) and polar  $\gamma^{AB}$  [ $J m^{-2}$ ] (acid-base) interactions (Van Oss et al., 1994):

$$\gamma = \gamma^{LW} + \gamma^{AB}, \quad (55)$$

where  $\gamma^{AB}$  is a geometric mean of electron-acceptor (Lewis acid)  $\gamma^+$  and electron-donor (Lewis base)  $\gamma^-$  components (Norris et al. 1992):

$$\gamma^{AB} = 2(\gamma^+ \gamma^-)^{1/2}. \quad (56)$$

The Lifshitz-van der Waals component of the interfacial free energy,  $\gamma_{SL}^{LW}$ , is given as:

$$\gamma_{SL}^{LW} = ((\gamma_S^{LW})^{1/2} - (\gamma_L^{LW})^{1/2})^2 \quad (57)$$

and the polar component of the interfacial free energy,  $\gamma_{SL}^{AB}$ , is given as:

$$\gamma_{SL}^{AB} = 2((\gamma_S^+ \gamma_S^-)^{1/2} + (\gamma_L^+ \gamma_L^-)^{1/2} - (\gamma_S^+ \gamma_L^-)^{1/2} - (\gamma_L^+ \gamma_S^-)^{1/2}). \quad (58)$$

### ***Measurements of contact angle and calculation of surface free energy***

Contact angle can be measured directly by observation of a small drop of a liquid settled on solid surface using a goniometer, that is illustrated in Fig. 93.

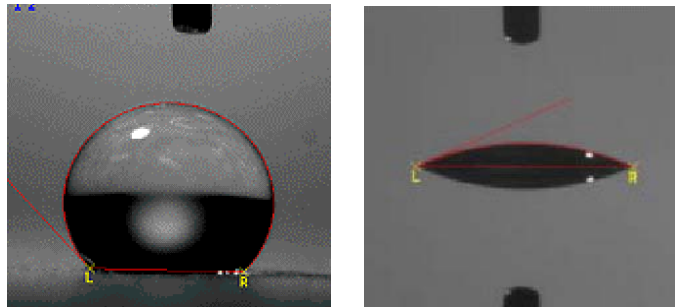


***Fig. 93. Goniometric measurement of contact angles on nonwetable (left) and wettable (right) surfaces***

However, Kwok and Neumann (1998) have recently shown that static contact angles measured by conventional goniometer techniques could be meaningless in the context of the Young equation. Basing on the literature contact angle data they

found that contact angles do not have to be discarded completely but a great caution is necessary to use them to determine solid surface tensions.

Because direct measurement of the contact angle, particularly for water on granular materials (soils) is almost impossible, one derives this from experiments on migration of a range of polar and nonpolar liquids (usually water, formamide, n-octane and n-decane) in the horizontal soil bed using a thin column wicking technique (Chibowski, 1992; Hajnos and Matyka-Sarzynska 1996, 1997).

In thin column wicking uses air-dry soil samples screened by 1mm sieve are placed in a few mm in diameter glass columns and compacted by vibrations. Some of the columns are dried in vacuum by 2 days (bare solids) and some are precontacted with the saturated vapor of the given liquid by 48h (vapor covered solids). The columns are positioned horizontally and joined with a given liquid via a cellulose wick, immersed in the bulk liquid. The time and distance of the migrating liquid are measured. Dependencies of the migration time vs. square of the migration distance in the thin column wicking experiment are linear. If a liquid enters the soil bed, its migration velocity at any distance is lower on the bare (dry) surface than on the vapor covered (wet) surface. Polar liquids (water and formamide) did not migrate in the hydrophobic material even in samples precovered with the respective vapors. Only apolar liquids (n-octane and n-decane) enter the columns thus this is only possible to estimate the dispersion component of the surface free energy.

The horizontal migration of the liquid in a porous body can be described by the Washburn equation modified by Chibowski and Holysz (1992):

$$l^2 = (R_{trans} t / 2\eta) \Delta G, \quad (59)$$

where  $R_{trans}$  [m] is an effective average radius of the capillary system in a porous body responsible for the transport of a liquid,  $t$  [s] is the time of migration of a liquid to the distance  $l$  [m],  $\eta$  [Pa s] is the viscosity of the liquid and  $\Delta G$  [J m<sup>-2</sup>], defined for convenience to be positive, is the change in free energy accompanying the wetting process of the unit area of the solid.

The effective capillary radius is calculated from Eq. 59 using the migration data of n-alkane on the solid covered with an equilibrium liquid film (so-called duplex film formed at saturated vapor pressure) assuming that in this case  $\Delta G = \gamma_L$  (Chibowski, 1992). One assumes the effective radius is the same for all other solid-liquid systems.

The free energy change accompanying the migration of a liquid on a bare solid,  $\Delta G_b$ , is expressed as:

$$\Delta G_b = \gamma_S - \gamma_L - \gamma_{SL}. \quad (60)$$

From the migration data of nonpolar liquids (e.g. n-alkanes which interact only by dispersion forces (Burghard 1985), for which  $\gamma_L = \gamma_{LLW} > 0$  and  $\gamma_{AB} = \gamma^+ = \gamma^- = 0$ ) on the bare solid one can easily find the dispersion component of the solid surface free energy using:

$$\Delta G_b = 2(\gamma_S^{LW} \gamma_L^{LW})^{1/2} - 2\gamma_L. \quad (61)$$

The difference between the free energy of the migration of a high surface tension liquid on a bare solid and on a solid covered by a vapor of this liquid is expressed as:

$$\Delta G_b - \Delta G_p = 2(\gamma_S^{LW} \gamma_L^{LW})^{1/2} + 2(\gamma_S^+ \gamma_L^-)^{1/2} + 2(\gamma_L^+ \gamma_S^-)^{1/2} - 2\gamma_L. \quad (62)$$

Knowing  $\gamma_{SLW}$  and solving a set of equations 17 using experimental migration data for at least two polar liquids on the bare and on the vapor covered solid one can find the surface free energy (SFE) of the solid and its components. Values of SFE,  $\gamma_{LW}$ ,  $\gamma^+$  and  $\gamma^-$  for a number of various liquids are available in the literature (e.g. Van Oss, 1998). Knowing the surface free energy components of the solid, the water contact angle can be calculated from Eq. 49.

Using water contact angle values, one can find the force of interaction  $F$  [N] occurring between soil solid particles joined via water layer of a defined shape. One frequently assumes that planar surfaces of solid particles are joined by a water film of the shape of a circle having the diameter  $d$  [m] and the thickness  $h$  [m]. In this case (Janczuk et al., 1993):

$$F = \frac{1}{2} \gamma_w [\pi d^2 h^{-1} \cos \alpha - \pi d]. \quad (63)$$

The  $h$  value should correspond to the distance between interacting soil particles and the  $d$  value to their magnitude. Thus the average distance between the particles can be approximated by the equivalent pore diameter ( $2 R_{trans}$ ) of the sample bed or by the dimension of the dominating particle fraction.

## WETTABILITY OF SOILS

Strong preponderance of electron-donicity is a common feature of most natural surfaces (Van Oss, 1994). The surface free energy of soils exhibits high contribution of dispersive Lifshitz-van der Waals interactions. The contribution of the electron-donor (Lewis base)  $\gamma^-$  interactions is high, however the electron-acceptor (Lewis acid)  $\gamma^+$  component is very low. Of course, the  $\gamma^-$  component seriously affects interactions of the polar liquids (water) with soils. As the overall amount of the polar interactions depends on the product of the electron acceptor and electron donor components (see Eqns 55-57), the acid-base  $\gamma^{AB}$  component is low due to low contribution of the  $\gamma^+$  component. Because the  $\gamma^+$  component of

the surface free energy is small for soils, their surfaces may be considered in practice as monopolar electron donors.

Dry humus-rich soil horizons exhibit only dispersive interfacial interactions. This is caused by exposure of hydrophobic parts of organic matter molecules while its hydrophilic parts are directed inside the residual moisture during drying. The hydrophobic character of these horizons is manifested also by very high water contact angles. Low wettability and high contact angles may lead to “hanging” of water within the (dry) soil bed causing low connectivity of water menisci.

Usually for characterizing soil water retention, full wettability (zero contact angle) of a solid phase is assumed (Walczak, 1984), despite high variations in contact angles occur between soils. This is particularly important for capillary filling processes (advancing contact angles). Differences in wettability are very important for water retention and transport processes and thus for soil management (Kramers and De Bano, 1965, Moseley and Dhir, 1996). Usually natural organic materials are hydrophobic (Tschapek 1973, Chassin et al., 1977) thus there exist a risk of the negative effect on soil water properties via an increase of soil hydrophobicity and decrease of wettability.

Strong effect of organic matter on wettability and surface free energy is a common feature in soils (Janczuk et al 1993). High wettability and high surface free energy of mineral soil horizons is due to high input of mineral surfaces. Contact angle values for various soils are illustrated in Fig. 94 (Hajnos 1999).

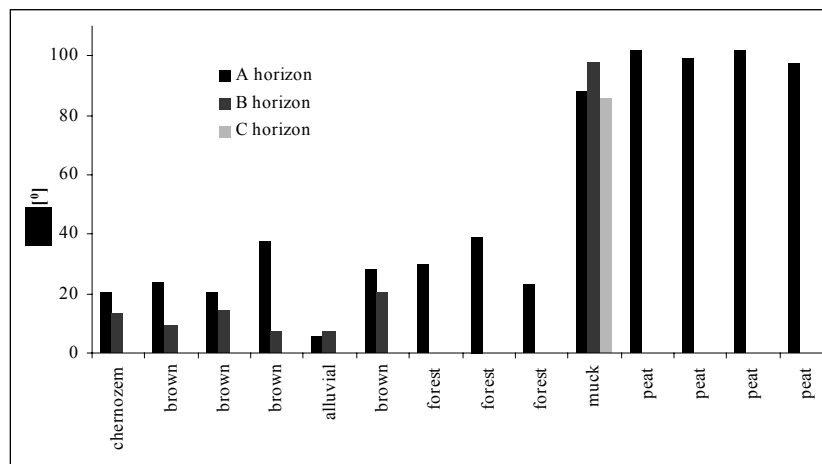


**Fig. 94.** Contact angle values for various soils.

The contact angle value exceeding 90 degs in organic soil horizons is a reason that the interactions of water with the humus rich horizons are weak, therefore the

force attracting soil particles via water layer ( $F$ ) is negative which can lead to the repulsion of soil particles and lacking of the soil structure stability that is illustrated in Fig. 95 for the same soils as in the previous figure.

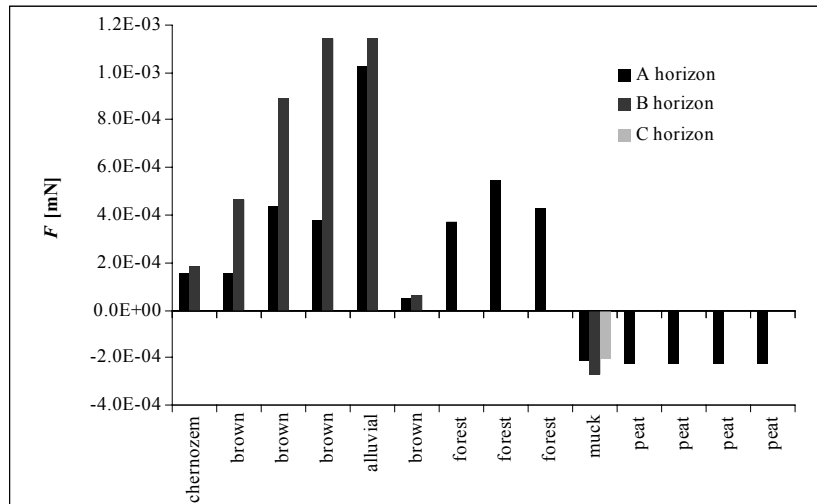


**Fig. 95.** Force attracting soil particles via water layer.

The importance of organic matter in formation of wettability, surface free energy and its components, and water contact angles is illustrated below on the example of kaolin enriched with different doses of humic acid. Figure 96. illustrates the behavior of surface free energy and water contact angles. In this figure, the ratio of a given parameter for the HA treated mineral to its value for the control mineral is presented on the y-axis.

The value of the surface free energy, as well as its Lifshitz-van der Waals and electron-donor components decrease with the increase of the HA concentration. The fastest decrease of these values occurs at the HA concentration of c.a.  $5 \cdot 10^{-5}$  w/w. The decrease of the electron-donor (Lewis base)  $\gamma$ - interactions reflects the decrease in the polar character of the surface due to the HA addition. The drop in dispersive Lifshitz-van der Waals interactions seems somewhat surprising taking into account the hydrophobic character of the HA. However, this may be due to some reorientation of the HA molecules on the kaolin surface leading to the exposure of some organic hydrophilic groups, being, however, less polar than these of the mineral. The water contact angle as well as the work of spreading increase with the HA concentration. Note that the increase of the ratio of the negative values of the WS indicates in fact that after the HA addition the

work of spreading becomes more negative i.e. water spreads worse on the HA covered kaolin surface. The fastest changes of the work of spreading and of the contact angle occurs also at the HA concentration of c.a.  $5 \cdot 10^{-5}$  w/w. At this very low HA concentration the hydrophilic surface of kaolin changes its character to hydrophobic due to accumulation of humic acid.

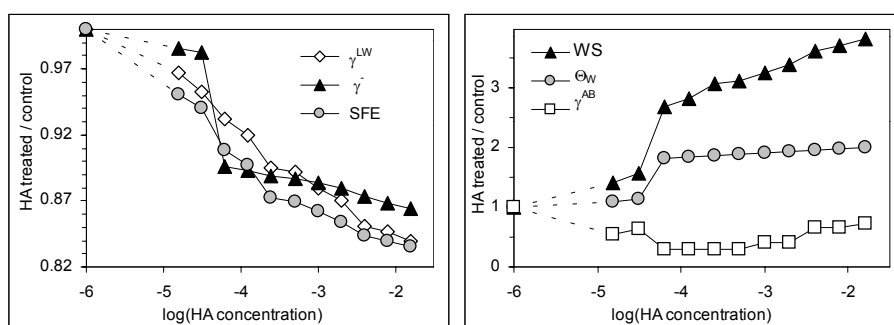


**Fig. 96.** Ratio of a given surface parameter for the HA enriched sample to the value of this parameter for pure kaolin as dependent on HA concentration. Abbreviations within the figure denote: SFE surface free energy,  $\gamma^{LW}$  Lifshitz-van der Waals component of the SFE,  $\gamma$  electron-donor (Lewis base) component of the SFE, WS work of spreading,  $\Theta_W$  contact angle of water,  $\gamma^{AB}$  acid-base component of the SFE.

In Fig. 97 one can see that the pressure of the water film present on the surface of kaolin decreases with the HA content. However, for both monomolecular and trimolecular films the sharp decrease in the film pressure occurs at HA concentration of around  $10^{-3}$  w/w, which is higher than that at which sharp changes of the other surface parameters studied were noted. The polar  $\gamma^{AB}$  (acid-base) component of the SFE decreases at minimum HA content and did not markedly change at higher HA loads.

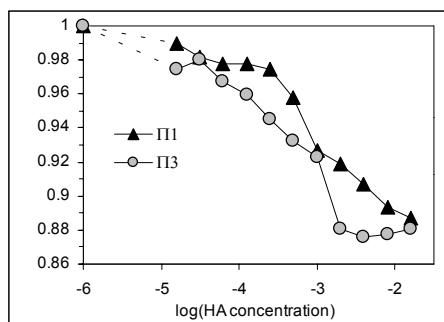


**Fig. 97.** Ratio of the pressure of the water film formed on the humic acid enriched sample to the value of this parameter for the pure kaolin as dependent on HA concentration. Abbreviations:  $\Pi 1$ -monomolecular film,  $\Pi 3$ -trimolecular film.

As presented in Fig. 98, under the experimental conditions applied, very low amount of the humic acid ( $5 \cdot 10^{-5}$  w/w) covers significant portion of the kaolin surface (c.a. 40%). Larger amounts of HA seem to locate on the previously covered surface, as far as the surface coverage changes only slightly due to HA concentration increase. This is the reason that the apparent thickness of the HA coating is proportional to the amount of the HA added.

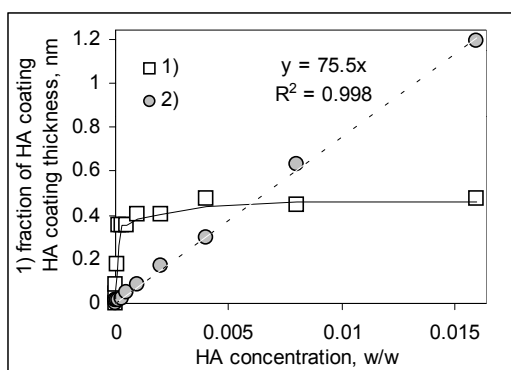


**Fig. 98.** Thickness of humic acid coating on kaolin surface (circles) and fraction of HA covered surface (squares) vs. HA concentration.

Very small amounts of humic acid cover significant part of the mineral surface with a very thin layer. Marked decrease of the mineral wettability by water is caused by low amounts of humic acid added.

Wettability of soils and their components depends also on the kind of dominating cations that is illustrated for exemplary soil minerals in Figs 99 and 100. The dominant factor responsible for changes in wettability seems to be the entropy of hydration of particular ions present on the surface in exchangeable forms.

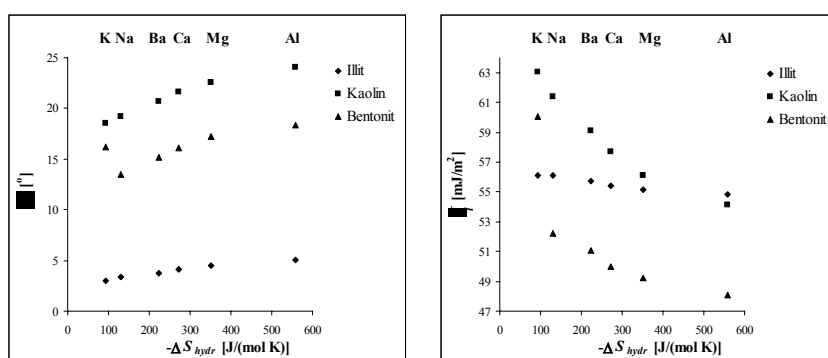


**Fig. 99.** Dispersive (left) and electron-donor (right) SFE components vs. entropy hydration of exchangeable surface cations.

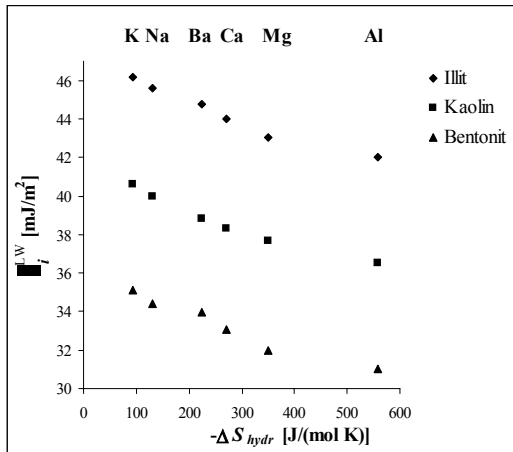


**Fig. 100.** Contact angle vs. entropy hydration of exchangeable surface cations for exemplary soil minerals.

Parameters of soil wettability govern the water storage properties in soils, that is illustrated in Fig. 101.

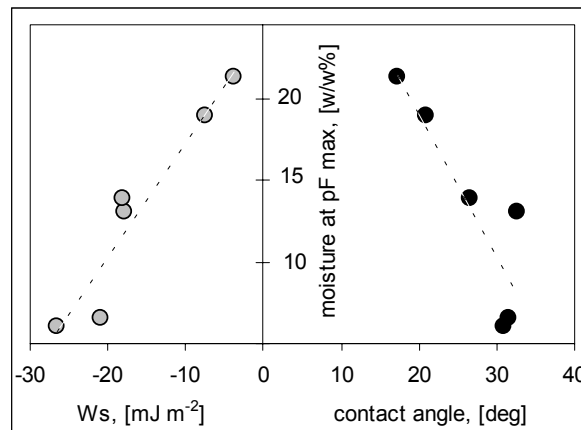


**Fig. 101.** Dependence of the amount of water stored at low moistures on the work of spreading and contact angle for exemplary soils.

As a consequence of variations in work of spreading and the contact angle one observes different amount of water stored in the soils at low moistures (high pF values).

## LITERATURE

1. Anderson AN McBratney AB Crawford JW 1998. Applications of fractals to soil studies. *Advances in Agronomy* 63 1-76
2. Aranovich G L 1992. The theory of polymolecular adsorption. *Langmuir* 8 736-739
3. Aslyng HC 1954. The lime and phosphate potentials of soils Solubility and Availability of Phosphates. Royal Agric Vet Coll Yearbook Copenhagen
4. Atanassova I 1995. Adsorption of Cu on Ca-vermiculite at high surface coverage. *Soil Science Agrochemistry and Ecology* 29 95- 97 In Bulg
5. Atanassova I Ilieva R 2003. Adsorption of Cu by smectite and kaolinite clays from natural deposits in Bulgaria. *Bulgarian Journal of Ecological Science* 9 673-678
6. Avnir D Farin D Pfeifer P 1985. Surface geometric irregularity of particulate materials. The fractal approach. *J Colloid Interface Sci* 103 112-123
7. Avnir D Jaroniec M 1989. An isotherm equation for adsorption on fractal surfaces.
8. Azooz RH Arshad MA Franzluebbbers AJ 1996. Pore size distribution and hydraulic conductivity affected by tillage in northwestern Canada. *Soil Sci Soc Am J* 60 1197-1201
9. Baccouche A Srasra E El Maaoui M 1998. Preparation of Na-P1 and sodalite octahydrate zeolites from interstratified illite-smectite. *Applied Clay Science* 13 255-273
10. Bache BW 1979. Activity Ratio Encyclopedia of Soil Science. Fairbridge RW Finkl CW Eds Dowden Hutchinson and Ross Stroudsburg
11. Balard H Saada A Papirer E Siffert B 1997. Energetic surface heterogeneity of illites kaolinites. *Langmuir* 13 1256-1269
12. Balci S 1999. Effect of heating and acid pre-treatment on pore size distribution of sepiolite. *Clay Minerals* 34 647-653
13. Bandosz TJ Jagiello J Andersen B Schwartz JA 1992. Inverse gas chromatography study of modified smectite surfaces. *Clays and Clay Minerals* 40 306-310
14. Bauer A Velde B 1999. Smectite transformation in high molar KOH solutions. *Clay Minerals* 34 259 – 273
15. Bennett MK Zisman WA 1959. Relation of wettability by aqueous solutions to the surface constitution of low-energy solids. *J Phys Chem* 63 1241-1263

16. Bird NR Perrier E Rieu M 2000. The water retention function for a model of soil structure with pore and solid fractal distributions. *European J Soil Sci* 51 55-63
17. Bloom PR 1979. Titration behavior of aluminum organic matter. *Soil Sci Soc Am J* 43 815-817
18. Bogda A Chodak T 1991. Mineralogical and physico-chemical properties of soils from the devastated forest area in Izerskie Mountains. *Proc 7th Euroclay Conf Dresden* 113-118
19. Boldyrev A 1983. *Physical colloid chemistry*. High school Ed Moscow 408pp (in Russian)
20. Bolt GH 1982. *Soil Chemistry B Physico-chemical Models*. Elsevier Amsterdam
21. Boyle JR Voigt GK Sawhney BL 1967. Biotite flakes Alteration by chemical and biological treatment. *Science* 155 193-195
22. Brackensiek DL Rawls WR Lodgson SD Edwards WM 1992. Fractal description of macroporosity. *Soil Sci Soc Am J* 56 1721-1723
23. Breen C Madejova J Komadel P 1995. Correlation of catalytic activity with infra-red <sup>29</sup>Si MAS NMR and acidity data for HCl-treated fine fractions of montmorillonites. *Applied Clay Science* 10 219-230
24. Breen C Watson R 1998. Acid-activated organoclays preparation characterization and catalytic activity of polycation-treated bentonites. *Applied Clay Science* 12 479-494
25. Brown D Rhodes CN 1995. Acid-treated and ion exchanged montmorillonite catalysts dependence of activity on composition. *Proc Euroclay'95* Leuven A Elsen P Grobet M Keung H Lehman R Schoonheydt and H Toufar Eds 189-190
26. Brunauer S Emmet PH Teller E 1938. Adsorption of gases in multimolecular layers. *Journal of American Chemical Society* 60 309-314
27. Burghardt W 1985. Bestimmung der Benetzungseigenschaften von Moor-bodenlösungen durch Kontaktwinkelmessung. *Z Pfl Bodenk* 148 66-72
28. Cases JM Berend I Francois M Uriot JP Michot LJ Thomas F 1997. Mechanism of adsorption and desorption of water vapor by homoionic montmorillonite 3 The Mg Ca Sr and Ba exchanged forms. *Clays and Clay Minerals* 45 8-22
29. Cerofolini GF 1974. Localized adsorption on heterogeneous surfaces. *Thin Solid Films* 23 129-152

30. Charlot G 1969. Methods of analytical chemistry. Chemistry Ed Moscow 1206pp Ru
31. Chassin P Nakaya N le Berre B 1977 Influence des substances humiques sur les propriétés des argiles II Adsorption des acides humiques et fulviques par la montmorillonite. *Clay Minerals* 12 261-271
32. Chermak JA Rimstidt JD 1987. The hydrothermal transformation of kaolinite to muscovite/illite. *Geochimica et Cosmochimica Acta* 54 2979-2990
33. Chernoberezkij J 1980. On the nature of the suspension effect. Habilitation thesis. St Peterbourg University (in Russian)
34. Chibowski E 1992. Solid surface free energy components determination by the thin-layer wicking technique. *J Adhesion Sci Technol* 6 1069-1090
35. Chibowski E Gonzales-Caballero F 1993. Theory and practice of thin layer wicking. *Langmuir* 9 330
36. Chibowski E Holysz L 1992. Use of the Washburn equation for surface free energy determination. *Langmuir* 8 710-716
37. Chibowski E Staszczuk P 1988. Determination of surface free energy of kaolinite. *Clays Clay Minerals* 36 455-461
38. Chiou C T Lee J-F Boyd A 1990. The surface area of soil organic matter. *Environ Sci Technol* 24 1164-1166
39. Christidis GE Scott PW Dunham AC 1997. Acid activation and bleaching capacity of bentonites from the islands of Milos and Chios (Aegean Greece). *Applied Clay Science* 12 329-347
40. Cotton AF Wilkinson G 1977a. Advanced inorganic chemistry. Part I. Science and Art Ed Sofia 677 pp (in Bulgarian)
41. Cotton AF Wilkinson G 1977b. Advanced inorganic chemistry. Part II. Science and Art Ed Sofia 756 pp (in Bulgarian)
42. Crawford JW Matsui N 1996. Heterogeneity of the pore and solid volume of soil distinguishing a fractal space from its non-fractal complement. *Geoderma* 73 183-195
43. Cresser M Brillet M Skiba U 1989. The effect of acid deposition on soils in Acid Deposition. Sources Effects and Controls. JWS Longhurst Ed British Lib Techn Commun 169-196
44. Csillag J 1987. Comparison of calculated and measured ion activities and estimation of the reliability of potentiometric determination of ion activities in soil pastes and extracts. *Ionometry in Soil Science*. Russian Acad Sci Ed Puschino (in Russian)

45. Czachor H 1997. Solid phase geometry and pore space in agricultural granular materials on example of mineral soil. *Acta Agrophysica* 7 1-80
46. Davis LE 1943. Measurements of pH with the glass electrode as affected by soil moisture. *Soil Sci* 56 405-422
47. De la Villa RV Cuevas J Ramirez S Leguey S 2001. Zeolite formation during the alkaline reaction of bentonite. *European Journal of Mineralogy* 13 635-644
48. De Wit JCM Van Riemsdijk WH Nederlof MM Kinniburgh DG Koopal LK 1990. Analysis of ion binding on humic substances and the determination of intrinsic affinity distributions. *Analitica Chimica Acta* 232 189-207
49. Debicki R Filipek T Glinski J Sikora E eds 1994. Natural and anthropogenic causes and effects of soil acidification. *Zeszyty Problemowe Postepow Nauk Rolniczych* 413 1-334
50. Dechnik I Glinski J Kaczor A Kern H 1990. Effect of acid rain on soils and plants. *Problemy Agrofizyki* 60 1-70 (in Polish)
51. Dechnik I Stawiński J 1973. Surface area in physicochemical and physical investigations of soil properties. *Problemy Agrofizyki* 6 (in Polish)
52. Dekany I Turi L Fonseca A Nagy JB 1999. The structure of acid treated sepiolites small-angle X-ray scattering and multi MAS-NMR investigations. *Applied Clay Science* 14 141-160
53. Douglas JT Goss MJ Hill D 1981. Measurement of pore characteristics in a clay soil under ploughing and direct drilling including use of a radioactive tracer  $^{144}\text{Ce}$  technique. *Soil Tillage Res* 1 11-18
54. Drief A Nieto F Sanchez-Navas A 2001. Experimental clay-mineral formation from a subvolcanic rock by interaction with 1 mole  $\text{dm}^{-3}$  NaOH solution at room temperature. *Clays and Clay Minerals* 49 92-106
55. Duchaufour PH 1968. *L'evolution des soils*. Masson et Cie Paris (in French)
56. Duchaufour PH 1972. *Processus de formation des soils* Academie de Nancy-metz (in French)
57. Duquette M Hendershot W 1993. Soil surface charge evaluation by back-titration. I Theory and method development. *Soil Sci Soc Am J* 57 1222-1228
58. Eberl DD Velde B Mc Cormick T 1993. Synthesis of illite-smectite from smectite at earth surface temperatures and high pH. *Clay Minerals* 28 49-60
59. Ehrburger-Dolle F 1999. A new way to analyze adsorption isotherms. *Langmuir* 15 6004-6015

60. Elonen P 1971. Particle-size analysis of soils. *Acta Agral Fenn* 122 65-81
61. Emmerson WW Bond RD 1962. The rate of water entry into dry sand and calculation of the advancing contact angle. *Aust J Soil Res* 1 9-16
62. Fanning DS Keramidas VZ El-Desosky MA 1989. Micas. in: *Minerals in Soil Environments 2nd Edition* JB Dixon and SB Weed Eds SSSA Book Series 1 Madison Wisc 527-634
63. Feller C Shouller E Thomas F Rouiller J Herbillon AJ 1992. N<sub>2</sub>-BET specific surface areas of some low activity clay soils and their relationships with secondary constituents and organic matter contents. *Soil Sci* 153 293-299
64. Filippidis A Godelitsas A Charistos D Misaelides P Kassoli-Fournaraki A 1996. The chemical behavior of natural zeolites in aqueous environments Interactions between low-silica zeolites and 1 mole dm<sup>-3</sup> NaCl solutions of different initial pH-values. *Applied Clay Science* 11 199-209
65. Fowkes FM 1964. Attractive forces at interface. *Ind Eng Chem* 56 56-40
66. Frank U Gebhardt H 1991. Weathering of silicates and destruction of clay minerals as a consequence of severe soil acidification in selected forest locations of Northern Germany. *Proc of 14th International Congress of Soil Science Kyoto VII* 61-65
67. Friedrichsberg D 1984. *Colloid chemistry*. Chemistry Ed Leningrad 368 pp (in Russian)
68. Fripiat J J Chaussidon A Jelli 1971. *Chimie-Physique des phenomenes de surface Applications aux oxides et aux silicates*. Masson et Cie Paris 387 pp (in French)
69. Ganev S 1987. Strongly acidic and weakly acidic nature of soil acidity and determining the liming rate of acid soils. *Sofia Forestry* 24 1 19-25 Bg
70. Ganev S 1990. *Contemporary soil chemistry*. Science and Art Ed Sofia 371 pp (in Bulgarian)
71. Gawlik J 1992. Water holding capacity of peat formations as an index of the state of their secondary transformation. *Polish J of Soil Sci* 2 121-126
72. Gawlik J Harkot W 2000. Influence of the kind of moorsh and the state of its transformation on the germination and growth of *Lolium perenne* in pot plant experiment during spring-summer cycle. *Acta Agrophysica* 26 25-40
73. Gerdes WF 1966. A New Instrument - The Streaming Current Detector. 12th National Analysis Instrument Symposium Houston TXUSA
74. Gilbert M Laudelout H 1965. Exchange properties of hydrogen ions in clays. *Soil Sci* 100157-162

75. Goates JR and Anderson K 1956. Acidic properties of Quartz. *Soil Science* 81 277-282
76. Good RJ Chaudhury MK 1991. Theory of adhesive forces across interfaces I The Lifshitz-van der Waals component of interaction and adhesion. *Fundamentals of adhesion* ed LH Lee, Plenum Press NY
77. Gregg SJ Sing KSW 1967. Adsorption Surface Area and Porosity. Academic Press London and New York
78. Grim R 1959. Clay mineralogy. Moscow 452 pp (in Russian)
79. Hajnos M 1998. Mercury intrusion porosimetry as compared to other methods characterizing microstructure of soil materials. *Zeszyty Problemowe Postepow Nauk Rolniczych* 461 523-537
80. Hajnos M 1999. Surface free energy and its components as parameters determining wettability and aggregation state of selected clay minerals and soils. *Acta Agrophysica* 17 1-112
81. Hajnos M Jozefaciuk G Sokolowska Z Greiffenhagen A Wessolek G 2003. Water storage surface and structural properties of sandy forest humus horizons. *J Plant Nutr Soil Sci* 166 5 625-634
82. Hajnos M Korsunskaja L Pachepsky Y 2000. Soil pore surface properties in managed grasslands. *Soil & Tillage Research* 55 63-70
83. Hajnos M Matyka-Sarzynska D 1996. Determination of surface free energy components of Kaolin by the thin-layer wicking technique. *Polish J Soil Sci* XXIX 39-45
84. Hajnos M Matyka-Sarzynska D 1997. Comparison of receding contact angles and solid surface free energy components of modified kaolin from thin-layer wicking technique and sessile drop method. *Polish J Soil Sci* XXX 45-52
85. Hall PL Astill DM 1989. Adsorption of water by homoionic exchange forms of Wyoming bentonite SWy1. *Clays and Clay Minerals* 37 355-363
86. Harris L B 1968. Adsorption on a patchwise heterogeneous surface I Mathematical analysis of the step-function approximation of the local isotherm. *Surface Science* 10 129-145
87. Harris LB 1969. Adsorption on a patchwise heterogeneous surface III Errors incurred in using the condensation approximation to estimate the energy distribution on a Hill-De Boer adsorbent. *Surface Science* 15 182-187
88. Hernandez MA 2000. Nitrogen-sorption characterization of the microporous structure of clinoptilolite-type zeolites. *Journal of Porous Materials* 7 443-454

89. Hoffmann C Renger M Hajnos M Sokolowska Z Jozefaciuk G Marschner B 1999. Reactions of sewage farm soils to different irrigation solutions in a column experiment. 1 Solid phase physicochemical properties. *Z Pfl Boden* 162 653-659
90. Huang WL 1993. The formation of illitic clays from kaolinite in KOH solution from 225 to 350°C. *Clay and Clay Minerals* 41 645-654
91. Hunter R 1993. *Introduction to Modern Colloid Science*. Oxford Science
92. Jackson ML Sherman GD 1953. Chemical weathering of clay minerals in soils. *Advances in Agronomy* 5 219-318
93. James RO Parks GA 1982. Characterization of Aqueous Colloids by their Electrical Double-Layer and Intrinsic Surface Chemical Properties. in: EJ Matijewic ed *Surface and Colloid Science Vol 12* Plenum Press New York 119-216
94. Janczuk B Hajnos M Zdzienicka A Jozefaciuk G 1991. The relationship between water film pressure and surface free energy of soil clay fraction. *Polish J Soil Sci XXIV* 131-138
95. Janczuk B Jozefaciuk G Hajnos M Bialopiotrowicz T Kliszcz A 1993. Surface free energy of a soil clay fraction in relation to aggregate stability. *Clay Minerals* 28 145-148
96. Janek M and Lagaly G 2001. Proton saturation and rheological properties of smectite dispersions. *Appl Clay Sci* 19 121-130
97. Jaroniec M 1995. Evaluation of the fractal dimension from a single adsorption isotherm. *Langmuir* 11 2316-2317
98. Jaroniec M Brauer P 1986. Recent progress in determination of energetic heterogeneity of solids from adsorption data. *Surface Sci Reports* 6 65-117
99. Jaroniec M Kruk M 1997. Fractal analysis of composite adsorption isotherms by using density functional theory data for argon in slitlike pores. *Langmuir* 13 1031-1035
100. Jaroniec M Rudzinski W Sokolowski S Smarzewski R 1976. Determination of energy distribution function from observed adsorption isotherms. *Journal of Colloid and Polymer Science* 253 164-166
101. Johansen RT Dunning HN 1959. Water vapor adsorption on clays. in: *Clays and Clay Minerals* E Ingerson Ed US Geol Surv Earth Sci Ser Monogr 2 Pergamon Press NY
102. Jovanovic N Janackovic J 1991. Pore structure and adsorption properties of an acid activated bentonite. *Applied Clay Sci* 6 59-68

103. Jozefaciuk G 1998. Changes of surface properties of soils and clay minerals in acidification and alkalization processes. Model studies. *Acta Agrophysica* 15 1-116
104. Jozefaciuk G 2002. Effect of acid and alkali treatment on surface-charge properties of selected minerals. *Clays and Clay Minerals* 50 646-655
105. Jozefaciuk G Bowanko G 2002. Effect of acid and alkali treatment on surface areas and adsorption energies of selected minerals. *Clays and Clay Minerals* 50 771-783
106. Jozefaciuk G Hajnos M Sokolowska Z Stawinski J Polubesova T Ponizovskij A 1993. Adhesion of humic acids to nonreactive surfaces effects on surface free energy and wettability of glass. *Intern Agrophysics* 7 235-240
107. Jozefaciuk G Hoffmann C Renger M Marschner B 2000. Effect of extreme acid and alkali treatment on surface properties of soils. *Journal of Plant Nutrition and Soil Science* 163 595-601
108. Jozefaciuk G Muranyi A Alekseeva T 2002. Effect of extreme acid and alkali treatment on soil variable charge. *Geoderma* 109 225-243
109. Jozefaciuk G Muranyi A Fenyvesi E 2001. Effect of cyclodextrins on surface and pore properties of soil clay minerals. *Environmental Science & Technology* 35 4947-4952
110. Jozefaciuk G Muranyi A Fenyvesi E 2003. Effect of randomly methylated beta-cyclodextrin on physical properties of soils. *Environmental Science & Technology* 37
111. Jozefaciuk G Muranyi A Szatanik-Kloc A Csillag J Wlodarczyk T 1999. Changes of pore system of a brown forest soil under acid degradation in a laboratory experiment. *Polish J Soil Sci* XXXII 23-32
112. Jozefaciuk G Muranyi A Szatanik-Kloc A Farkas C Gyuricza C 2001. Changes of surface fine pore and variable charge properties of a brown forest soil under various tillage practices. *Soil Tillage Res* 59 127-135
113. Jozefaciuk G Shin JS 1996. A modified back-titration method to measure soil titration curves minimizing soil acidity and dilution effects. *Korean J Soil Sci Fertilizer* 29 321-327
114. Jozefaciuk G Shin JS 1996. Distribution of apparent surface dissociation constants of some Korean soils as determined from back titration curves. *Korean Journal of Soil Science and Fertilizer* 29 328-335
115. Jozefaciuk G Shin JS 1996. Water vapor adsorption on soils. I Surface areas and adsorption energies as calculated by the BET and a new Aranovich theories. *Korean J Soil Sci and Fertilizer* 29 86-91

116. Jozefaciuk G Shin JS 1996. Water vapor adsorption on soils. II Estimation of adsorption energy distributions using local BET and Aranovich isotherms. *Korean J Soil Sci and Fertilizer* 29/3 218-225
117. Jozefaciuk G Sokołowska Z Hajnos M Hoffmann C Renger M 1996. Large effect of leaching of DOC on water adsorption properties of a sandy soil. *Geoderma* 74 125-137
118. Jozefaciuk G Sokolowska Z Sokolowski S Alekseev A Alekseeva T 1993. Changes of mineralogical and surface properties of water dispersible clay after acid treatment of soils. *Clay Minerals* 28 145-148
119. Jozefaciuk G Stawinski J Arsova A Urumova A 199. The influence of Al on negative soil charge. *Zesz Probl Post Nauk Roln Warsaw* 398 79-81
120. Jozefaciuk G Szatanik-Kloc A Muranyi A 1998. Effect of wetting on pore system of soils and minerals as determined by mercury intrusion porosimetry. *Polish J Soil Sci* 21 19-24
121. Keenan AG Mooney RW Wood LA 1951. The relation between exchangeable ions and water adsorption on kaolinite. *Journal of Physical Colloid Chemistry* 55 1462-1474
122. Keren R 1986. Reduction of the cation-exchange capacity of montmorillonite by take-up of hydroxy Al polymers. *Clays and Clay Minerals* 22 41-47
123. Kokotov J Zolotarev P Elkin T 1986. Theoretical base of the ion-exchange. *Chemistry Ed Leningrad* 375pp (in Russian)
124. Komadel P Schmidt D Madejova J Cícel B 1990. Alteration of smectites by treatments with hydrochloric acid and sodium carbonate solutions. *Applied Clay Science* 5 113-122
125. Kononowa MM 1966. *Soil organic matter*. Pergamon Elmsford NY
126. Konstankiewicz K Stawinski J 1976. The use of the mercury porosimeter for studies of some soil properties. *Polish J Soil Sci* IX 3-10
127. KoopalLK Van Riemsdijk WK Roffey MG 1987. Surface ionization and complexation models a comparison of methods for determining model parameters. *Journal of Colloid and Interface Science* 118 117-136
128. Kooyman PJ van der Waal P Van Bekkum H 1997. Acid dealumination of ZSM-5. *Zeolites* 18 50-53
129. Kortum G 1966. *Lehrbuch der Elektrochemie*. Verlag Chemie GmbH
130. Kozak E Sokolowska Z Sokolowski S Wierzchos J 1996. Surface fractal dimension of soil materials from pore size distribution data. I A comparison of two methods of determination. *Polish J Soil Sci* XXVIII/2 77-85

131. Kozak E Stawinski J Wierzchoś J 1991. Reliability of mercury intrusion porosimetry results for solids. *Soil Sci* 152 1325-1328
132. Kramers JS De Bano LF 1965. Soil nonwettability A neglected factor in watershed management. *Water Resour Res J* 1 283-286
133. Kunze GW 1965. Pretreatment for mineralogical analysis. in: Black CA ed *Soil Analysis Part I*. Amer Soc Agron Madison Wi 568-577
134. Kutilek M Nielsen DR 1994. *Soil Hydrology*. GeoEcology textbook Catena Verlag Cremlingen-Destedt Germany pp 1-357
135. Kwok DY Neumann AW 1998. Contact angles and surface energetics. *Progress Colloid Polymer Science* 109 170-184
136. Lal R Hall GF Miller FP 1989. Soil degradation. 1Basic processes. *Land Degrad Rehabilitation* 1 51-69
137. Lawrence GP 1977. Measurement of pore sizes in fine-textured soils A review of existing techniques. *J Soil Sci* 28 527-540
138. Lazarov D 2001. *Inorganic Chemistry*. Ed "Kl Ohridski" Sofia 631 pp (in Bulgarian)
139. Leon y Leon CA 1998. New perspectives in mercury porosimetry. *Adv in Colloid and Interface Sci* 76-77 342-372
140. Lipiec J Hatano R Slowinska-Jurkiewicz A 1998. The fractal dimension of pore distribution patterns in variously-compacted soil. *Soil Tillage Res* 47 61-66
141. Low PF 1961. Physical chemistry of clay-water interaction. *Advances in Agronomy* 40 269-327
142. Madejova J Bujdak J Janek M Komadel P 1998. Comparative FT-IR study of structural modifications during acid treatment of dioctahedral smectites and hectorite. *Spectrochimica Acta A Molecular and Biomolecular Spectroscopy* 54 1397-1406
143. Mandelbrot BB 1983. *The Fractal Geometry of Nature*. Freeman San Francisco
144. Mc Bride M 1976. Origin and position of exchange sites in kaolinite An ESR study. *Clays and clay minerals* 24 88-92
145. Mc Bride M 1989. *Surface Chemistry of Soil Minerals*. in: *Minerals in Soil Environments*. JB Dixon and SB Weed Eds SSSA Book Series No1 Madison Wisc USA
146. Mc Bride M 1997. A critique of diffuse double layer models applied to colloid and surface chemistry. *Clays and Clay Minerals* 45 598-608

147. Michel JC Riviere LM Bellon-Fontaine MN 1998. Characterization of the wettability of organic substrates peat and composed bark by adsorption measurements. *Int Symp Of Growing Media and Hydrophobics Windsor Canada*
148. Moise JC Bellat JP Methivier A 2001. Adsorption of water vapor on X and Y zeolites exchanged with barium. *Microporous and Mesoporous Materials* 43 91-101
149. Moseley WA Dhir VK 1996. Capillary pressure-saturation relations in porous media including the effect of wettability. *J Hydrology* 178 33-53
150. Mrad I Ghorbel A Tichit D and Lambert JF 1997. Optimisation of the preparation of an Al-pillared clay thermal stability and surface acidity. *Appl Clay Sci* 12 349-364
151. Myriam M 1998. Structural and textural modifications of palygorskite and sepiolite under acid treatment. *Clays and Clay Minerals* 46 225-231
152. Nederlof MM De Wit JC Riemsdijk WH Koopal LK 1993. Determination of proton affinity distributions for humic substances. *Environmental Science and Technology* 27 846-856
153. Nederlof MM Venema P Van Riemsdijk WH Koopal LK 1991. Modeling variable charge behaviour of clay minerals. in: *Proceedings of 7th Euroclay Conference Dresden Storr M Henning KH Adolphi P eds* 795-800
154. Neimark AV 1990. Calculating fractal dimensions of adsorbents. *Adsorption Sci Technol* 7 210-219
155. Neimark AV 1990. Determination of surface fractal dimension from the results of an adsorption experiment. *Russ J Phys Chem* 64 1398-1403
156. Neimark AV 1992. A new approach to determination of the surface fractal dimension of porous solids. *Physica A* 191 258-262
157. Newman ACD 1985. The interaction of water with clay mineral surfaces. in: *Chemistry of Clays and Clay Minerals Mineralogical Society Monograph No 6 ACD Newman ed Longman Scientific and Technical* 237-274
158. Newman RH Tate KR 1980. Soil characterized by <sup>31</sup>P nuclear magnetic resonance. *Commun Soil Sci Plant Anal* 11 835-842
159. Niklasson GA 1993. Adsorption on fractal structures application to cement materials. *Cem Conc Res* 23 1153-1158
160. Norris J Giese RF Van Oss CJ Constanzo PM 1992. Hydrophobic nature of organo-clays as a Lewis acid/base phenomenon. *Clay Clay Minerals* 40 327-334

161. Notario JS Garcia JE Caceres JM Arteaga IJ Gonzalez MM 1995. Characterization of natural phillipsite modified with orthophosphoric acid. *Applied Clay Science* 10 209-217
162. Ochiai M Ozao Y Yamazaki Y 1992. Self-similarity law of particle-size distribution and energy law in size distribution of solids. *Physica A* 191 292-300
163. Orlov D 1985. *Soil chemistry Univ of Moscow Ed Moscow* 376 pp Ru
164. Oscik J 1982. *Adsorption PWS Ellis Horwood Ltd Publish Chichester*
165. Pachepsky YA Polubesova TA Hajnos M Sokolowska Z Jozefaciuk G 1995. Parameters of surface heterogeneity from laboratory experiments on soil degradation. *Soil Sci Soc Am J* 59/2 410-417
166. Pachepsky YA Polubesova TA Hajnos M Sokolowska Z Jozefaciuk G 1995. Fractal parameters of pore surface area as influenced by simulated soil degradation. *Soil Sci Soc Am J* 59 68-75
167. Pachepsky YA Ritchie JC Gimenez D 1997. Fractal modelling of airborne laser alimetry data. *Remote Sens Environ* 61 150-161
168. Pachepsky YaA Crawford JW Rawls WJ Editors 2000. *Fractal in Soil Science*. Elsevier Amsterdam
169. Parks GA 1965. The isoelectric points of solid oxides solid hydroxides and aqueous hydroxo complex systems. *Chemical Review* 65 177-198
170. Paustian K Elliott T Carter M 1998. Tillage and crop management impacts on soil C storage use of long-term experimental data. *Soil Tillage Res* 47 vii-xii
171. Peech M Hydrogen-Ion Activity 1965. in: *Methods of Soil Analysis*. CA Black Ed Agronomy Series 9 914-926
172. Peech M Olsen RA Bolt GH 1953. The significance of potentiometric measurements involving liquid junction in clay and soil suspensions. *Soil Sci Soc Am Proc* 17164-167
173. Perfect E 1999. Estimating soil mass fractal dimensions from water retention curves. *Geoderma* 88 221-231
174. Perfect E Kay BD 1995. Applications of fractals in soil and tillage research. A review. *Soil & Tillage Research* 36 1-20
175. Perfect E Zhai Q Blevins RL 1997. Soil and tillage effects on the characteristic size and shape of aggregates. *Soil Sci Soc Am J* 61 1459-1465
176. Petersen LW Moldrup P Jacobsen OH Rolston DE 1996. Relation between soil specific area and soil physical and chemical properties. *Soil Sci* 161 9-21

177. Petit S Righi D Madejova J and Decarreau A 1999. Interpretation of the infrared  $\text{NH}_4^+$  spectrum of the  $\text{NH}_4^+$ -clays application to the evaluation of the layer charge. *Clay Minerals* 34 543-549
178. Pfeifer P Cole MW 1990. Fractals in surface science scattering and thermodynamics of adsorbed films. *New J Chem* 14 221-232
179. Pfeifer P Obert M 1989. Fractals Basic concepts and terminology. in: *The fractal approach to Heterogeneous Chemistry*. Avnir D Ed. J Willey and Sons
180. Polish Standard PN-Z-19010-1 1999. Soil Quality. Determination of the soil surface area – adsorption of water vapour method. (in Polish)
181. Polubesova TA Pachepsky YA Hajnos M Jozefaciuk G Sokolowska Z 1997. Comparison of three techniques to assess surface heterogeneity of solids in soils. *Int Agrophysics* 11 189-198
182. Rampazzo N and Blum WEH 1991. Decrease of layer charge in 21 clay minerals through soil acidification. in: *Proceedings of 7th Euroclay Conference Dresden*. M Storr KH Henning and P Adolphi eds 863-864
183. Rasiah V Kay BD Perfect E 1993. New mass-based model for estimating fractal dimension of soil aggregates. *Soil Sci Soc Am J* 57 891-895
184. Rassineux F Griffault L Meunier A Berger G Petit S Vieillard P Zellagui R Munoz M 2001. Expandability-layer stacking relationship during experimental alteration of a Wyoming bentonite in pH 135 solutions at 35 and 60°C. *Clay Minerals* 36197-210
185. Ravichandran J Sivasankar B 1997. Properties and catalytic activity of acid-modified montmorillonite and vermiculite. *Clays and Clay Minerals* 45 854-857
186. Raychev T 1996. Influence of organo-mineral interactions on colloid-chemical state of the soil adsorbent. D Sci Thesis. “N Poushkarov” Inst Sofia 161 pp Bg
187. Raychev T Arsova A Popandova S Jozefaciuk G Sokolowska Z Hajnos M 2001. Mechanisms of chelate formation during organo-mineral melioration of heavy metals polluted acid soils. *Bulg J of Agr Sci* 7 43-47 Sofia
188. Raychev T Arsova A Popandova S Jozefaciuk G Sokolowska Z Hajnos M 2001 Role of chelating processes in formation of buffer systems under organo-mineral melioration of Cu and Zn polluted acid soils. *Bulg J of Agr Sci* 7 167-174 Sofia
189. Raychev T Jozefaciuk G Sokolowska Z 2003. Effect of organic matter removal on fractal dimension of soil clay fraction. *Ecology and Future* 3-4 73-74

190. Roquerol R Avnir D Fairbridge CW Everett DH Haynes JH Pernicone N Ramsay JDF Sing KSW Unger KK 1994. Recommendations for the characterization of porous solids. *Pure Appl Chem* 66 1739-1758
191. Rudzinski W Everett DH 1991. Adsorption of gases on heterogeneous surfaces. Academic Press London
192. Rudzinski W Jagiello J Grillet Y 1982. Physical adsorption of gases on heterogeneous solid surfaces evaluation of the adsorption energy distribution from adsorption isotherms and heats of adsorption. *Journal of Colloid and Interface Science* 87 478-491
193. Ruiz R Blanco C Pesquera C González F Benito I López JL 1997. Zeolitization of a bentonite and its application to the removal of ammonium ion from waste water. *Applied Clay Science* 12 73-83
194. Rupert JP Granquist WT Pinnavaia TJ 1987. Catalytic properties of clay minerals. in: *Chemistry of Clays and Clay Minerals*. Mineralogical Society Monograph No 6 ACD Newman ed Longman Scientific and Technical 237-274
195. Sano T Uno Y Wang ZB Ahn CH Soga K 1999. Realumination of dealuminated HZSM-5 zeolites by acid treatment and their catalytic properties. *Microporous and Mesoporous Materials* 31 89-95
196. Sapozhnikov PM 1985. Relationship between the swelling of some soils and specific surface categories and the energetics of soil moisture. *Sov Soil Sci* 17 87-93
197. Schall N Simmler-Hubenthal H 1995. Surface modifications of montmorillonite and resulting possibilities for use as an adsorbent. in: *Proc Euroclay'95 Leuven*. A Elsen P Grobet M Keung H Lehman R Schoonheydt and H Toufar Eds 24-25
198. Schmidt PW 1989. Use of Scattering to Determine the Fractal Dimension. in: *The Fractal Approach to Heterogeneous Chemistry*. ed D Avnir J Willey and Sons New York pp 67-79
199. Schnitzer M 1991. Soil Organic matter-The next 75 years. *Soil Sci* 151 1 41-59
200. Schnitzer M Khan S U 1978. Soil organic matter. Elsevier Sci Publ Comp NY
201. Schofield RK Taylor AW 1955. Measurements of the activities of bases in soils. *J Soil Sci* 6137-146
202. Schofield RK Taylor AW 1955. The measurement of soil pH. *Soil Sci Soc Am Proc* 17164-167

203. Shin-Jyung Kang Kazuhiko Egashira 1997. Modification of different grades of Korean natural zeolites for increasing cation exchange capacity. *Applied Clay Science* 12 131-144
204. Sing KSW 1982. Reporting physisorption data for gas/solid systems with the special reference to the determination of surface area and porosity. *Pure&Appl Chem* 54 2201-2218
205. Singh U Uehara G 1986. Electrochemistry of the double-layer Principles and applications to soils. in: *Soil Physical Chemistry*. DL Sparks EdCRC Press Inc Boca Raton Florida
206. Sinitsyn VA Aja SU Kulik DA Wood SA 2000. Acid-base surface chemistry and sorption of some lanthanides on K<sup>+</sup>-saturated marlehead illite. I Results of an experimental investigation. *Geochim Cosmochim Acta* 64 185-194
207. Sławinski C Sokolowska Z Walczak R Borowko R Sokolowski S 2002. Fractal dimension of peat soils from adsorption and from water retention experiments. *Colloids and Surfaces A Physicochemical and Engineering Aspects* 208 289-301
208. Sokolowska Z 1989. Role of energetic heterogeneity in soil adsorption processes. *Problems of Agrophysics* 58 1-126 in Polish
209. Sokolowska Z 1992. On the role of energetic and geometric heterogeneity in sorption of water vapor by soils. Application of the fractal approach. *Geoderma* 52 59-72
210. Sokolowska Z Borowko M Reszko-Zygmunt J Sokolowski S 2002. Adsorption of nitrogen and water vapor by alluvial soils. *Geoderma* 107 33-54
211. Sokolowska Z G Jozefaciuk S Sokolowski A Urumova-Pesheva 1993. Adsorption of water vapor by soils. Investigations of the influence of organic matter iron and aluminum on energetic heterogeneity of soil clays. *Clays Clay Miner* 44 346-352
212. Sokolowska Z Hajnos M Borowko M Sokolowski S 1999. Adsorption of nitrogen on thermally treated peat soils. The role of energetic and geometric heterogeneity. *J Coll Interface Sci* 2191-10
213. Sokolowska Z Hajnos M Bowanko G 2000. Nitrogen adsorption study of the surface properties of the secondary transformed peat-moorsh soils. *Acta Agrophysica* 26 65-73
214. Sokolowska Z Hajnos M Dabek-Szreniawska M 1999. Relation between adsorption of water vapour specific surface area and soil cultivation. *Polish J Soil Sci XXXII/2* 3-12

215. Sokolowska Z Hajnos M Jozefaciuk G Hoffmann C Renger M 1996. Influence of surface coverage with humic acid on water vapor adsorption properties of kaolin and quartz. *Z Pfl Bodenk* 160 327-331
216. Sokolowska Z Hajnos M Jozefaciuk G Kozak E Arsova A 1995. Profile distribution of water adsorption properties of some representative Bulgarian soils. *Soil Sci Agrochem and Ecology* 30 171-173
217. Sokolowska Z Jozefaciuk G Sokolowski S Renger M Wilczynski A 1993. Water vapour adsorption as related to liming of acidic sandy forest soils. *Z Pfl Bodenk* 156 495-499
218. Sokołowska Z Sokołowski S 1999. Influence of humic acid on surface fractal dimension of kaolin analysis of mercury porosimetry and water vapour adsorption data. *Geoderma* 88 233-249
219. Sposito G 1984. *The surface chemistry of soils*. Oxford Univ Press NY Clarendon Press Oxford
220. Srasra E Trabelsi-Ayedi M 2000. Textural properties of acid activated glauconite. *Applied Clay Science* 17 71-84
221. Sridharan A Venkatappa Rao G 1972. Pore size distribution of soils from mercury intrusion porosimetry data. *Soil Sci Soc Am Proc* 36 980-981
222. Stawinski J Glinski J Ostrowski J Stepniewska Z Sokołowska Z Bowanko G Jozefaciuk G Księżopolska A Matyka-Sarzynska D 2000. Spatial characteristics of surface area of Polish arable soils. *Acta Agrophysica* 33 1-52 (in Polish)
223. Stevenson J 1982. *Humus chemistry genesis composition and reaction*. J Wiley and Sons NY
224. Suarez Barrios M de Santiago Buey C Garcia Romero E Martin Pozas J M 2001. Textural and structural modifications of saponite from Cerro del Aguila by acid treatment. *Clay Minerals* 36 483-488
225. Sucha V Srodon J Clauer N Elsass F Eberl D D Kraus I Madejova J 2001. Weathering of smectite and illite-smectite under temperate climatic conditions. *Clay Minerals* 36 403-419
226. Sumner ME 1994. Measurement of soil pH problems and solutions. *Commun Soil Sci Plant Anal* 257&8 859-879
227. Sun Kou MR Mendioroz S Munoz V 2000. Evaluation of the acidity of pillared montmorillonites by pyridine adsorption. *Clays Clay Min* 48 528-536
228. Suraj G Iyer CSP Lalithambika M 1998. Adsorption of cadmium and copper by modified kaolinites. *Applied Clay Science* 13 293-306

229. Swieboda R Kocjan R 2004. Porosimetric curves of modified silica. *Acta Agrophysica* 110 185-210
230. Tanji KN 1995. Agricultural salinity assessment and management. *Sci Publ Jodhpur India* 1-545
231. Tatlier M Erdem-Senatalar A 1999. Method to evaluate the fractal dimensions of solid adsorbents. *J Phys Chem B* 103 4360-4365
232. Taubald H Bauer A Sucha T Geckeis H Satir M 2000. Experimental investigation of the effect of high-pH solutions on the Opalinus Shale and the Hammerschmiede Smectite. *Clay Minerals* 35 515-524
233. Thomas GW Hargrove WL 1984. The Chemistry of Soil Acidity. in: F Adams Ed *Soil Acidity and Liming*. Agronomy Series 12 Madison Wise
234. Tombacz E Szekeres M Baranyi L Micheli B 1998. Surface modification of clay minerals by organic polyions. *Colloids and Surfaces A* 141 379-384
235. Toth T Jozefaciuk G 2002. Physicochemical properties of a solonchic toposequence. *Geoderma* 106 1-2 137-159
236. Tschapek M 1984. Criteria for determining the hydrophilicity-hydrophobicity of soils. *Z Pfl Bodenk* 147 138-149
237. Tschapek M Pozzo Ardizzi G de Bussetti SG 1973. Wettability of humic acid and its salts. *Z Pflanzen Bodenk* 135 16-31
238. Turcotte DL 1986. Fractals and fragmentation. *J Geophys Res* 91B2 1921-1926
239. Turner RC 1958. A theoretical treatment of the pH of calcareous soil. *Soil Sci* 86 32-34
240. Tyler SW Wheatcraft SW 1992. Fractal scaling of soil particle-size distributions analysis and limitations. *Soil Sci Soc Am J* 56 362-369
241. Ulrich B 1990. An Ecosystem Approach to Soil Acidification. in: *Soil Acidity*. Ulrich B and Sumner ME eds Springer-Verlag 28-79
242. Van Olphen H 1977. *An Introduction to Clay Colloid Chemistry*. 2nd Edition. John Wiley and Sons NY London Sydney Toronto
243. Van Oss C J 1994. *Interfacial forces in aqueous media*. Marcel Dekker Inc Publ New York 1-440
244. Van Oss CJ Chaudhury MK Good RJ 1998. Interfacial Lifshitz-van der Waals and polar interactions in macroscopic systems. *Chem Rev* 88 927-941
245. Van Reeuwijk LP ed 1986. *Procedures for soil analysis*. International Soil Reference Information Centre Wageningen

246. Van Riemsdijk WH Koopal LK De Wit JCM 1987. Heterogeneity and electrolyte adsorption intrinsic and electrostatic effects. *Neth J Soil Sci* 35 241-257
247. Volzone C Hipedinger N 1997. Mercury porosimetry of compacted clay minerals. *Z Pfl Bodenkunde* 160 357-360
248. Volzone C Thompson JG Melnitchenko A Ortiga J Palethorpe SR 1999. Selective gas adsorption by amorphous clay-mineral derivatives. *Clays and Clay Minerals* 5 647-657
249. Walczak R 1984. Model studies on a dependence of soil water retention on soil solid phase parameters. *Problems of Agrophysics* 41 (in Polish)
250. Wallace A 1994. Soil acidification from use of too much fertilizers. *Communications in Soil Science and Plant Analysis* 25 87-92
251. Warren CJ Dudas MJ and Abboud SA 1992. Effects of acidification on the chemical composition and layer charge of smectite from calcareous till. *Geoderma* 40 731-739
252. Wershaw RL 1994. Membrane-micelle model for humus in soils and its relation to humification. *US Geological Survey Water-Supply Paper* 2410 1-45
253. Wilczynski W Renger M Jozefaciuk G Hajnos M Sokolowska Z 1993. Surface area and CEC as related to qualitative and quantitative changes of forest soil organic matter after liming. *Z Pflanzenernahr Bodenk* 156 235-238
254. Yatsu E 1988. *The Nature of Weathering. An Introduction.* Sozosha Tokyo
255. Ylagan RF Altaner SP Pozzuoli A 2000. Reaction mechanisms of smectite illitization associated with hydrothermal alteration from Ponza Island Italy. *Clays and Clay Minerals* 48 610-631
256. Yongfu Xu Songyu Liu 1999. Fractal character of grain-size distribution of expansive soils. *Fractals* 7 359-366

## SYMBOLS AND ABBREVIATIONS:

$A$	adsorption potential
$C$	constant in adsorption equation
$d$ [m]	diameter
$D$	micropore fractal dimension
$D_s$	fractal dimension of mesopore surface
$E_a$ [J mol <sup>-1</sup> ]	adsorption energy
$E_c$ [J mol <sup>-1</sup> ]	condensation energy of the adsorbate
$F$ [N]	force
$f()$	fraction of a measurable given in parentheses
$\Delta G$ [J m <sup>-2</sup> ]	free energy change
$h$ [m]	thickness
$l$ [m]	distance of migration
$L$ [mol <sup>-1</sup> ]	Avogadro number
$M$ [kg]	molecular mass of the adsorbate
$N$ [kg kg <sup>-1</sup> ]	amount adsorbed
$N_m$ [kg kg <sup>-1</sup> ]	monolayer capacity
$p$ [Pa]	equilibrium adsorption or desorption pressure
$p_0$ [Pa]	saturated pressure of the adsorbate
$\underline{R}$ [J mol <sup>-1</sup> K <sup>-1</sup> ]	universal gas constant
$r, R$ [m]	pore radius
$R_{trans}$ [m]	effective pore radius for transport of a liquid
$S$ [m <sup>2</sup> kg <sup>-1</sup> ]	surface area
$T$ [K]	temperature of the measurements
$t$ [s]	time of migration
$V$ [m <sup>3</sup> kg <sup>-1</sup> ]	pore volume
$x$	ratio of $p/p_0$
$\alpha$ [deg]	solid-liquid contact angle
$\gamma$ [J m <sup>-2</sup> ]	surface free energy
$\eta$ [Pa s]	viscosity of the liquid
$\theta(p)$	total adsorption isotherm
$\omega$ [m <sup>2</sup> ]	area occupied by a single adsorbate molecule

**SUBSCRIPTS:**

av     average  
mic    micropores  
mes    mesopores  
mac    macropores  
L      liquid  
S      solid  
SL     solid/liquid interface

**SUPERSCRIPTS:**

- (minus)     electron donor  
+ (plus)      electron acceptor  
AB            polar (acid-base)  
LW            nonpolar (Lifshitz-van der Waals)